Physics Beyond the Standard Model: Supersymmetry

M.M. Nojiri[1,2], **T. Plehn**[3], **G. Polesello**[4] *(conveners & editors)*,

M. Alexander[3], *B.C. Allanach*[5], *A.J. Barr*[6], *K. Benakli*[7], *F. Boudjema*[8], *A. Freitas*[9], *C. Gwenlan*[10], *S. Jäger*[11], *S. Kraml*[12], *S. Kreiss*[3], *R. Lafaye*[13], *C.G. Lester*[14], *N. Kauer*[15], *C. Milstène*[16], *C. Moura*[7], *G.S. Muanza*[17], *A.R. Raklev*[5,14], *M. Rauch*[3], *M. Schmitt*[18], *S. Sekmen*[19], *P. Skands*[11,20], *P. Slavich*[8,11], *A. Sopczak*[21], *M. Spannowsky*[22], *D.R. Tovey*[23], *E. Turlay*[24], *C. F. Uhlemann*[15], *A.M. Weber*[25], *P. Zalewski*[26], *and D. Zerwas*[24]

[1] KEK Theory Group and Graduate University for Advanced Study (SOUKENDAI), Tsukuba, Japan; [2] Institute for the Physics and Mathematics of the Universe (IPMU), University of Tokyo, Kashiwa City, Japan; [3] SUPA, School of Physics, University of Edinburgh, Scotland; [4] INFN, Sezione di Pavia, Pavia, Italy; [5] DAMTP, CMS, University of Cambridge, UK; [6] Department of Physics, University of Oxford, UK; [7] LPTHE, Université Pierre et Marie Curie — Paris VI et Université Denis Diderot — Paris VII, France; [8] LAPTH, Annecy-le-Vieux, France; [9] Zurich University, Switzerland; [10] Department of Physics and Astronomy, UCL, London, UK; [11] Theory Group, Physics Department, CERN, Geneva, Switzerland; [12] LPSC, UJF Grenoble 1, CNRS/IN2P3, INPG, Grenoble, France; [13] LAPP, Université Savoie, IN2P3/CNRS, Annecy, France; [14] Cavendish Laboratory, University of Cambridge, UK; [15] Institut für Theoretische Physik, Universität Würzburg, Germany; [16] Fermilab, Batavia, U.S.; [17] IPN Lyon, Villeurbanne, France; [18] Northwestern University, Evanston, U.S.; [19] Department of Physics, Middle East Technical University, Ankara, Turkey; [20] Theory Group, Fermilab, Batavia U.S.; [21] Department of Physics and Astromony, Lancaster University, UK; [22] Institut für Theoretische Physik, Universität Karlsruhe, Germany; [23] Department of Physics and Astronomy, University of Sheffield, UK; [24] LAL, Université Paris-Sud, IN2P3/CNRS, Orsay, France; [25] Max Planck Institut für Physik (Werner Heisenberg Insitut), München, Germany; [26] Soltan Institute for Nuclear Studies, Warsaw, Poland

Abstract

This collection of studies on new physics at the LHC constitutes the report of the supersymmetry working group at the Workshop 'Physics at TeV Colliders', Les Houches, France, 2007. They cover the wide spectrum of phenomenology in the LHC era, from alternative models and signatures to the extraction of relevant observables, the study of the MSSM parameter space and finally to the interplay of LHC observations with additional data expected on a similar time scale. The special feature of this collection is that while not each of the studies is explicitely performed together by theoretical and experimental LHC physicists, all of them were inspired by and discussed in this particular environment.

Contents

[1] K. Benakli and C. Moura
[2] S. Kraml and A.R. Raklev
[3] R. Lafaye, T. Plehn, M. Rauch, E. Turlay, and D. Zerwas
[4] A.J. Barr, C. Gwenlan and C.G. Lester
[5] M.M. Nojiri, G. Polesello and D.R. Tovey
[6] G.S. Muanza

[7] N. Kauer and C.F. Uhlemann
[8] B.C. Allanach, F. Boudjema and A.M. Weber
[9] M. Alexander, S. Kreiss, R. Lafaye, T. Plehn, M. Rauch, and D. Zerwas
[10] S. Jäger, T. Plehn and M. Spannowsky
[11] P. Zalewski
[12] A. Sopczak, A. Freitas, C. Milsténe and M. Schmitt
[13] S. Kraml and S. Sekmen

[14] participating/corresponding authors: B.C. Allanach, P. Skands and P. Slavich

Aim and structure of this collection [1]

With the first LHC data around the corner, the great common goal of theoretical and experimental high–energy physics appears to be in close reach: over the coming years, we will have to try to understand the origins of electroweak symmetry breaking and the role of the TeV scale from the data rolling in. This effort can only be successful if theorists and experimentalists work in close collaboration, following the well–known spirit of the Les Houches workshops. This collaboration of course starts with the proper understanding of QCD, the theory which describes any kind of particle production at the LHC, but which also describes the main backgrounds which Higgs and new–physics searches have to battle. However, due to the complexity of LHC data on the one hand, and of the new–physics models at the TeV scale on the other hand, the interaction between theorists and experimentalists needs to go much further. Realistically, we expect that any new–physics search at the LHC will require theorists to formulate viable and predictive hypotheses which are implemented in state-of-the-art simulation and extraction tools. Such models can guide experimental searches towards the of course yet unknown ultraviolet completion of the Standard Model, even if at least all but one known models for new physics at the LHC will be soon ruled out.

Over recent years, high–energy theorists have hugely expanded the number of viable ultraviolet completions of the Standard Model. The main guiding principle of all of these models is still electroweak symmetry breaking. There are essentially two paths we can follow to explain the weak–scale masses of gauge bosons and of (third–generation) fermions: first, we can assume the minimal Higgs sector of our Standard Model to hold, which leads to the hierarchy problem. Without solving this problem, the Standard Model appears to be incomplete as a fundamental theory valid to all mass scales up to the Planck scale. Such ultraviolet completions are particularly attractive if they allow us to incorporate dark–matter candidates or unification scenarios. Supersymmetry is in particular in the experimental community definitely the most carefully studied completion, but extra dimensions or little–Higgs models are alternatives worth studying. The alternative path to describe electroweak symmetry breaking are strongly interacting models, which avoid predicting a fundamental Higgs boson. Such models have recently become more viable, if combined for example with extra dimensions.

As indicated by its title, this working group focuses on supersymmetry as one example for an ultraviolet completion of the Standard Model with the usual Higgs mechanism. However, simply writing down one supersymmetric version of the Standard Model does not suffice in view of the almost infinite number of LHC analyses which would be possible to study such models. As a matter of fact, signatures which until recently were thought to be typical for supersymmetry, namely jets plus missing energy plus maybe like–sign dileptons are by now mainstream signals for extra dimensions, little–Higgs models, or even strong interactions. Therefore, this collection of projects should first be considered as studies of models which lead to typical supersymmetry signatures, mostly beyond the naive inclusive ‘missing energy plus jets’ analysis. The obvious question is how with the LHC running we would go about to understand what the underlying theory of such signatures could be. Secondly, we include studies on version of a supersymmetric Standard Model which deviate from the simple MSSM. Which means that even supersymmetry as an underlying principle does not have to look exactly like we naive think it should look. It is a healthy development that theoretical physics has moved beyond its focus on the minimal supersymmetric ultraviolet extension of the Standard Model, while at the same time, not all alternatives in and beyond supersymmetry need to be studied including full detector simulations.

Independent of our ‘preferred’ models, theorists need to carefully formulate viable TeV–scale models, including variations of key models which allow us to test predictions for example of the MSSM. These alternatives can for example be driven by the similarity of signatures or by the aim to test certain underlying theory structures. In supersymmetry such models obviously involve Dirac gauginos (altering

[1] T. Plehn

the Majorana nature for example of the gluino or the dark–matter agent). Naively matching the two degrees of freedom of an on-shell gluon with those of a gluino only allows us to write down a Majorana gluino. In extended supersymmetric models this requirement does not need to exist. On the other hand, even assuming minimal supersymmetry an extended Higgs sector like in the NMSSM, should be tested carefully. Moreover, supersymmetric spectra with a hierarchy between gauginos and scalars maintain many advantages of supersymmetry, like unification and a dark–matter agent, while avoiding flavor constraints at the expense of introducing fine tuning. Due to the organization of the complete document, in this chapter of the Les Houches proceedings we limit ourselves to variations of the MSSM, deferring models like extra dimensions or little–Higgs to another collection of articles in the same volume.

In a second step, theorists and experimentalists need to develop strategies to extract information on TeV–scale physics from LHC data. In the standard MSSM scenarios, studying the kinematics of cascade decays has been shown to be a spectacularly successful, even in the presence of missing energy from a dark–matter agent escaping the detector unseen. There are, however, many more or less experimentally complex ways to use LHC observables to extract information on the masses of new states from LHC data. The information can come from the general underlying mass scale is event samples including physics beyond the Standard Model, or from any combination with cascade information. Of course, such studies are not limited to supersymmetry, but they can in principle be used for any new–physics signatures with decays from strongly interacting new–physics states down to a weakly interacting dark–matter particle.

Whatever we are looking for at the LHC, technically correct simulations of new–physics events are crucial, if we ever want to extract the fundamental parameters from their comparison with data. There is no good reason to try to extract new physics from 21st-century LHC data using 20th-century Monte–Carlos and methods. The past years have seen impressive progress in incorporating new–physics signals in modern Monte–Carlo tools, including for example the proper simulation of many–particle final states beyond a naive narrow–width approximation. This particular problem is being studied in the supersymmetric framework, but it is at least as relevant for new–physics models which predict more degenerate mass spectra, like for example generic universal extra dimensions.

Obviously, LHC data on TeV–scale physics will not come into a data–free world. There is a wealth of information we have already collected on such physics models, and during the LHC era we expect much more of it. The long list of current and future complementary data includes electroweak precision data, the muon's anomalous magnetic moment, precision–flavor physics, dark–matter measurements linked with big–bang nucleosynthesis, and most importantly at some stage the high–precision data from a future ILC. In particular, when it comes to measuring as many model parameters of the TeV–scale Lagrangian as possible, the proper combination of all these pieces of information is crucial to our understanding of the ultraviolet extension of the Standard Model. Only once we can claim a solid understanding of the TeV scale we should attempt to extrapolate our physics picture to very large mass scales, to finally determine if our underlying theory can really be a fundamental theory of Nature. After all, the LHC is not going to be the last, but the first major experiment allowing us to carefully study the TeV scale and determine the fundamental parameters of physics beyond the weak scale over the coming years!

The last section in this collection follows a great tradition of the Les Houches workshops: the successful definition and implementation of interfaces between computer tools used by the theoretical and experimental high–energy community.

At this stage, the conveners of the SUSY session would like to express their gratitude of course to the organizers of this inspiring and enjoyable workshop. Moreover, we would like to thank all the young collaborators in Les Houches and elsewhere, who have made possible the impressive studies presented in this collection.

1. A model for dirac and majorana gaugino masses [1]

1.1 Introduction

Massive fermions can appear either as Majorana or Dirac. Because the latter allow charged states, they are easier to detect . And, in fact, all identified fermionic masses are of Dirac type. The nature of neutrinos masses remains unknown, and unveiling it is the main challenge for double beta decays experiments. It is then legitimate to ask about the form of the masses of new fermions that could be detected by LHC.

In the minimal extension (MSSM) masses of gauginos are of Majorana type. Obtaining Dirac ones requires pairing up with new fermions that should then arise as components of extra chiral fields in the adjoint representation. The easiest way to incorporate these new states is to make the gauge fields as parts of $N = 2$ multiplets. Such a scheme is present in an extra-dimensional picture where the $N = 2$ fields appear as bulk states (in the absence of a projection) while the chiral matter appear as localized states in $N = 1$ representations. In such a set-up Dirac masses have been shown to appear naturally in the presence of an anomalous $U(1)$ as a result of new operators that mix the MSSM fields with the anomalous $U(1)$ [1, 2, 3, 4, 5, 6]. It was later shown that such operators can be generated by loop effects if the supersymmetry breaking sector is in an $N = 2$ representation [7, 8, 9], and that the quartic tree-level Higgs potential is in fact also modified [9]. Such models where studied as primarely based on the only presence of D -term breaking suffer from two issues. First, in the minimal set-up the adjoint scalar have tachyonic masses[2, 9]. Second, typical supersymmetry breaking model would lead to both D and F -terms. The latter will fix the first issue, but also turn on new sources for sof terms, in particular Majorana masses for the gauginos.

Here, we will take a different, more phenomenological approach. We will provide with the corresponding Lagrangian containing an $N = 2$ extended gauge sector, and we will not address the origin of the soft masses.

1.2 Primer

We will start by fixing our conventions for the spinorial notation as well as for the MSSM, and then we will proceed to extend the gauge sector.

Spinors notation

A Dirac fermion $_D$ has four components which can be assembled into two-component spinors :

$$_D = \quad (1)$$

where $^- = \ -^-\ _$ and $^-\ _ = (\ \ )$. Here is the completely antisymmetric tensor and $^{12} = 1$. We adopt for the matrices the following representation:

$$= \quad ; \quad ^5 = i^{0\ 1\ 2\ 3} = \quad (2)$$

where $^!$ are the Pauli matrices and the notation $= (1; ^!\ )$ and $^- = (1; \ ^!\ )$ is used. A Dirac mass term here takes the form:

$$^-_D \ _D = \quad + \ ^-\ ^-; \quad (3)$$

with the spinor products and $^-\ ^-$ defined as $=$ and $^-\ ^- = ^-\ _\ ^-$, where, again, we use the notation $=$. A Majorana fermion can also be written as:

$$_M = \quad ; \quad (4)$$

[1] K. Benakli and C. Moura

with the Majorama mass term:

$$\bar{}_{M}\ _{M} = \quad + \bar{\bar{}}; \tag{5}$$

Below we will always use left handed fermions. The Dirac fermion representing a lepton is:

$$^{(l\ )}_{D} = \begin{pmatrix} \bar{}^{(l^{+})} \\ ^{(l\ )} \end{pmatrix} \tag{6}$$

where $^{(l\ )}$ is the left-handed lepton field and $\bar{}^{(l^{+})}$ is the charge conjugated of the left-handed anti-lepton field: $\bar{}^{(l^{+})} - = \ -(\ ^{(l^{+})})$. Then, its Dirac mass will be written $m_{D}[\ ^{(l\ )}\ ^{(l^{+})} + \bar{}^{(l^{+})}\bar{}^{(l\ )}]$.

Supersymmetry

The generic supersymmetric Lagrangian density for a gauge theory discussed here take the form [2].

$$L = L_{gauge} + L_{chiral} + L_{minimal\ coupling}: \tag{7}$$

Here, the gauge kinetic Lagrangian is given by:

$$L_{gauge} = \quad \frac{1}{4}F^{a}F \quad ^{a} + i\bar{}^{a}\bar{} \ (D \quad)^{a} + \frac{1}{2}D^{a}D_{a} \tag{8}$$

where F is the gauge boson field strength, and D are the associated gaugino and and auxiliary field, respectively. D is the gauge covariant derivative. Here, the index a is a gauge symmetry group index corresponding to the generator T^{a}.

The chiral Lagrangian is written as:

$$L_{chiral} = D \quad _{i}D \quad _{i} + i\bar{}_{i}\bar{} \ D \quad _{i} + F_{i}F_{i} + \quad \frac{@W}{@\ _{i}}F_{i} \quad \frac{1}{2}\frac{@^{2}W}{@\ _{i}@\ _{i}}\ _{i}\ _{j} + h.c: \ : \tag{9}$$

Here the chiral fermion $_{i}$, the boson $_{i}$, and the auxiliary field F_{i} belong to the same gauge group representation and form an $N = 1$ multiplet . The index i labels the different chiral multiplets. The superpotential W is an holomorphic function of the fields $_{i}$.

Finally, the last piece in the supersymmetric Lagrangian density is:

$$L_{minimal\ coupling} = \quad g(\ _{i}T^{a}\ _{i})D^{a} \quad \sqrt{2}g\ ^{h}(\ _{i}T^{a}\ _{i})\ ^{a} + \bar{}^{a}(\bar{}_{i}T^{a}\ _{i})\ ^{i} \tag{10}$$

where g is the gauge coupling contant. The last two terms in (10) will be important to us as the scalar field takes a vacuum expectation value (the Higgs multiplets), producing bilinears in the fermions, thus mass terms.

1.3 MSSM

The field content of the MSSM is presented in table 1. Note that all the chiral fermions are left-handed, the charge conjugation label c allows to use the appropriate antiparticles. At the renormalisable level, the MSSM has the superpotential:

$$W = y_{u}^{ij}u_{i}^{c}Q_{j} \quad H_{u} \quad y_{d}^{ij}d_{i}^{c}Q_{j} \quad H_{d} \quad y_{e}^{ij}e_{i}^{c}L_{j} \quad H_{d} + \quad H_{u} \quad H_{d}: \tag{11}$$

The indices $i;j$ are family indices and runs from 1 to 3. The $3 \quad 3$ y matrices are the Yukawa couplings and the parameter is a Dirac mass for the Higgsinos. The " " denotes the $SU(2)$ invariant couplings, for example: $Q \quad H_{u} = \tilde{u}_{L}H_{u}^{0} \quad \tilde{d}_{L}H_{u}^{+}$.

[2] In this subsection and the next we follow closely the presentation of Refs [10].

Names		Spin 0	Spin 1/2	Spin 1	SU(3), SU(2), $U(1)_Y$
left-handed	Q	$(\tilde{u}_L\ ;\tilde{d}_L)$	$(u_L\ ;d_L)$		**3**, **2**, 1/3
quarks	u^c	$\tilde{u}^c_L$	u^c_L		$\overline{\mathbf{3}}$, **1**, -4/3
(3 families)	d^c	$\tilde{d}^c_L$	u^c_L		$\overline{\mathbf{3}}$, **1**, 2/3
leptons	L	$(\tilde{}_{eL}, \tilde{e}_L)$	$(\ _{eL}\ ; e_L)$		**1**, **2**, -1
(3 families)	e^c	$\tilde{e}^c_L$	e^c_L		**1**, **1**, 2
Higgs	H_u	$(H^+_u\ ; H^0_u)$	$(\tilde{H}^+_u\ ; \tilde{H}^0_u)$		**1**, **2**, 1
	H_d	$(H^0_d ; H_d\ )$	$(\tilde{H}^0_d ; \tilde{H}_d\ )$		**1**, **2**, -1
gluons	g		$\tilde{g}$	g	**8**, **1**, 0
W	W		$\tilde{W}\ ; \tilde{W}^0$	$W\ ; W^0$	**1**, **3**, 0
B	B		$\tilde{B}$	B	**1**, **1**, 0

Table 1: Chiral and gauge multiplet fields in the MSSM

Soft breaking

The breaking of supersymmetry is parametrized by a set of terms, labelled soft as they preserve the absence of quadratic divergences. The possible soft breaking terms in the MSSM are quite limited, there are gaugino masses for each gauge group, squarks mass terms, sleptons mass terms, Higgs mass terms and triple scalar couplings. We are primarily interested the gaugino masses given by:

$$\frac{1}{2}(M_3\tilde{g}\,\tilde{g} + M_2\tilde{W}\,\tilde{W} + M_1\tilde{B}\tilde{B} + h.c.) \tag{12}$$

Note that these are Majorama masses. Two of these terms for $\tilde{W}^{1,2}$ combine as a Dirac mass for $\tilde{W}$.

Neutralino masses

The neutral fermions of interest are the higgsinos $\tilde{H}^0_u$ and $\tilde{H}^0_d$ and the gauginos, bino $\tilde{B}$ and wino $\tilde{W}^0$. The mass terms for these fields in the MSSM have three origins:

The soft breaking terms for the bino and wino,

$$\frac{1}{2}(M_2\tilde{W}^0\tilde{W}^0 + M_1\tilde{B}\tilde{B} + h.c.): \tag{13}$$

The two last terms in equation (10) generate a mixing between $(\tilde{B}\ ;\tilde{W}^0)$ and $(\tilde{H}^0_u ; \tilde{H}^0_d)$. These mass terms are parametrized by the vev of the Higgs scalars $< H^0_u > \ v_u$ and $< H^0_d > \ v_d$. Using $\tan\ = v_u/v_d$, one can then express them in terms of , the weak gauge bosons masses m_W and m_Z and the weak mixing angle $_W$ as

$$\left[\, m_Z\ \cos\ _W\ (\cos\ \tilde{H}^0_d\tilde{W}^0\ \ \sin\ \tilde{H}^0_u\tilde{W}^0) + \sin\ _W\ (\sin\ \tilde{H}^0_u\tilde{B}\ \ \cos\ \tilde{H}^0_d\tilde{B}) + h.c.\right. \tag{14}$$

The term in the superpotential W contributes to the higgsinos masses ,

$$\tilde{H}^0_u ; \tilde{H}^0_d + h.c. \tag{15}$$

Chargino masses

Here we consider the charged higgsinos $\tilde{H}^+_u$ and $\tilde{H}_d$ and the charged gauginos $\tilde{W}^+$ and $\tilde{W}$. In the MSSM the origin of the chargino mass terms is completely analogous to those presented in subsection 1.3, they take here the following form:

$$M_2\tilde{W}^+\tilde{W} \tag{16}$$

$$\sqrt{2}m_W\ \sin\ \tilde{H}^+_u\tilde{W} \qquad \sqrt{2}m_W\ \cos\ \tilde{H}_d\tilde{W}^+ + h.c. \tag{17}$$

$$\tilde{H}^+_u ; \tilde{H}_d + h.c. \tag{18}$$

1.4 Extended susy gauge sector

We now consider the scenario where the gauge sector arise in multiplets of $N = 2$ supersymmetry while matter states are in $N = 1$ SUSY representations. Moreover, the Higgs multiplets H_u and H_d are assumed to form an $N = 2$ hypermultiplet.

The field content for the gauge sector is described in table 2. Note that for each $N = 1$ gauge multiplet present in the MSSM one need to introduce one extra scalar and fermionic fields. The latter are differentiated by a symbol ^{0} (see table 2).

Names	Spin 0	Spin 1/2	Spin 1	$SU(3), SU(2), U(1)_Y$
gluons	g	$\tilde{g}, \tilde{g}^0$	g	**8**, **1**, 0
W	W, W^0	$\tilde{W}, \tilde{W}^0, \tilde{W}^0, \tilde{W}^{00}$	W, W^0	**1**, **3**, 0
B	B	$\tilde{B}, \tilde{B}^0$	B	**1**, **1**, 0

Table 2: N = 2 gauge supermultiplets fields

In addition to the Majorana masses, Dirac ones can now be written. We will extended the MSSM soft terms to include

$$\frac{1}{2}(M_3^0 \tilde{g}^0 \tilde{g}^0 + M_2^0 \tilde{W}^0 \tilde{W}^0 + M_1^0 \tilde{B}^0 \tilde{B}^0) \quad (M_3^D \tilde{g} \tilde{g}^0 + M_2^D \tilde{W} \tilde{W}^0 + M_1^D \tilde{B} \tilde{B}^0) + h.c. \quad (19)$$

where M_i are Majorana and M_i^D are Dirac masses.

The $N = 2$ supersymmetry in the gauge sector introduces new couplings analogous to the two last terms in equation (10). These lead to new bilinear mixing terms between gauginos and higgsinos when the Higgs scalars H_u^0 and H_d^0 acquire vevs.

Neutralinos:

$$\left[m_Z \sin_W (\sin \tilde{H}_d^0 \tilde{B}^0 + \cos \tilde{H}_u^0 \tilde{B}^0) \quad \cos_W (\cos \tilde{H}_u^0 \tilde{W}^{00} + \sin \tilde{H}_d^0 \tilde{W}^{00}) \right] + h.c. \quad (20)$$

Charginos:

$$\sqrt{2} m_W \cos \tilde{H}_u^+ \tilde{W}^0 + \sqrt{2} m_W \sin \tilde{H}_d \tilde{W}^{0+} + h.c. \quad (21)$$

1.5 Fermionic mass matrix

We now put all the previous terms together and describe the resulting mass matrices for both neutral and charged gauginos and higgsinos when both Majorana and Dirac term are present.

Neutralinos

The neutralino mass terms are presented in equations (13)-(15), (19) and (20). The neutralino mass matrix, in the $(\tilde{B}^0, \tilde{B}, \tilde{W}^{00}, \tilde{W}^0, \tilde{H}_d^0, \tilde{H}_u^0)$ basis is:

$$M_{Neut} = \begin{pmatrix} M_1^0 & M_1^D & 0 & 0 & m_Z s_W s & m_Z s_W c \\ M_1^D & M_1 & 0 & 0 & m_Z s_W c & m_Z s_W s \\ 0 & 0 & M_2^0 & M_2^D & m_Z c_W s & m_Z c_W c \\ 0 & 0 & M_2^D & M_2 & m_Z c_W c & m_Z c_W s \\ m_Z s_W s & m_Z s_W c & m_Z c_W s & m_Z c_W c & 0 & \\ m_Z s_W c & m_Z s_W s & m_Z c_W c & m_Z c_W s & & 0 \end{pmatrix} \quad (22)$$

where $c_W = \cos_W$, $s_W = \sin_W$, $c = \cos$ and $s = \sin$.

Clearly this $6 \quad 6$ matrix will provide in general very long expressions for the neutralino mass eigenstates. A simple case is when the m_Z dependent terms in (22) are relatively small compared to

the other entries, and can be treated as perturbations. Moreover, the gaugino Majorama masses are symmetric in the primed and unprimed fermions: $M_1^0 = M_1$ and $M_2^0 = M_2$. In this case the higgsino mass eigenstates are given (approximately) by the combinations

$$\tilde{H}_S^0 \simeq \frac{1}{\sqrt{2}}(\tilde{H}_u^0 + \tilde{H}_d^0) \quad ; \quad \tilde{H}_A^0 \simeq \frac{1}{\sqrt{2}}(\tilde{H}_u^0 - \tilde{H}_d^0) \tag{23}$$

both having mass squared ^{2}. The neutral gaugino mass eigenstates are given, to leading order in m_Z/M_i, by

$$\tilde{B}_S = \frac{1}{\sqrt{2}}(\tilde{B} + \tilde{B}^0) \quad ; \quad \tilde{B}_A = \frac{1}{\sqrt{2}}(\tilde{B} - \tilde{B}^0) \tag{24}$$

$$\tilde{W}_S^0 = \frac{1}{\sqrt{2}}(\tilde{W}^0 + \tilde{W}^{00}) \quad ; \quad \tilde{W}_A^0 = \frac{1}{\sqrt{2}}(\tilde{W}^0 - \tilde{W}^{00}) \tag{25}$$

with masses

$$m_{\tilde{B}_S} \simeq M_1 + M_1^D \; ; \quad m_{\tilde{B}_A} \simeq M_1 - M_1^D \tag{26}$$

$$m_{\tilde{W}_S^0} \simeq M_2 + M_2^D \quad m_{\tilde{W}_A^0} \simeq M_2 - M_2^D : \tag{27}$$

One can express the ratio between Dirac and Majorama masses by the angle ^{D} defined by $\tan {}^D = M^D/M$. Alternatively, the angle ^{D} is measured by

$$\sin 2{}_B^D = \frac{m^2_{\tilde{B}_S} - m^2_{\tilde{B}_A}}{m^2_{\tilde{B}_S} + m^2_{\tilde{B}_A}} \tag{28}$$

and

$$\sin 2{}_W^D = \frac{m^2_{\tilde{W}_S^0} - m^2_{\tilde{W}_A^0}}{m^2_{\tilde{W}_S^0} + m^2_{\tilde{W}_A^0}} : \tag{29}$$

Charginos

The mass terms for the charginos can be expressed in the form

$$\frac{1}{2}((v^-)^T M_{Ch} v^+ + (v^+)^T M_{Ch}^T v^- + h.c) \tag{30}$$

where we addopted the basis $v^+ = (\tilde{W}^{0+}; \tilde{W}^+; \tilde{H}_u^+)$, $v^- = (\tilde{W}^{0-}; \tilde{W}^-; \tilde{H}_d^-)$. Collecting all the terms presented in equations (16)-(18), (19) and (21) leads to the chargino mass matrix :

$$M_{Ch} = \begin{pmatrix} 0 & M_2^0 & \sqrt{2} m_W \cos \\ M_2^D & \sqrt{2} m_W \sin & M_2 \sqrt{2} m_W \cos \\ \sqrt{2} m_W \sin & M_2 & \end{pmatrix} : \tag{31}$$

This nonsymmetric mass array is diagonalized by separate unitary transformations in the basis v^+ and v^-, $M_{Ch}^{diag} = U^\dagger M_{Ch} V$, where the matrices U and V are unitary.

For the simple case considered in the previous subsection, where the m_Z dependent terms can be treated as perturbations and $M_2^0 = M_2$, the higgsino mass eigenstates will be given approximately by $\tilde{H}_u^+$ and $\tilde{H}_d^-$, both having mass squared ^{2}. The charged gaugino mass eigenstates will be given, to leading order in m_Z/M_i, by the combinations

$$\tilde{W}_S^+ \simeq \frac{1}{\sqrt{2}}(\tilde{W}^+ + \tilde{W}^{0+}) \quad ; \quad \tilde{W}_A^+ \simeq \frac{1}{\sqrt{2}}(\tilde{W}^+ - \tilde{W}^{0+}) \tag{32}$$

$$\tilde{W}_S \simeq \frac{1}{\sqrt{2}}(\tilde{W}^+ + \tilde{W}^{0\prime}) \quad ; \quad \tilde{W}_A \simeq \frac{1}{\sqrt{2}}(\tilde{W}^+ - \tilde{W}^{0\prime}) \tag{33}$$

with squared masses

$$m^2_{\tilde{W}^+_S} \simeq (M_2 + M_2^D)^2 \qquad m^2_{\tilde{W}^+_A} \simeq (M_2 - M_2^D)^2 \tag{34}$$

$$m^2_{\tilde{W}^0_S} \simeq (M_2 + M_2^D)^2 \qquad m^2_{\tilde{W}^0_A} \simeq (M_2 - M_2^D)^2 \tag{35}$$

Note that, in this limit, the winos have approximate degenerate masses: $m^2_{\tilde{W}^{0\prime}_S}$ $m^2_{\tilde{W}^+_S}$ $m^2_{\tilde{W}^0_S}$ and $m^2_{\tilde{W}^{0\prime}_A}$ $m^2_{\tilde{W}^+_A}$ $m^2_{\tilde{W}^0_A}$.

Gluinos

Since gluinos $\tilde{g}$ and $\tilde{g}^0$ are in color octet representation, they cannot mix with any other fermion, the only possible gluino masses are the soft ones presented in (12) and (19). In the basis $(\tilde{g}^0, \tilde{g})$ the gluino mass matrix is simply

$$M_{Gluino} = \begin{pmatrix} M_3^0 & M_3^D \\ M_3^D & M_3 \end{pmatrix} : \tag{36}$$

We will illustrate two limits. The first one is when gaugino Majorama masses are symmetric in the primed and unprimed fermions: $M_3^0 = M_3$. The analysis of the gluino mass matrix in this case follows closely the discussion after (23). The gluino mass eigenstates are

$$\tilde{g}_S = \frac{1}{\sqrt{2}}(\tilde{g} + \tilde{g}^0) \quad ; \quad \tilde{g}_A = \frac{1}{\sqrt{2}}(\tilde{g} - \tilde{g}^0) \tag{37}$$

with masses

$$m_{\tilde{g}_S} = M_3 + M_3^D \; ; \qquad m_{\tilde{g}_A} = M_3 - M_3^D \; ; \tag{38}$$

and the ratio between Dirac and Majorama masses is parameterized by the angle $\tan\beta_g^D = M_3^D/M_3$, alternatively by

$$\sin 2\beta_g^D = \frac{m^2_{\tilde{g}_S} - m^2_{\tilde{g}_A}}{m^2_{\tilde{g}_S} + m^2_{\tilde{g}_A}} : \tag{39}$$

The second limit is when one of the Majorama masses, say M_3^0, is very small compared to the other entries of the mass matrix (36). In this limit, the gluino mass eigenstates are given approximately by

$$\tilde{g}_1 \simeq \cos\theta\, \tilde{g} - \sin\theta\, \tilde{g}^0 \quad ; \quad \tilde{g}_2 \simeq \sin\theta\, \tilde{g} + \cos\theta\, \tilde{g}^0 \tag{40}$$

where

$$\tan\theta = \frac{1}{2}\cot\beta_g^D \left(1 + \sqrt{1 + 4\tan^2\beta_g^D}\right) \tag{41}$$

and, as before, $\tan\beta_g^D = M_3^D/M_3$. The gluino masses are

$$m_{\tilde{g}_1} \simeq \frac{M_3}{2}\left(1 + \sqrt{1 + 4\tan^2\beta_g^D}\right) \quad ; \quad m_{\tilde{g}_2} \simeq \frac{M_3}{2}\left(1 - \sqrt{1 + 4\tan^2\beta_g^D}\right) \tag{42}$$

and the ratio between Dirac and Majorana masses is parameterized

$$\sin^2\beta_g^D = \frac{|m_{\tilde{g}_1} m_{\tilde{g}_2}|}{m^2_{\tilde{g}_1} + m^2_{\tilde{g}_2} + |m_{\tilde{g}_1} m_{\tilde{g}_2}|} : \tag{43}$$

1.6 Interactions

We turn now to the interactions between the extended supersymmetric sector and the MSSM fields. First, we remind the interactions between the MSSM gauginos, the higgsinos and the scalar Higgs:

$$\frac{g}{\sqrt{2}} H_u \, i\tilde{H}_u \tilde{W}^i + H_d \, i\tilde{H}_d \tilde{W}^i \qquad \frac{g'}{\sqrt{2}} H_u \tilde{H}_u \tilde{B} \quad H_d \tilde{H}_d \tilde{B} \tag{44}$$

where g and g' are the $SU(2)$ and $U(1)_Y$ coupling constants.

Due to the fact that the two Higgs H_u and H_d form a $N = 2$ hypermultiplet, their interactions with the new fermions W'^0 and B'^0 are

$$\frac{g}{\sqrt{2}} \Big[H_u \quad (i\tilde{H}_d)\tilde{W}'^0 i + H_d \quad (i\tilde{H}_u)\tilde{W}'^0 i \Big] \qquad \frac{g'}{\sqrt{2}} H_d \; \tilde{H}_u \tilde{B}'^0 \quad H_u \; \tilde{H}_d \tilde{B}'^0 \; : \tag{45}$$

One can straightforwardly verify that these interactions lead upon electroweak breaking to the gaugino-higgsino mixing present in the neutralino and chargino mass matrices .

1.7 New scalars

The $N = 2$ vector multiplets include, in addition to the new fermions dicussed above, scalar fields in the adjoint representation. We denote these states as $_g$, $_W$ and $_B$. They couple to the Higgs chiral fields (now in an $N = 2$ hypermultiplet) in the superpotential, and through their F-term modify the tree-level Higgs scalars quartic terms in the potential by the new terms:

$$\frac{g^2}{2} \sum_i \quad H_u \quad i H_d^{\dagger 2} \quad \frac{g'^2}{2} \Big| H_u \quad H_d \Big|^2 : \tag{46}$$

These scalar should not remains massless, but get soft terms as:

$$\frac{1}{2} m^2_{3S} \; g \; g \quad \frac{1}{2} m^2_{3A} \; g \; g \quad \frac{1}{2} m^2_{2S} \; W \; W \quad \frac{1}{2} m^2_{2A} \; W \; W \quad \frac{1}{2} m^2_{1S} \; B \; B : \frac{1}{2} m^2_{1A} \; B \; B : \tag{47}$$

with $m^2_{iS} > m^2_{iA}$. If the masses in (47) are big compared to the Higgs mass, these fields can be integrated out and in the low energy theory the scalar potential is the one in the MSSM plus the contributions coming from the quartic terms (46) [9]. Note that the latter contribution disappears, if instead, the integration out is supersymmetric (due to a large supersymmetric mass).

Acknowledgements

We wish to thank the organizers of the ”Les Houches: TeV Colliders” for their hospitality.

2. NMSSM in disguise: discovering singlino dark matter with soft leptons [1]

2.1 Introduction

The Next-to-Minimal Supersymmetric Standard Model (NMSSM) provides an elegant solution to the problem of the MSSM by the addition of a gauge singlet superfield $\hat{S}$ [11, 12, 13, 14]. The superpotential of the Higgs sector then has the form $\hat{S}(\hat{H}_d \hat{H}_u) + \frac{1}{3}\hat{S}^3$. When $\hat{S}$ acquires a vacuum expectation value, this creates an effective term, hSi, which is automatically of the right size, *i.e.* of the order of the electroweak scale.

The addition of the singlet field leads to a larger particle spectrum than in the MSSM: in addition to the MSSM fields, the NMSSM contains two extra neutral (singlet) Higgs fields – one scalar and one pseudoscalar – as well as an extra neutralino, the singlino. Owing to these extra states, the phenomenology of the NMSSM can be significantly different from the MSSM; see chapter 4 of [15] for a recent review and references. In particular, the usual LEP limits do not apply to singlet and singlino states. Moreover, the singlino can be the lightest supersymmetric particle (LSP) and a cold dark matter candidate.

In this contribution, we investigate the LHC signature of a SPS1a-like scenario, supplemented by a singlino LSP. In such a setup, gluinos and squarks have the 'conventional' SUSY cascade decays into the bino-like neutralino, $\tilde{\chi}_2^0$ B, which then decays into the singlino LSP, $\tilde{\chi}_1^0$ S, plus a pair of opposite sign same-flavour (OSSF) leptons. (The $\tilde{\chi}_2^0$ decay proceeds dominantly through an off-shell slepton.) A dark matter relic density of h^2 $0{:}1$ is obtained if the $\tilde{\chi}_1^0$ and/or $\tilde{\chi}_2^0$ annihilate through pseudoscalar exchange in the s-channel.

One peculiar feature of this scenario is that the mass difference between $\tilde{\chi}_1^0$ and $\tilde{\chi}_2^0$ is always small; it reaches at most 12 GeV, and is often much smaller. The leptons originating from the $\tilde{\chi}_2^0 ! \tilde{\chi}_1^0 l^+ l$ decay hence tend to be soft. In the standard SUSY analysis, requiring $p_T(l) > 20$ GeV, there is a risk of missing these leptons and wrongly concluding to have found the MSSM instead of the NMSSM, with $\tilde{\chi}_2^0$ as the LSP and dark matter candidate (discovery of the additional Higgs states will also be very difficult at the LHC in this scenario). The aim of this contribution is to show the feasibility of detecting the $\tilde{\chi}_2^0 ! \tilde{\chi}_1^0 l^+ l$ decay and measuring the singlino–bino mass difference by looking for soft di-leptons.

We use the NMHDECAY [16, 17] program to compute the NMSSM mass spectrum and Higgs branching ratios, and to evaluate the LEP bounds; SPHENO [18] is used to calculate the sparticle branching ratios, and MICROMEGAS [19, 20] for the relic density. The SUSY-breaking parameters of our scenario are listed in Table 1. The main difference to the original SPS1a [21] is that we choose $M_1 = 0{:}5M_2 = 120$ GeV, leading to a $\tilde{\chi}_2^0$ mass of $' 115$ GeV, in order to evade LEP bounds when adding the singlino and singlet Higgses. To obtain a singlino LSP, we choose 10^2 and $0{:}1$. This way $\tilde{\chi}_1^0$ 99% S, and $m_{\tilde{\chi}_2^0}$ hardly varies with and ($0{:}1$ GeV). In addition, the trilinear Higgs couplings A and A are chosen such that $m_{\tilde{\chi}_i^0} + m_{\tilde{\chi}_j^0} \quad m_{A_2}$ for at least one combination of $i;j = 1;2$, to achieve $0{:}094 \quad h^2 \quad 0{:}135$ [22]. We thus obtain a set of NMSSM parameter points with varying $m \quad m_{\tilde{\chi}_2^0} \quad m_{\tilde{\chi}_1^0}$.

The four points used for this study are summarised in Table 2. Points A–D have $m = 9{:}7, 3{:}0, 1{:}5$ and $0{:}9$ GeV, respectively. The SM-like second neutral scalar Higgs, S_2, has a mass of 115 GeV for all these points, consistent with the LEP limit. On the other hand, the lightest neutral scalar S_1 and the

[1] S. Kraml and A.R. Raklev

M_1	M_2	M_3	e	$M_{L_{1;3}}$	M_{E_1}	M_{E_3}	M_{Q_1}	M_{U_1}	M_{D_1}	M_{Q_3}	M_{U_3}	M_{D_3}
120	240	720	360	195	136	133	544	526	524	496	420	521

Table 1: Input parameters in [GeV] for our SPS1a-like scenario. The NMSSM-specific parameters are given in Table 2.

Point	[10 ^{2}]	[10 ^{3}]	A	A	m $_{\sim_1^0}$	m $_{A_1}$	m $_{A_2}$	m $_{S_1}$	h ^{2}		($\sim_2^0$)
A	1:49	2:19	37:4	49:0	105:4	88	239	89	0:101	7	10 ^{11}
B	1:12	1:75	42:4	33:6	112:1	75	226	100	0:094	9	10 ^{13}
C	1:20	1:90	39:2	53:1	113:8	95	256	97	0:094	1	10 ^{13}
D	1:47	2:34	39:2	68:9	114:5	109	259	92	0:112	4	10 ^{14}

Table 2: NMSSM benchmark points used in this study. Masses and other dimensionful quantities are in [GeV].

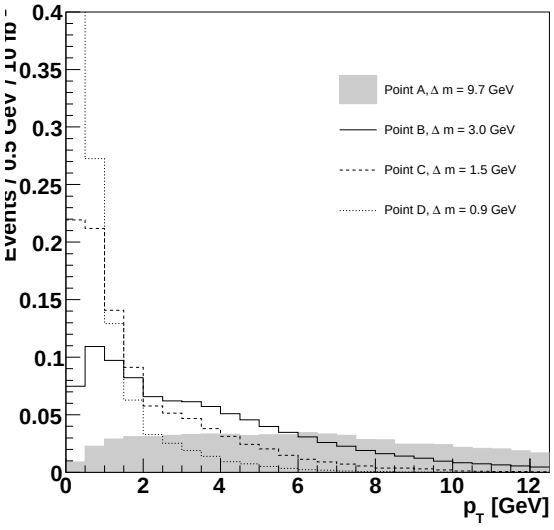

Fig. 1: p_T distributions for leptons from the decay $\sim_2^0 \; ! \; \sim_1^0 l^+ l$ in benchmark points A–D. All distributions are normalised to unity over the whole momentum range.

lighter pseudoscalar A_1 are mostly singlet states, and can hence be lighter than 114 GeV. Concerning the neutralino annihilation, for Point A the dominant channel is $\sim_2^0 \sim_2^0 \; ! \; bb$, contributing 88% to h vi. For Point B, $\sim_1^0 \sim_1^0$, $\sim_1^0 \sim_2^0$ and $\sim_2^0 \sim_2^0$ annihilation to bb contribute 10% , 15% , and 50% , respectively. Point C has again dominantly $\sim_2^0 \sim_2^0$, while Point D has about 50% $\sim_2^0 \sim_2^0$ and 35% $\sim_1^0 \sim_2^0$ annihilation.

Figure 1 shows the resulting p_T distributions for leptons from decays to singlinos for all four benchmark points. Clearly, cuts on lepton transverse momentum of even 10 GeV will remove the wast majority of events for points B–D. However, one should notice that the distributions have considerable tails beyond the simple mass difference m , due to the boost of the $\sim_2^0$.

2.2 Monte Carlo analysis

We perform a Monte Carlo simulation of the benchmarks described above by generating both SUSY signal and SM background events with `PYTHIA 6.413` [23]. The generated events are then put through a fast simulation of a generic LHC detector, `AcerDET-1.0` [24]. Although `PYTHIA` does not contain a framework for generating NMSSM events *per se*, it has the capability to handle the NMSSM spectrum and its decays. Since our scenario predicts the same dominant cross section as in the MSSM, namely gluino and squark pair-production, with negligible interference from the non-minimal sector, we use the built-in MSSM machinery for the hard process, and generate only squark and gluino pair-production.

The detector simulation is done with standard `AcerDET` settings, with one exception: for detecting decays to the singlino the detector response to soft leptons is vital. We therefore parametrise the

efficiency of electron and muon identification as a function of lepton p_T. For muons we base ourselves on the efficiencies shown in Figure 8-5 and 8-9 of the ATLAS TDR [25]; for electrons we use the same parametrisation scaled down by 0.82. While this is certainly not a perfect description of the real ATLAS or CMS efficiencies during data taking, it incorporates some of the most important effects in an analysis, such as an absolute lower limit for lepton identification, at around 2–3 GeV for muons, and a difference in electron and muon efficiencies. However, it does not address other important issues, e.g. mis-identification of charged pions as electrons. To improve on these simple assumptions one would need a full simulation of the detectors, or efficiencies from data, which is clearly beyond the scope of this contribution.

We generate events corresponding to 10 fb ^{1} of both signal and background (some with weights). Our background consists of large p_T-binned samples of QCD $2 ! 2$ (10M), W +jet (4M), Z +jet (3M), $W W = W Z = Z Z$ (1M) and $t\bar{t}$ (5M) events. For the signal, PYTHIA gives a LO cross section of 24 pb for squark and gluino pair-production, thus 240 000 events are generated per benchmark point.

We begin our analysis along the lines of the 'standard' di-lepton edge analysis. To isolate the SUSY signal from SM background we apply the following cuts:

Require at least three jets with $p_T > 150;100;50$ GeV.

Require missing transverse energy $E_T > max(100\,GeV;0.2M_{e})$, where the effective mass M_{e} is the sum of the p_T of the three hardest jets plus missing energy.

Require two OSSF leptons with $p_T > 20;10$ GeV.

After these cuts the background is small and consists mainly of $t\bar{t}$, with some vector boson events surviving. The resulting di-lepton invariant mass distributions for points B and D can be seen in the left and right panels, respectively, of Fig. 2. The contribution from decays of $\tilde{\chi}_3^0$ to $\tilde{\chi}_2^0$ via right and left-handed sleptons are shown in red and blue, other SUSY events, where the leptons mainly come from chargino or stau decays, in light grey, and the remaining SM background in dark grey. For the B benchmark point there is a small excess of events coming from decays of $\tilde{\chi}_2^0$ to singlinos (yellow) at low invariant masses, that survives due to other harder leptons in the event. However, all such events are removed for benchmark point D because of the hard lepton p_T cut.[2] In this case one would miss the singlino and take the $\tilde{\chi}_2^0$ to be the LSP dark matter candidate.

It is clear that to increase sensitivity to the disguised NMSSM scenario, one needs to lower the lepton p_T cuts. However, this opens the possibility for large increases in background. While most of this background, from uncorrelated leptons, can in principle be removed by subtracting the corresponding opposite sign opposite-flavour (OSOF) distribution, assuming lepton universality, large backgrounds will increase the statistical error and a soft lepton sample is more vulnerable to non-universality from e.g. pion decays. The result of completely removing the p_T requirement on the leptons is shown for benchmark points B and D in the left and right panels of Fig. 3, respectively. While there is indeed an increase in backgrounds, the effect on the signal is much more significant. For both benchmarks, the decay to the singlino is now visible as a large excess at low invariant masses. We have also tested scenarios with smaller values of m, and find that we have a significant excess down to $m \prime 0.6$ GeV, with the assumptions on lepton efficiencies described above.[3]

In the standard di-lepton analysis the edges of the red and blue distributions shown in Fig. 2 can be used to determine the relationship between the neutralino and slepton masses, in our scenario $m^2_{\tilde{\chi}_3^0} \quad m^2_{\tilde{l}}$ and $m^2_{\tilde{l}} \quad m^2_{\tilde{\chi}_2^0}$. We extract additional information by also determining the position of the edge at low invariant masses, fitting a Gaussian-smeared step function to the OSOF subtracted distribution, shown in Fig. 4. In subtracting the OSOF distribution we have taken into account the asymmetry induced by the the difference in electron and muon efficiencies. This fit determines the mass difference m, since

[2] Green denotes lepton combinations with one lepton from a slepton decay chain and the other from a decay to a singlino. The few pure singlino events at higher invariant masses are due to mis-combinations of leptons from different $\tilde{\chi}_2^0$ decays.

[3] In fact, for such small mass differences we may also see displaced vertices due to the long lifetime of the $\tilde{\chi}_2^0$.

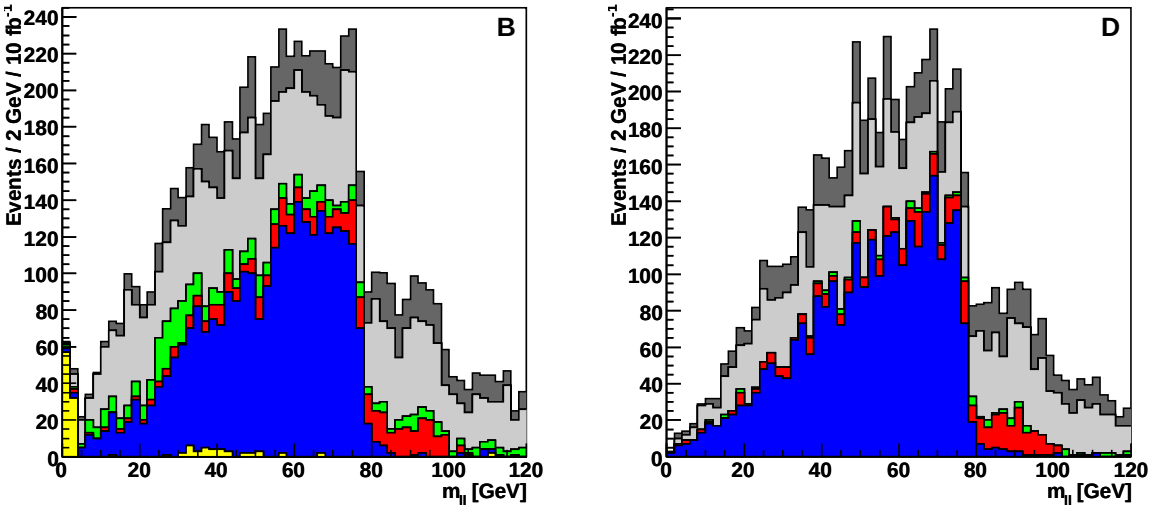

Fig. 2: Di-lepton invariant mass distributions for point B (left) and point D (right) with standard lepton p_T cuts. See text for colour coding.

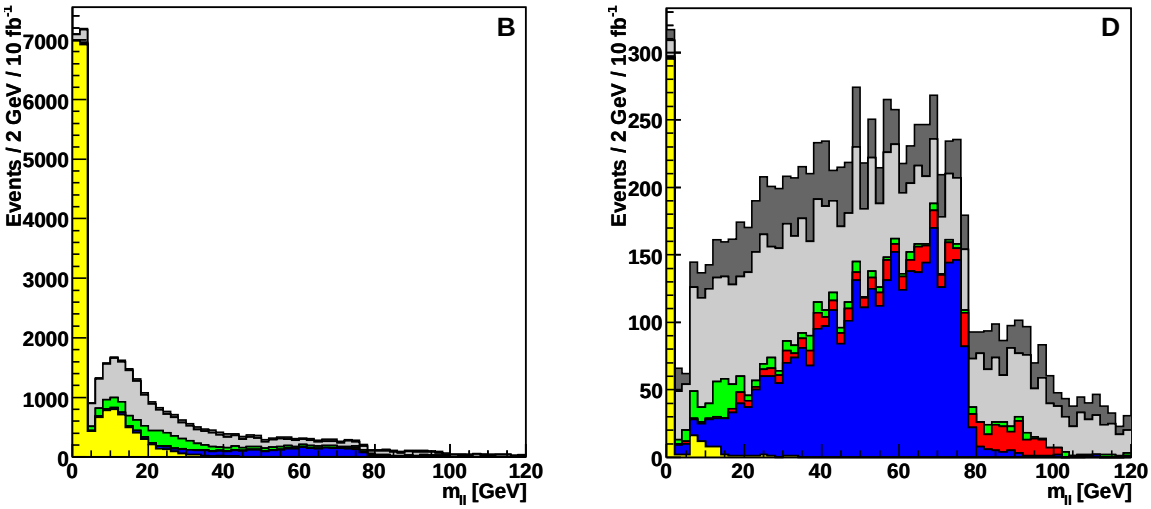

Fig. 3: Di-lepton invariant mass distributions for point B (left) and point D (right) without lepton p_T cuts.

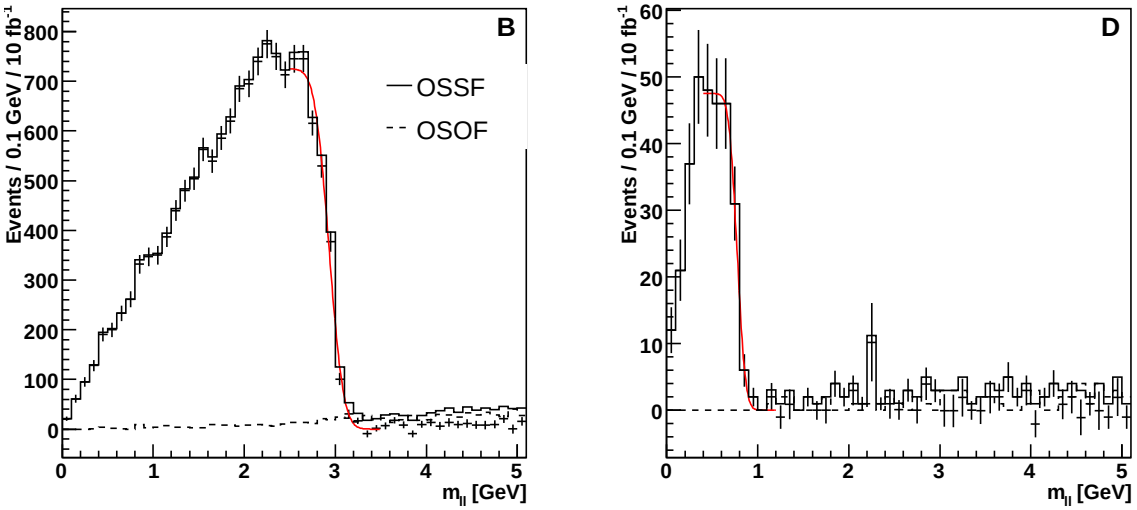

Fig. 4: Di-lepton invariant mass distributions for point B (left) and point D (right) after OSOF subtraction.

$m_{ll}^{max} = m_{\tilde{\chi}_2^0} - m_{\tilde{\chi}_1^0}$. For point B the result of the fit is $m_{ll}^{max} = 2.93 \pm 0.01$ GeV, to be compared with the nominal value of 3.05 GeV, while for point D the result is $m_{ll}^{max} = 0.77 \pm 0.02$ GeV, with a nominal value of 0.87 GeV. Both results are significantly on the low side with respect to the small statistical errors. We speculate that this systematic error is at least in part due to the step function used in the fit to the edge, and that a more sophisticated description will give results closer to the nominal values.

A final comment is in order concerning early discoveries: in fact, since all SUSY cascades will contain the decay to a singlino, the lower edge in the di-lepton distribution may appear much earlier than the 'standard' decay through a slepton, if at all present, provided that the soft leptons are searched for.

2.3 Conclusions

We have demonstrated that lowering the requirements on lepton transverse momentum in the standard di-lepton edge of SUSY searches may reveal unexpected features, such as the NMSSM in disguise. While our numerical results are sensitive to the exact lepton efficiencies, to be measured at the experiments, and while there may be additional backgrounds not simulated, such as multi gauge boson and/or multi jet final states, the OSOF subtraction procedure ensures that the background is removable and the NMSSM scenario in question is discoverable down to very small mass differences $m = m_{\tilde{\chi}_2^0} - m_{\tilde{\chi}_1^0}$.

Acknowledgements

ARR wishes to thank the members of the Cambridge Supersymmetry Working Group for many useful discussions, and acknowledges funding from the UK Science and Technology Facilities Council (STFC).

3. The MSSM with decoupled scalars at the LHC [1]

3.1 Introduction

Assuming a large soft–breaking scale for all MSSM scalars [26, 27, 28, 29, 30] pushes squarks, sfermions and heavy Higgses out of the reach of the LHC without affecting the gaugino sector. Even though the hierarchy problem will not be solved without an additional logarithmic fine tuning in the Higgs sector, such models can be constructed to provide a good dark–matter candidate and realize grand unification while minimizing proton decay and FCNCs. We investigate their LHC phenomenology, with all scalars decoupled from the low–energy spectrum. We focus on gaugino–related signatures to estimate the accuracy with which its underlying parameters can be determined [31, 32].

3.2 Phenomenology

The spectrum at LHC mass scales is reduced to the Standard–Model with a light Higgs, plus gauginos and Higgsinos. At the high scale M_S the effective theory is matched to the full MSSM and the usual renormalization group equations apply. The Higgsino mass parameter and the ratio $\tan$ in the Higgs sector correspond to their MSSM counter parts. The gaugino masses $M_{1,2,3}$ and the Higgs-sfermion-sfermion couplings unify, and M_S replaces the sfermion and the heavy Higgs' mass parameters. This set resembles the mSUGRA parameter set except for $\tan$ now playing the role of a matching parameter (with all heavy Higgses being decoupled) rather than that of an actual vev ratio [33].

We select our parameter point lead by three constraints: first, we minimize the amount of fine tuning necessary to bring the light Higgs mass into the 100 to 200 GeV range and reduce M_S to 10 TeV, which is still outside the LHC mass range. Another reason for this low breaking scale is that we want the gluino to decay inside the detector (preferably at the interaction point) instead of being long–lived [34, 29]. Heavier sfermions increase the life time of the gluino such that it creates a displaced vertex or even hadronizes [35].

Secondly, we obtain the correct relic dark–matter density $h^2 = 0{:}111^{+0{:}006}_{0{:}008}$ [36] by setting $= 290$ GeV and $M_2(M_{GUT}) = 132{:}4$ GeV or $M_2(M_{weak}) = 129$ GeV. This corresponds to the light–Higgs funnel $m_{LSP} \quad M_2{=}2 \quad m_h{=}2$, where the s-channel Higgs exchange enhances the LSP annihilation rate. And finally, m_h needs to be well above the LEP limit, which we achieve by choosing $\tan = 30$. We arrive at a parameter point with $m_h = 129$ GeV, $m_{\tilde{g}} = 438$ GeV, chargino masses of 117 and 313 GeV, and neutralino masses of 60, 117, 296, and 310 GeV, using a modified version of SuSpect which decouples the heavy scalars from the MSSM RGEs [30, 37]. The neutralinos/charginos $\tilde{\chi}^0_2$ and $\tilde{\chi}_1$ as well as $\tilde{\chi}^0_4$ and $\tilde{\chi}_2$ are degenerate in mass. All neutralinos/charginos and most notably the gluino are much lighter than in the SPS1a parameter point, which greatly increases all LHC production cross sections. It is important to note that this feature is specific to our choice of parameters and not generic in heavy–scalar models.

Table 1 shows the main (NLO) cross sections at the LHC [38, 39]. The SUSY production is dominated by gluino pairs whose rate is eight times that of the SPS1a point: the lower gluino mass enlarges the available phase space, while in addition the destructive interference between s and t–channel diagrams is absent. The second largest process is the $\tilde{\chi}_1\,\tilde{\chi}^0_2$ production, which gives rise to a 145 fb of

[1] R. Lafaye, T. Plehn, M. Rauch, E. Turlay, and D. Zerwas

$\tilde{g}\tilde{g}$	63 pb	$\tilde{} \; \tilde{g}$	0.311 pb
$\tilde{} \; \tilde{}^0$	12 pb	$\tilde{}^0 \tilde{g}$	0.223 pb
$\tilde{} \; \tilde{}$	6 pb	$\tilde{}^0 \tilde{}^0$	0.098 pb
Total			82 pb

Table 1: NLO cross sections for SUSY pair production at the LHC. Branching ratios are not included.

observables		systematic error		statistical error	theory error
m_h	128.8 GeV	0.1%	energy scale	0.1%	4%
$m_{\tilde{\chi}_2^0} - m_{\tilde{\chi}_1^0}$	57 GeV	0.1%	energy scale	0.3%	1%
(3ℓ)	145.2 fb	5%	luminosity	3%	20%
$g \to b\bar{b}$ or $t\bar{t}$	0.11	5%	b tagging	0.3%	20%
(gg)	68.2 pb	5%	luminosity	0.1%	20%

Table 2: Summary of all observables and their errors. We assume an integrated luminosity of $100\ \text{fb}^{-1}$.

hard-jet free, e and μ trilepton signal, more than a hundred times that of the SPS1a parameter choice.

3.3 Observables

The first obvious observable is the light Higgs mass m_h. Although slightly higher than in most MSSM points, m_h can still be measured in the Higgs decay to two photons [40]. The systematic error on this measurement is mainly due to the uncertainty of the electromagnetic energy scale.

A measurement of the gluino pair production cross section appears feasible and can be very helpful to determine M_3 [41]. Most gluinos (85%) will decay through a virtual squark into a chargino or a neutralino along with two jets. The chargino will in turn decay mostly into the LSP plus two leptons or jets. Such events would then feature at least 4 hard jets, a large amount of missing energy and possibly leptons. The main backgrounds are $t\bar{t}$ pairs (590 pb) and W + jets (4640 pb) as well as Z + jets (220 pb). Despite these large cross sections, we have checked using a fast LHC-like simulation that most of the background can be eliminated by requiring a minimal number of hard jets or by applying standard cuts on the missing energy or the effective mass $M_{\text{eff}} = \not{E}_T + \sum_j p_{Tj}$. The main source of systematic errors on the cross section is the 5% error on the luminosity. The theory error on the cross section we estimate to 20%.

The next relevant observable is the trilepton signal. After gluino pairs, the second–largest rate comes from the direct production of $\tilde{\chi}_1^\pm \tilde{\chi}_2^0$, with 22% of $\tilde{\chi}_1^\pm$ s decaying through a virtual W into an electron or muon, a neutrino and the LSP. Similarly, 7% of $\tilde{\chi}_2^0$s decay through a virtual Z into an opposite–sign–same–flavor lepton pair (OSSF) and the LSP. The resulting signal features three leptons (two of them with OSSF), missing energy from the LSPs and the neutrino, and no jet from the hard process. The backgrounds are mainly $W\,Z$ (386 fb) and $Z\,Z$ (73 fb), the latter with one missed lepton. Taking into account all branching ratios [42], the trilepton signal has a rate of 145 fb. Without any cuts, the identification efficiencies of 65% (e) and 80% (μ) leave us with 110 to 211 fb for the background and 40 to 74 fb for the signal, depending on the number of electrons and muons in the final state. A dedicated study with the appropriate tools would evidently provide a better understanding of signal and background. As in the previous case, the main source of systematic errors is the luminosity. We also take the theory error on the value of the trilepton cross section to be roughly 20%.

For the trilepton signal we can define a kinematic observable: 10% of $\tilde{\chi}_2^0$s decay into an OSSF lepton pair and the LSP. The distribution of the invariant mass of the leptons features a kinematic upper edge at $m_{\tilde{\chi}_2^0} - m_{\tilde{\chi}_1^0}$. Such an observable gives precious information on the neutralino sector and hence on M_1. Its systematic error is dominated by the lepton energy scale. The statistical error we estimate to be of the order of 1%, from a ROOT fit of the $M_{\ell\ell}$ distribution. Finally, we use the ratio of gluino decays including a b quark to those not including a b. We roughly assume a systematic error of 5% due to the b tagging and 20% on the theory prediction.

Table 2 summarizes the central values and errors for all observables we use. The third and fourth columns give the experimental systematic errors and their sources, the fifth column gives the statistical errors corresponding to a few years of the LHC's nominal luminosity ($100\ \text{fb}^{-1}$). The last column gives a conservative estimate of the theory uncertainties.

3.4 Parameter determination

To study the effects of the different error sources, we first look at a low–statistics scenario and ignore all theory uncertainties. Then, we choose the limit of high statistics to estimate the ultimate precision barrier imposed by experimental systematical errors. Finally, we look at the effect of theory errors by including them into the previous set. We expect the theory errors to dominate, based on the currently available higher–order calculations. We use the parameter extraction tool SFitter [31], which in parallel to Fittino [32] was developed for this kind of problem.

With no information on the squark and sfermion sector, except for non-observation, we are forced to fix M_S and A_t in our fits. Moreover, we set $M_2 = M_1$ at the unification scale M_{GUT}, lacking enough information from the neutralino/chargino sector. Using Minuit, we then fit the remaining parameters to the LHC observables. The ^{2} minimum we identify using Migrad, while Minos determines the approximately Gaussian errors. Note that in a more careful SFitter study we would use flat theory errors [43, 31], but given the huge difference in computing time we employ a Gaussian approximation in this preliminary study. Our distant starting point is $(M_1; M_3; \tan\ ;\ ) = (100; 200; 10; 320)$.

Table 3 shows the result of the different fits. It is interesting to note that $\tan$ is undetermined except in the case of infinite statistical and theory's accuracy. This is due to the fact that only one of the five Higgs masses is measured. We present a study on the determination of $\tan$ from $(g\ \ 2)$ elsewhere in this volume. The quality of the trilepton and gluino signals gives very good precision on the determination of M_1 and M_3, even with low statistics. Including theory errors indeed decreases the accuracy but still allows for a determination of the mass parameters: M_3 only depends on the large gluino rate and its decays, explaining its relative stability for smaller statistics. The weakly interacting M_1 and M_2 suffer a larger impact from the theory errors, because they depend on the trilepton rate and also on the $b$to non-$b$gluino–decay ratio, both of which bear a large theory error.

3.5 Outlook

The MSSM with heavy scalars is built to satisfy current experimental and theoretical constraints on physics beyond the Standard Model while keeping some of the features of the TeV–scale MSSM. At the LHC, light gauginos and Higgsinos will lead to sizeable production rates, allowing us to study these new states.

The main observable channels are gluino pairs and the tri-leptons, whose hard-jet free channel makes it a fairly clean channel with respect to Standard–Model and SUSY backgrounds. Additional observables such as the light Higgs mass, the $(m_{\tilde{\chi}_2^0}\ \ m_{\tilde{\chi}_1^0})$ kinematic edge and the b-to-non-b gluino–decay ratio give us access to most parameters at the level of a few percent with 100 fb ^{1} luminosity, based on experimental uncertainties. Theory errors increase the error bands on the model parameters to $O(15\%)$.

Obviously, the scalar sector including $\tan$ is only poorly constrained, if at all. New complementary observables could improve this limitation. Similarly, a look at other parameter points would be

parameter	nominal	fitted	low stat.		1 stat.		1 stat.+ theory	
M_2	132.4 GeV	132.8 GeV	6	5%	0.24	0.2%	21.2	16%
M_3	132.4 GeV	132.7 GeV	0.8	0.6%	0.16	0.1%	5.1	4%
	290 GeV	288 GeV	3.8	1.3%	1.1	0.4%	48	17%
$\tan$	30	28.3	60	undet.	1.24	4%	177	undet.
M_1	132.4 GeV	132.8 GeV	$= M_2$					
A_t	0		fixed					
M_S	10 TeV		fixed					

Table 3: Result of the fits. Errors on the determination of the parameter are given for the three error sets described in the text.

needed to remove the specific properties of the point studied and to provide a more complete view of the LHC discovery potential of a MSSM with decoupled scalars.

Acknowledgements

We would like to thank the organizers of the great Les Houches 2007 workshop *Physics at TeV-Scale Colliders*.

4. Finding the SUSY mass scale [1]

4.1 Introduction

In the past it has been suggested that a good starting point for the determination of the mass scale of new susy or other exotic particles is the "effective mass" distribution [44, 45]. There are a number of slightly different definitions of M_E and the phrase "mass scale" [46] but a typical definition of M_E would be

$$M_E = p_T^{miss} + \sum_i p_{T(i)}; \quad (1)$$

in which p_T^{miss} is the magnitude of the event's missing transverse momentum and where $p_{T(i)}$ is the magnitude of the transverse momentum of the i-th hardest jet or lepton in the event.

All definitions of M_E are motivated by the fact that new TeV-scale massive particles are likely to be produced near threshold, and so by attempting to sum up the visible energy in each event, one can hope to obtain an estimate of the energy required to form the two such particles. Broadly speaking, the peak in the M_E distribution is regarded as the mass-scale estimator.

Although the effective mass is a useful variable, and simple to compute, it has undesirable properties: The desired correlation between M_E and the mass scale relies on the assumption that the particles are produced near threshold. While it is true that the cross sections will usually *peak* at threshold, they can have significant tails extending to $\sqrt{\hat{s}}$ values considerably beyond the threshold value. It is very hard to make *precise* statements about the mass scale from M_E alone.

In this letter we introduce a variable, m_{TGen}, which is designed to make more precise measurements of the mass scale by using event kinematics, rather than simple energy sums or ad-hoc rules. The aim is to produce event-by-event lower bound on the mass of pair-produced heavy particles. The variable has been constructed so that it is our ignorance about the ancestry of the final state particles, and the loss of information from the invisible massive heavy particles.

A solution already exists for the simplest case of interest – in which the final state consists of only two visible particles (plus the invisibles). For this case there is no combinatorial problem, as one can assume that each visible particle belongs to one of the initial heavy particles (e.g. one jet comes from each squark parent). The variable defined for that case is known as m_{T2} and is described in [47, 48].

The generalisation to the case of arbitrary numbers of final state visible particles is the subject of this letter and is called m_{TGen}. m_{TGen} is defined to be the smallest value of m_{T2} obtained over all possible partitions of momenta in F into two subsets and – each subset representing the decay products of a particular "side" of the event. Note that m_{T2} is itself defined in terms of p_T and m (respectively the transverse momentum and mass of one side of the event), p_T and m (respectively the transverse momentum and mass of the other side of the event), and (the mass of each of the unobserved particles which are supposed to have been produced on each side of the event) as follows:

$$m_{T2} \quad (p_T; p_T; p_T^{miss}; m \quad ; m \quad ; \quad) \quad \min_{q_T^{(1)} + q_T^{(2)} = p_T^{miss}} \max \left[m_T^2 (p_T; q_T^{(1)}; m \quad ; \quad); m_T^2 (p_T; q_T^{(2)}; m \quad ; \quad) \right] : \quad (2)$$

where

$$m_T^2 (p_T; p_T; m \quad ; \quad) \quad m^2 + \quad ^2 + 2(E_T E_T \quad p_T \quad p_T) \quad (3)$$

in which

$$E_T = \sqrt{(p_T)^2 + m^2} \quad \text{and} \quad E_T = \sqrt{(p_T)^2 + \quad ^2} \quad (4)$$

and likewise for ! . With the above definition (in the case = $m_{\tilde{\chi}_1^0}$), m_{T2} generates and event-by-event lower bound on the mass of the particle whose decay products made up either of the two sides

[1] A.J. Barr, C. Gwenlan and C.G. Lester

of the event, under the assumption that the event was an event represents pair production followed by decay to the visible particles and an unseen massive particle on each side. When evaluated at other values of the above properties are retained approximately (see [47, 48, 49, 50, 51, 52]). There exist events which allow this lower bound to saturate, and so (in the absence of background) the upper endpoint of the m_{T2} distribution may be used to determine the mass of the particle being pair produced.

4.2 Example distributions

In this letter we show the results for simulations of an example particle spectrum for proton-proton collisions at LHC centre-of-mass energy of $\sqrt{s} = 14$ TeV. The HERWIG [53, 54, 55] Monte Carlo generator was used to produce inclusive unweighted supersymmetric particle pair production events. Final state particles (other than the invisible neutrinos and neutralinos) were then clustered into jets by the longitudinally invariant k_T clustering algorithm for hadron-hadron collisions[56] used in the inclusive mode with $R = 1.0$ [57]. Those resultant jets which had both pseudo-rapidity ($= \ln \tan /2$) satisfying $|| < 2$ and transverse momentum greater than 10 GeV/c were used to calculate m_{TGen} and M_E .

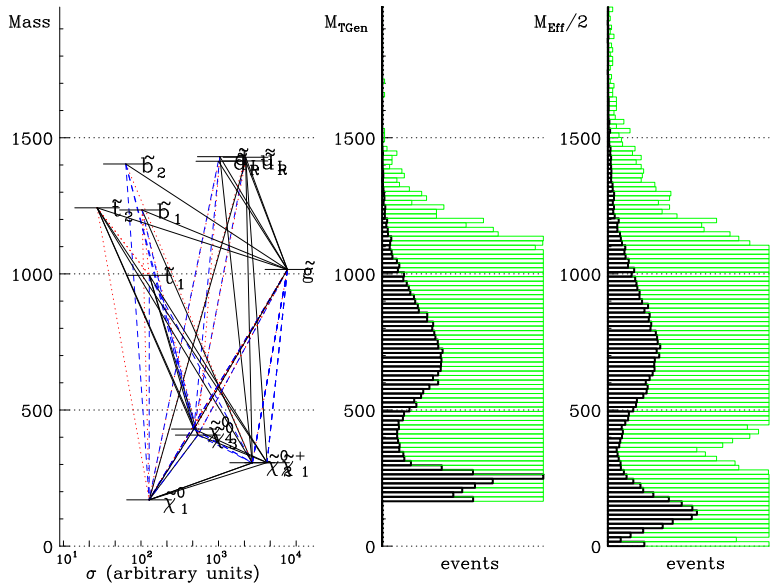

Fig. 1: On the left hand side is a graphical representation of the susy mass spectrum of the point described in the text. The vertical positions of the particles indicate their masses. The horizontal positions of the centres of the bars indicate the relative LHC production cross-section (arbitrary units). The lines joining particles indicate decays with branching fractions in the following ranges: greater than 10^{-1} solid; 10^{-2} ! 10^{-1} dashed; 10^{-3} ! 10^{-2} dotted. The middle plot shows the distribution of our variable, M_{TGen}, with M_{TGen} increasing vertically to ease comparison with the spectrum. The right hand plot shows the distribution of another variable, M_E =2, where M_E is defined in eq. 1. In both the M_{TGen} and the M_E plots, the lighter shading shows the histograms with the number of events multiplied by a factor of twenty, so that the detail in the upper tail may be seen.

In figure 1 we show the distributions of M_{TGen} and M_E for a sample point with a spectrum, defined by the mSUGRA parameters: $m_0 = 1200$ GeV, $m_{\frac{1}{2}} = 420$ GeV, $\tan = 10$, $m_t = 174$ GeV, < 0, The spectrum and branching ratios were calculated using Isajet[58] version 7.58. In these plots we assume it is possible to accurately assign all visible momenta to the correct category F or G, i.e. “interesting final state momenta” versus “initial state radiation”. Plots in which this is not assumed look similar and can be found in [59]. The HERWIG initial state radiation and underlying event have

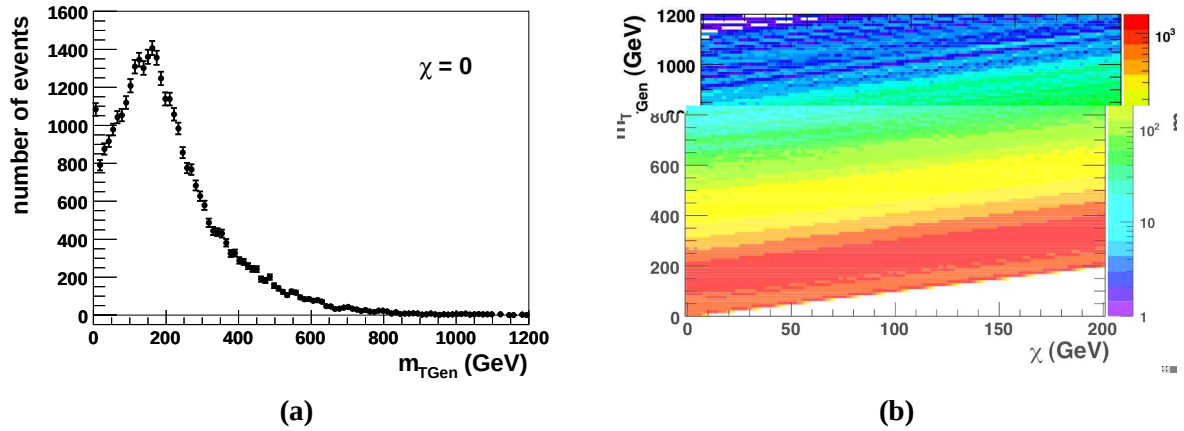

Fig. 2: M_{TGen} distributions for a Les Houches blind data sample as described in the text. **(a)** Invisible particle mass, $= 0$. **(b)** The colour scale shows the number of events with a particular value of M_{TGen} (y-axis) as a function of the input invisible particle mass, (x-axis).

been switched off, and the parameter which is required to calculate M_{TGen} has been set to the mass of the lightest supersymmetric particle.

It can be seen that, as intended, the upper edge of the distributions gives a very good indication of the mass of the heaviest pair-produced sparticle. Other supersymmetric points show similar behaviour [59]. This means that the position of the upper edge of m_{TGen} can be used to find out about the mass scale of any semi-invisibly decaying, heavy, pair-produced particles.

Furthermore, a change in slope can be observed at lower masses due to significant pair production of lower-mass particles (e.g. chargino and/or neutralino pairs). Therefore it is also possible in principle to extract from information about several different mass scales.

In figure 2 we plot the m_{TGen} distribution for events from the Les Houches 2007 blind data sample[2]. We select events which have at least one jet with $j\,j < 3{:}2$ and transverse momentum greater than 400 GeV, and also have missing transverse momentum greater than 70 GeV. We veto any event containing an electron, muon or photon with transverse momentum greater than 20 GeV.[3] There is no evidence for an end-point in the distribution, like the one seen in figure 1 or in the other examples in [59]. Neither is there evidence for any "kinks" in the m_{TGen} distribution when plotted as a function of the invisible particle mass, (figure 2b). Such end-points and kinks would be expected if the events contained many-body or cascade decays of strongly interacting objects to visible and invisible heavy particles [49, 50, 51, 52], and so disfavours a model of this type.

4.3 Conclusions

In conclusion, m_{TGen} could be a useful variable for determining mass scales at the LHC. If you are interested in using it, contact the authors for the code and let us know what you find.

Acknowledgements

The authors thank the scientific organisers of the Les Houches workshop for their hospitality and for liasing with the secretariat. CB and AB would like to thank the UK Science and Technology Facilities Council for their for the financial support of their fellowships. CGL would like to thank the Friends of Nature for extra pillows.

[2] Described in these proceedings

[3] Due to the lack of trigger information in the "blind sample".

5. A hybrid method for SUSY masses from fully identified cascade decays [1]

5.1 Introduction

This letter describes a new hybrid technique for improving the precision with which SUSY particle masses can be measured at the LHC. Existing techniques usually make use of the positions of end-points in experiment-wise distributions of invariant mass combinations of visible SUSY decay products [60, 61, 62], or use E_T^{miss} constraints from 'symmetric' events in which the same SUSY decay chain has participated in both 'legs' of the event [48]. In both cases some information regarding the events is discarded – in the former case event-wise E_T^{miss} information is not used in the experiment-wise end-point analysis, in the latter experiment-wise invariant mass end-point constraints are not used in the event-wise analysis. In this letter we describe a simple 'hybrid' technique which enables optimum use of both experiment-wise and event-wise information to fully reconstruct SUSY events and hence improve the mass measurement precision.

5.2 Description of technique

The new technique involves conducting a kinematic fit to each selected SUSY event, with the sparticle masses as free parameters. Crucially, the ^{2} function of the fit involves both event-wise E_T^{miss} constraints and experiment-wise invariant mass end-point constraints. It should be appreciated that without the E_T^{miss} constraints each event-wise fit is formally equivalent to solving the experiment-wise invariant mass end-point constraints for the individual sparticle masses, and consequently each fit will give the same value for each mass. The RMS values of the distributions of these masses will then be consistent with the mass precisions obtained from the conventional method involving solution of the end-point constraints. Addition of the event-wise E_T^{miss} constraints reduces the number of degrees-of-freedom of the kinematic fits and hence can improve the mass measurement precision. In this case the widths of the distributions of mass values obtained from different events for one Monte Carlo experiment are larger than those obtained when E_T^{miss} constraints are excluded, however the means of the distributions across many such experiments measure the masses more accurately.

5.3 Example: $\tilde{q}_L$ decays in SPS1a

At mSUGRA point SPS1a there is a significant branching ratio for the decay chain

$$\tilde{q}_L \to \tilde{\chi}_2^0 q \to \tilde{l}_R l q \to \tilde{\chi}_1^0 l l q: \qquad (1)$$

This chain provides 5 kinematic end-point mass constraints from invariant mass combinations of jets and leptons [63]:

$m(ll)^{max}$ = 77.08 0.08(scale) 0.05(stat) GeV
$m(llq)^{max}$ = 431.1 4.3(scale) 2.4(stat) GeV
$m(llq)^{min}$ = 203.0 2.0(scale) 2.8(stat) GeV
$m(lq)_{hi}^{max}$ = 380.3 3.8(scale) 1.8(stat) GeV
$m(lq)_{lo}^{max}$ = 302.1 3.0(scale) 1.5(stat) GeV

For this study unbiased samples equivalent to 100 fb ^{1} (one Monte Carlo 'experiment') of SPS1a signal events and $t\bar{t}$ background events were generated with HERWIG 6.4 [64, 54] and passed to a generic LHC detector simulation [65]. A lepton reconstruction efficiency of 90% was assumed.

Events were selected in which the above decay chain appears in both legs of the event with the following requirements:

N_{jet} 2, with $p_T(j2) >$ 100 GeV,

[1] M.M. Nojiri, G. Polesello and D.R. Tovey

$M_{eff2} = E_T^{miss} + p_T(j1) + p_T(j2) > 100$ GeV,

$E_T^{miss} > \max(100\text{ GeV}, 0.2M_{eff2})$,

$N_{lep} = 4$, where $lep = e, \mu$ (isolated) and $p_T(l4) > 6$ GeV,

2 Opposite Sign Same Flavour (OSSF) lepton pairs. If the pairs are of different flavour both pairs must have $m(ll) < m(ll)^{max}$. If both pairs are of the same flavour then one and only one of the two possible pairings must give two $m(ll)$ values which are both less than $m(ll)^{max}$. These pairings allocate the leptons to each leg of the event.

One and only one possible pairing of the two leading jets with the two OSSF lepton pairs must give two $m(llq)$ values less than $m(llq)^{max}$. These pairings allocate the jets to each leg of the event.

For each inferred leg of the event the maximum(minimum) of the two $m(lq)$ values must be less than $m(lq)^{max}_{hi(lo)}$. This ordering allocates the leptons to the `near` and `far` [61] positions in the decay chain.

The requirement of 4-leptons in two OSSF pairs and two high-p_T jets consistent with kinematic end-points, together with large E_T^{miss}, is effective at removing the majority of SM and SUSY backgrounds (see below).

Each selected event was fitted with MINUIT [66]. Free parameters were taken to be the four masses appearing in the decay chain: $m(\tilde{q}_L)$, $m(\tilde{\chi}_2^0)$, $m(\tilde{\tau}_R)$ and $m(\tilde{\chi}_1^0)$. The mass-shell conditions and measured momenta of the visible decay products for each leg were solved to determine the LSP four-momenta, giving two solutions for each leg. The χ^2 minimisation function was defined by:

$$\begin{aligned}
\chi^2 = & \left(\frac{m(ll)^{max}_{evt} - m(ll)^{max}_{expt}}{m(ll)^{max}}\right)^2 \\
& + \left(\frac{m(llq)^{max}_{evt} - m(llq)^{max}_{expt}}{m(llq)^{max}}\right)^2 + \left(\frac{m(llq)^{min}_{evt} - m(llq)^{min}_{expt}}{m(llq)^{min}}\right)^2 \\
& + \left(\frac{m(lq)^{max}_{hi,evt} - m(lq)^{max}_{hi,expt}}{m(lq)^{max}_{hi}}\right)^2 + \left(\frac{m(lq)^{max}_{lo,evt} - m(lq)^{max}_{lo,expt}}{m(lq)^{max}_{lo}}\right)^2 \\
& + \left(\frac{p_x(\tilde{\chi}_1^0(1)) + p_x(\tilde{\chi}_1^0(2)) - E_x^{miss}}{E_x^{miss}}\right)^2 + \left(\frac{p_y(\tilde{\chi}_1^0(1)) + p_y(\tilde{\chi}_1^0(2)) - E_y^{miss}}{E_y^{miss}}\right)^2 ; \qquad (2)
\end{aligned}$$

where `evt` denotes an expected end-point value derived from the masses in the event-wise fit with the formulae of Ref. [61], and `expt` denotes a 'measured' experiment-wise end-point value. The uncertainties in these 'measured' endpoints were those quoted above. The uncertainties on the measurements of the x and y components of E_T^{miss}, E_x^{miss} and E_y^{miss}, were given by $0.5\sqrt{E_T^{sum}}$ where E_T^{sum} is the scalar sum of jet p_T of the event. This function incorporating both event-wise E_T^{miss} constraints and experiment-wise end-point constraints was evaluated for each of the four pairs of $\tilde{\chi}_1^0$ momentum solutions obtained from solving the leg mass-shell conditions. Fitted masses were obtained when χ^2 was minimised for the event. Fitted masses were used in the subsequent analysis only if MINUIT judged the fit to have converged and $\chi^2_{min} < 35.0$.

Following application of the selection cuts described above and the requirements of fit convergence and low fit χ^2_{min} 38 SUSY 'signal' events with the above decay chain appearing in both legs were observed. 4 SUSY background events were observed, consisting of the above decay chain in both legs but with one or two leptonically decaying staus produced in the decays of the $\tilde{\chi}_2^0$'s. No $t\bar{t}$ background events were observed in 100 fb^{-1} equivalent data. More SM background events may be expected in a real experiment, given that effects such as charge and lepton mis-identification are not included in the fast detector simulation. Nevertheless the contribution is still expected to be negligible.

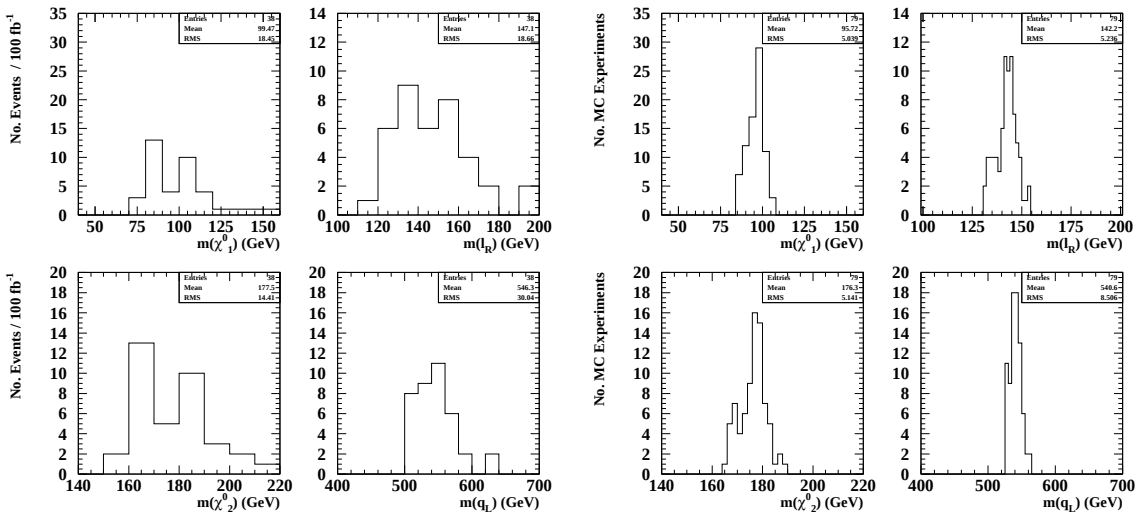

Fig. 1: Distributions of sparticle masses. The four distributions on the left are of masses obtained from event-wise fits, for one MC experiment. Each entry is obtained by minimising the ^{2} function shown in Eqn. 2. The four distributions on the right are likelihood distributions of sparticle masses obtained from 100 MC experiments. Each entry is the mean of an experiment-wise mass histogram such as those on the left.

Each event-wise fit generated one set of values for the sparticle masses, namely those values which minimise the broad ^{2} function in Eqn. 2. The distributions of these values for one Monte Carlo experiment are shown in Fig. 1(left). In order to demonstrate the performance of the technique and judge the uncertainties in the measurements the above procedure was repeated for 100 Monte Carlo experiments. For each experiment, kinematic end-point positions were sampled from gaussians with means and sigmas given by the means and uncertainties listed above. The five sampled end-point positions for each experiment were solved simultaneously with a MINUIT fit to give initial mass values for input to the MINUIT event-wise kinematic fits. For each experiment relative jet(lepton) energy scale values were sampled from gaussians of width 1%(0.1%) reflecting likely ultimate energy scale uncertainties at the LHC. Each experiment generated a set of sparticle mass histograms similar to those shown in Fig. 1(left). The means of these histograms for the 100 MC experiments were then used to construct likelihood histograms for the masses, shown in Fig. 1(right). The standard deviations of these histograms were taken to provide the uncertainties on the sparticle mass measurements.

Unbiased MC data equivalent to only one 100 fb ^{1} experiment were available for this study. For this reason the same events were used for each MC experiment, with just the end-point values and jet/lepton energy scales varying. The additional uncertainties in the final mass values expected from varying event samples were estimated from the mean statistical uncertainties in the mean experiment mass values as extracted from the event-wise distributions such as those shown in Fig. 1(left). We evaluated the experiment-by-experiment spread due to varying event samples as $= \frac{p}{n}$, where $$ is the RMS of the event-wise distributions as shown in Fig. 1(left), and n is the number of entries in each plot. These additional contributions were added in quadrature to the uncertainties obtained from the study. This approximation was checked with a second sample of SPS1a events equivalent to 100 different MC experiments, biased to force gluinos to decay to q_L, b or t, q_L to decay to $\tilde{}^0_2$ and $\tilde{}^0_2$ to decay to e or $\tilde{}$.

The results of this study are summarised in Table 1. For comparison purposes the analysis was initially carried out with the E_T^{miss} constraints removed from the ^{2} function. The measurement precisions are consistent with those obtained from the conventional end-point fitting method, as expected following

State	Input	End-Point Fit		Hybrid Method, E_T^{miss}		Hybrid Method, no E_T^{miss}	
		Mean	Error	Mean	Error	Mean	Error
$\tilde{\chi}_1^0$	96.05	96.5	8.0	95.8(92.2)	5.3(5.5)	97.7(96.9)	7.6(8.0)
$\tilde{l}_R$	142.97	143.3	7.9	142.2(138.7)	5.4(5.6)	144.5(143.8)	7.8(8.1)
$\tilde{\chi}_2^0$	176.81	177.2	7.7	176.4(172.8)	5.3(5.4)	178.4(177.6)	7.6(7.9)
$\tilde{q}_L$	537.2–543.0	540.4	12.6	540.7(534.8)	8.5(8.7)	542.9(541.4)	12.2(12.7)

Table 1: Summary of mass measurement precisions for SPS1a states. Column 2 lists masses used in the HERWIG generator, Columns 3 and 4 the fitted masses and uncertainties obtained from the conventional fit to kinematic end-points, Columns 5 and 6 the equivalent values obtained with the new technique and Columns 7 and 8 the equivalent values obtained with the new technique excluding E_T^{miss} constraints. Figures in parentheses are those obtained with the biased sample of non-repeated events. All masses are in GeV. The quoted mass range for $\tilde{q}_L$ excludes $\tilde{b}$squarks, which are produced less readily than the light squarks.

the reasoning outlined above. The analysis was then repeated including the E_T^{miss} constraints, giving an overall improvement in sparticle mass precisions 30% for all four masses considered. A similar improvement was found when using the biased sample of non-repeated events for different experiments.

Acknowledgements

The authors wish to thank the organisers of the Les Houches 2007 *Physics at TeV-Scale Colliders* workshop for what was once again an excellent and stimulating working environment. DRT wishes to acknowledge STFC for support.

6. A blind SUSY search at the LHC [1]

6.1 Introduction

Most of the SUSY prospects [67][68] at the LHC are based on simulations and analyses where the analyzer knows all the properties of the signal as well as those of the SUSY and Higgs backgrounds to this signal.

In constrast with these situations, we describe in this letter a new SUSY data challenge at the LHC which is called the "Blind SUSY Search Project" [69]. As name of this project suggests, here, the analyzer ignores the properties of the searched SUSY signal.

We have produced a 100 pb^{-1} pseudo-data (PsD_1) sample which consists in a randomized mixture of the Standard Model (SM) backgrounds and the inclusive Higgs and SUSY production of an unrevealed SUSY model. We also provide separate and independent samples of the SM backgrounds.

The aim of the challenge is to determine the type of underlying SUSY breaking mechanism as well as the corresponding parameters of the hidden SUSY model.

All of the samples are under a simple ROOT [70] format so as to propose this challenge not only to the experimental HEP community but also to the theorists.

The motivations for this challenge lie in the following questions. Let's hypothesize the presence of a SUSY signal at the LHC, can one:

determine the excess with respect to the SM expectations and quantify it?

handle the possible presence of several SUSY and Higgs signals and how does that affect the measurement of experimental observables (masses, mass differences, cross sections, ratios of branching fractions, spins,...)?

determine the type of underlying SUSY breaking mechanism at play (gravity or gauge or anomaly mediated)

distinguish different types of phenomenological hypotheses (R-parity conservation, phases, high scale unifications,...)?

evaluate the values of the parameters of the underlying SUSY model?

Part of such questions has been posed and partially answered in previous SUSY challenges. But most of them provided either an exclusive signal (ie: without all the decay channels open), or were missing the Higgs and SUSY background, or part of the SM backgrounds,... In the current challenge we tried to provide all of these pieces.

In section 2, we'll describe in some details how the samples were produced. In sections 3 and 4 respectively we'll explain how to access and how to analyze the data.

6.2 Samples production

Production tools

All the processes were generated using Pythia version 6.325 (v6.325) [71]. The SUSY mass spectrum and decay table in the v1.0 "SUSY Les Houches Accord" (SLHA)[72] format was read in by Pythia. The CTEQ6L1 [73] proton parton density functions (PDF) were utilized for all the processes through an interface to the LHAPDF [74] v5.2.3 package.

For the SM backgrounds and the Higgs processes the were decayed by Tauola [75] v2.6. However, because of missing pieces in the Tauola interface, the from SUSY processes were decayed by Pythia unabling to account for the spin correlations in these cases.

The ATLAS detector response was simulated using a personal fast simulation based on ATLFAST [76] v00-02-22. All the reconstructed quantities are simulated using smearing functions and the correspond-

[1] G.S. Muanza

ing variables are also used to mimic the trigger conditions[2] as described in the ATLAS High Level Trigger TDR [77]. Note that the events failing the trigger conditions were removed from the PsD$_1$ set, but not from the background samples. Obviously the Monte Carlo (MC) truth informations were removed from the PsD$_1$ set as well.

The output of the fast simulation is a PAW [78] ntuple which is subsequently converted into a root-tuple using ROOT v5.14.

For the samples normalization an integrated luminosity of 100 pb^{-1} was assumed and the Pythia leading order (LO) cross sections were used for the sake of simplicity. Nevertheless some background (sub)-processes with very high cross sections had to be arbitrarily taken out of the PsD$_1$ sample in order to keep the number of events to be produced within reasonable limits. Table 1 contains the full list of these pruned sub-processes:

Process	Pythia Process Index	Kinematical Cut
$qq \to qq$ (q = u=d=s=g)	MSEL = 1	$\hat{p}_T < 160$ GeV
$c\bar{c}$	MSEL = 4	$\hat{p}_T < 40$ GeV
$b\bar{b}$	MSEL = 5	$\hat{p}_T < 40$ GeV
+ jets	MSUB(14;29;115) = 1	$\hat{p}_T < 20$ GeV
Low mass resonances (; ; ;::;)	- -	- -
Elastic Scattering	-	-
Diffraction	-	-

Table 1: The list of high cross section processes that were removed from the PsD$_1$ sample.

The PsD$_1$ sample is stored in 7 root-tuples and contains in total 4.5M events for a total size of 12 Gb.

Each background root-tuples contains exactly 100k events. In total there are 1593 such root-tuples for a total statistics of 159.3M events that amount to 424 Gb.

All the other details about the events generation can be found on the project website: [69].

6.3 Access to data

The full dataset was too large to be kept on disk. Therefore it is stored on tape at the Lyon Computing Center, except for the PsD$_1$ sample which can also be downloaded from the project website.

For those who have an account at this Computing Facility, the samples are available on HPSS[79] in the cchpssd0=hpss=in2p3:fr=home=muanza=GDR_SUSY=SUSY_Blind= directory. And the following sub-directories: Pseudo_DATA=final=0=100_inv_pb=, BKGD=<bkgd_process> and ANALYSIS=SKIMMING=MET150= respectively contain the PsD$_1$, the SM background and the skimmed ($\not{E}_T > 150$ GeV) samples.

For those who don't have an account at the Lyon Computing Center, there's a possible data access using SRB[80]. The participant has to be registered as an SRB user. This can be done by sending me an email at muanza@in2p3:fr. Then the participant needs to install an SRB client on his (her) computer to be able to list and copy the root-tuples. The main SRB directory is

=home=muanza:ccin2p3=GDR_SUSY=SUSY_Blind= and all the sub-directories structure is that of HPSS.

All the useful details about SRB are explained on the projcet website.

[2]The participants are asked to present results only with events passing at least one of these conditions.

6.4 Data analysis

Template analysis program

A template analysis tarball is provided on the project website

(http://www.clued0.fnal.gov/%7Emuanza/Blind_SUSY/Analysis/Run_Analysis.tar.gz). It can either be used as is or be hacked by the participants. In any case, the most useful information for those who'd like to write their own analysis code are the cross sections of all the SM backgrounds. They can be found in the "proc_xsect" array at the top of the Analysis.C file.

Some illustrations of the PsD_1 *sample*

Here are some plots advertising the project. They were produced after rejecting the events not passing any trigger requirements[3].

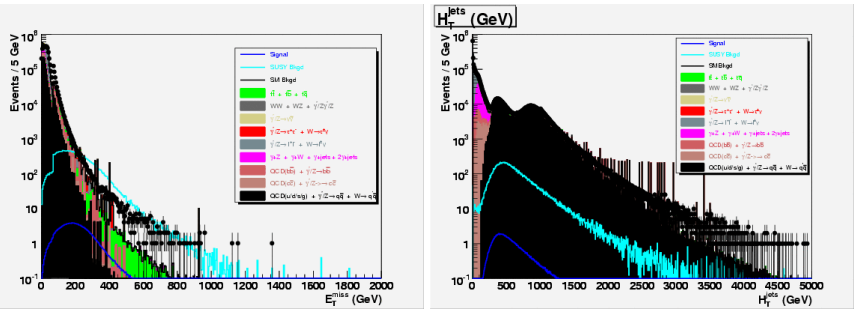

Fig. 1: The distributions of the missing (left) and scalar (right) $\mathrm{E_T}$ after rejecting the events failing the trigger requirements. A SUSY signal (dark blue) studied in [81] and its SUSY background (light blue) are superimposed only for illustrative purposes.

These plots exhibit an excess of pseudo-data events in the high missing and scalar $\mathrm{E_T}$ tails...

Signal templates production

A tarball of the production package is available on the project website

(http://www.clued0.fnal.gov/%7Emuanza/Blind_SUSY/Production/running_susyblind.tar.gz). The analyzers have to produce their SLHA input cards for their preferred SUSY models and to produce signal templates using the production tarball. This way they can test ideas about possible signals that could explain the difference between the PsD_1 sample and the SM background.

6.5 Conclusions and prospects

We have proposed a special SUSY data challenge at the LHC that includes the full Higgs and SUSY inclusive production for an unrevealed SUSY model on top of the SM backgrounds.

The aim of this challenge is to subject to a blind analysis possible strategies to disentangle a given Higgs or SUSY signal in the presence of simultaneous contributions from different other Higgs and SUSY processes. And to see how well these strategies enable to determine the properties of the SUSY model under study.

We look forward for participants to this challenge to present their analysis of this first pseudo-data sample. We are eager to see what experimental observables they'll have measured, what will be their uncertainties estimates. We are expecting their initial best guess for the values of the hidden SUSY model parameters. And we also suggest they provide the SUSY fitter groups [82][83] with their observables and uncertainties so as to find out what global fits could teach us about in this blind analysis context.

[3] A code for simulating the trigger conditions can be found in the ana:HLT() function of the ana.C file in the analysis tarball

Acknowledgements

We would like to thank the IPN Lyon and the IN2P3 for their financial support.

7. Off-shell effects for decay processes in the MSSM [1]

7.1 Introduction

Theoretical arguments and experimental observations indicate that new particles or interactions play an important role at the TeV scale, which will become directly accessible at the Large Hadron Collider (LHC) and its planned complement, the International Linear Collider. In the near future we can therefore anticipate ground-breaking discoveries that reveal physics beyond the Standard Model (BSM) and allow to gain insight into the structure of the fundamental theory. Theoretically appealing extensions of the Standard Model often feature numerous additional interacting heavy particles. The phenomenology of supersymmetric (SUSY) theories, for example, is characterized by sparticle production and cascade decays, which lead to many-particle final states and scattering amplitudes with complex resonance structure. In order to extract the additional Lagrangian parameters of an extended theory from collider data, theoretical predictions are required that match the experimental accuracies. In theoretical calculations production and decay stages can be factorized by means of the narrow-width approximation (NWA), which effectively results in on-shell intermediate states. Its main advantage is that sub- and nonresonant as well as nonfactorizable amplitude contributions can be neglected in a theoretically consistent way, resulting in significant calculational simplifications at tree and loop level. For these reasons, the NWA is employed in nearly all studies of BSM physics. We note that it is implicitly applied whenever branching ratios are extracted from scattering cross sections. A reliable NWA uncertainty determination is therefore crucial. Given the width Γ and mass M of an unstable particle, the uncertainty of the NWA is commonly estimated as $\mathcal{O}(\Gamma/M)$. With $\Gamma/M \lesssim 2\%$, its uncertainty is expected to be small in comparison to, for instance, QCD corrections.

Recently, two circumstances have been observed in which the NWA is not reliable: the first involves decays where a daughter mass approaches the parent mass [84], the second involves the convolution of parton distribution functions with a resonant hard scattering process [85]. We are thus motivated to investigate when and why the NWA is not appropriate in the context of cascade decays in the Minimal Supersymmetric Standard Model (MSSM). We first consider a typical example, namely $\tilde{g}\tilde{e}_L$ production at the LHC, i.e. in proton-proton collisions at 14 TeV, with the subsequent cascade decay $\tilde{g} \to \tilde{e}_L s$ and $\tilde{e}_L \to e_1 c$ at the SPS1a' benchmark point [86, 21] in the MSSM parameter space. Phenomenologically, to consider a squark decay into the LSP candidate $\tilde{e}_1^0$ would be more natural, but the resulting complete Feynman amplitude features a complicated resonance structure whose study we leave to future work. Even for the gluino decay chain considered here, interference arises from $\tilde{g} \to (\tilde{e}_L \to e_1 s)c$. However, it does not exceed the expected NWA uncertainty and can therefore be neglected. We focus on off-shell effects for the resonant $\tilde{e}_L$ state (with $M = 570$ GeV and $\Gamma = 5.4$ GeV at SPS1a') and hence treat the chargino as stable and the gluino in NWA with spin correlations. As shown in Fig. 1, the NWA error substantially exceeds the expectation of $\Gamma(\tilde{e}_L)/M(\tilde{e}_L) < 1\%$ when the strange squark mass approaches either the chargino or gluino mass of 184 and 607 GeV, respectively.[2] Note that the region where the NWA is inappropriate is not restricted to mass configurations where the Breit-Wigner shape is cut off kinematically, i.e. where $M(\tilde{e}_L) \gtrsim M(e_1) + \Gamma(\tilde{e}_L)$ or $M(\tilde{g}) \gtrsim M(\tilde{e}_L) + \Gamma(\tilde{e}_L)$.

7.2 Resonant $1 \to 3$ decays in the MSSM

The example in Sec. 7.1 suggests resonant $1 \to 3$ decays as smallest unit that features the amplified off-shell effects. Giving type (4-momentum, mass) for each particle, we define a resonant $1 \to 3$ decay by

$$T_I(P_I, M_I) \to T_1(p_1, m_1); T(q, M) \text{ and } T(q, M) \to T_2(p_2, m_2); T_3(p_3, m_3): \tag{1}$$

The width of the intermediate particle with momentum q is . Type can be scalar (S), fermion (F) or vector boson (V). In the MSSM, 48 generic processes exist and are identified with type codes $T_I T_1 T\text{-}T T_2 T_3$. For each process we have systematically scanned the MSSM parameter space for the maximum deviation $|R|$ of off-shell ($_{\text{off-shell}}$) and NWA ($_{\text{NWA}}$) decay rate predictions, where $R = (_{\text{off-shell}}/_{\text{NWA}} - 1)/(\Gamma/M)$. Note that in R, coupling constants typically cancel with the exception of the relative strength of the chiral components of SFF and VFF vertices, which has been varied in addition to the masses and width. From this survey [88] we conclude that large deviations $|R|$ do not occur for configurations with a resonance mass that is very far from kinematical bounds. The NWA exploits that in the limit $\Gamma \to 0$ the squared propagator $D(q^2) \equiv [(q^2 - M^2)^2 + (M\Gamma)^2]^{-1}$ is asymptotically equal to $2K_{\text{NWA}}(q^2 - M^2)$ with $K_{\text{NWA}} = 1/(2M\Gamma) = \int_{-\infty}^{\infty} D(q^2)\,dq^2/(2\pi)$. The Breit-Wigner shape is thus effectively integrated out. The origin of unexpectedly large deviations for configurations where kinematical bounds are outside the resonance region is that the q^2-dependence of the residual integrand significantly distorts the peak

[1] N. Kauer and C.F. Uhlemann

[2] The tools of Ref. [87] were used in our calculations.

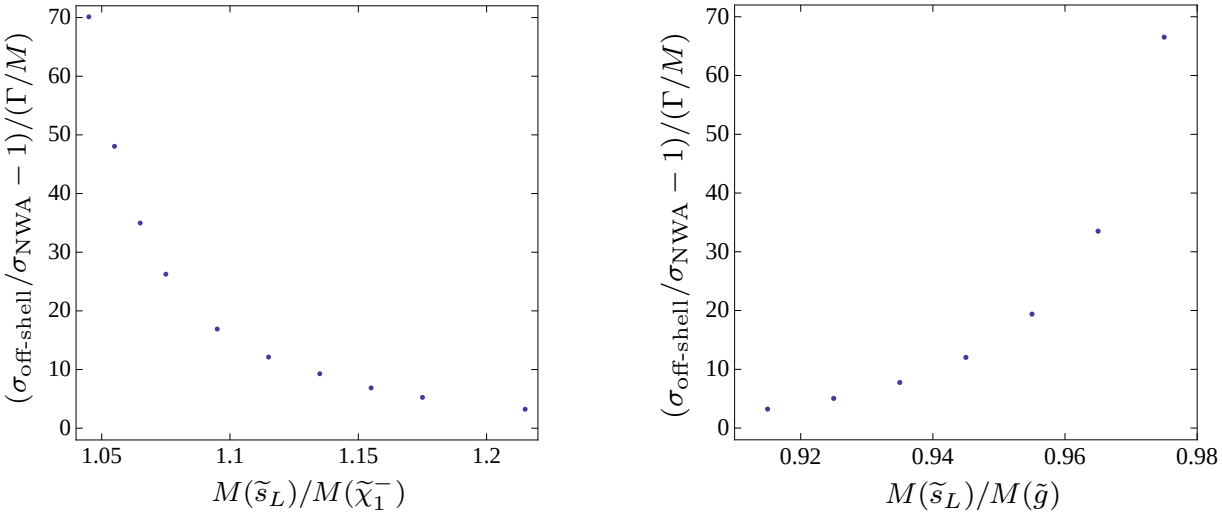

Fig. 1: The accuracy of the NWA cross section normalized to the conventionally expected uncertainty is shown for $\tilde{g}\tilde{u}_L$ production at the LHC followed by the cascade decay $\tilde{g} \to \tilde{s}_L s$ and $\tilde{s}_L \to \tilde{\chi}_1^- c$ in the MSSM at SPS1a' for a variable strange squark mass that approaches the chargino mass (left) and the gluino mass (right).

and tail of $D(q_I^2)$. We find that the effect is most pronounced for the decay process SSS-SSV. We thus use it to demonstrate the distortion. With $m_1 = m_2 = 0$, the q_I^2-integrand is given by

$$1 - \frac{q_I^2}{M_I^2} \quad 1 - \frac{m_3^2}{q_I^2} \quad \frac{(q_I^2 - m_3^2)^2}{m_3^2} \quad \frac{1}{(q_I^2 - M^2)^2 + M^2\Gamma^2} : \tag{2}$$

The 1st- and 2nd-stage decay PS elements contribute the first and second factor, respectively. The 2nd-stage decay matrix element gives the third factor. When $m_3^2 \gg M^2$ the second and third factor effect a strong deformation of $D(q_I^2)$, which, together with the resulting large deviations, is displayed in Fig. 2. The deviation grows with increasing power of the deforming factors. When M approaches the lower kinematic bound, $\mathcal{R}$ is sensitive to the type of the 2nd-stage decay, which determines the power of the factor that deforms the Breit-Wigner peak. While this factor enhances the Breit-Wigner tail, the factor of the 1st-stage decay suppresses it. And vice versa for the upper bound. We find stronger effects for SSV, VSV, FFV, VVV and SVV than for FSF, SFF, VFF, VSS and SSS vertices. Using our generic results we probe resonant $1 \to 3$ decays at SPS benchmark points [21]. Decays with larger deviations are shown in Table 1.

Affected decays generally have a small branching ratio due to similar-mass configurations. For example, BR = 1.3% for the decay mode $\tilde{\chi}_1^+ \to \tilde{\chi}_1^0 ud$ at SPS1a. It proceeds via the intermediate states W^+ (resonant), $\tilde{u}_L$ and $\tilde{d}_L$ (nonresonant). The resonant W^+ contribution with $\mathcal{R} = \Gamma/M = 13\%$ (see Table 1) induced by the mass ratio $(m_1 + M)/M_I = 0.975$ dominates, and the off-shell prediction including the nonresonant contributions deviates by about 11% from the NWA prediction. Since the 1st-decay stage is not affected by QCD corrections, this error is particularly significant. For a detailed discussion of effects at SPS points including cascade decay segments we refer to Ref. [88].

7.3 Conclusions

When the NWA is applied to decay chains the approximation error will exceed order Γ/M for mass configurations in an extended vicinity of segment kinematical bounds due to a significant distortion of the Breit-Wigner peak and tail, which is effected by the q^2-dependence of the phase space elements and residual matrix elements. In phenomenological studies of affected models, fully off-shell tree-level Monte Carlos [87] should thus be used even though it requires more computing resources. For decay processes involving strongly interacting particles QCD corrections are known to be large [89, 90, 91] and need to be taken into account. For this purpose, a suggestive NWA improvement is proposed in Ref. [92]. We have chosen the MSSM to illustrate how large off-shell effects can occur in extended models, but emphasize that the effects do not depend on SUSY.

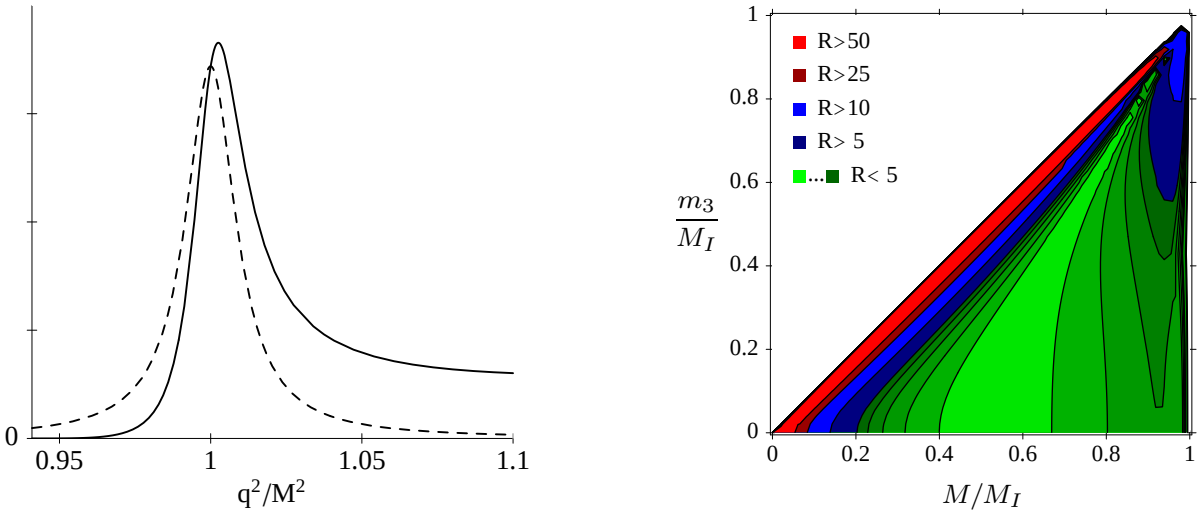

Fig. 2: Resonant $1 \to 3$ decay SSS-SSV (see main text) with $\Gamma/M = 0.01$: The graph displays the q^2-dependence of the Breit-Wigner (dashed) that is integrated out in the NWA and of the complete integrand of Eq. 2 (solid) for $m_3 = M_3$. The contour plot shows R, the resulting off-shell-NWA deviation in units of Γ/M, as function of m_3 and M with $m_1 = m_2 = 0$.

decay process	SPS	R	Γ/M [%]
$\tilde{g} \to d\tilde{d}_L \to dd\tilde{\chi}_1^0$	1a	9.54	0.935
$\tilde{g} \to d\tilde{d}_L \to dd\tilde{\chi}_1^0$	5	11.4	0.956
$\tilde{g} \to u\tilde{u}_L \to uu\tilde{\chi}_1^0$	1a	5.98	0.976
$\tilde{g} \to u\tilde{u}_L \to uu\tilde{\chi}_1^0$	5	9.46	0.975
$\tilde{\chi}_1^+ \to \tilde{\chi}_1^0 W^+ \to \tilde{\chi}_1^0 ud$	1a	5.21	2.49
$\tilde{\chi}_1^+ \to \tilde{\chi}_1^0 W^+ \to \tilde{\chi}_1^0 e^+ \nu_e$	1a	5.21	2.49
$\tilde{g} \to b\tilde{b}_2 \to bb\tilde{\chi}_1^0$	4	6.43	1.11
$\tilde{g} \to u\tilde{u}_L \to ud\tilde{\chi}_1^+$	9	114	1.19
$\tilde{g} \to d\tilde{d}_L \to du\tilde{\chi}_1^+$	9	209	1.19

Table 1: R, the off-shell-NWA deviation in units of Γ/M, for resonant $1 \to 3$ decays at SPS benchmark points.

Acknowledgements

N. Kauer would like to thank the Ecole de Physique des Houches and the Galileo Galilei Institute for Theoretical Physics for the hospitality and the INFN for partial support during the completion of this work. This work was supported by the BMBF, Germany (contract 05HT1WWA2).

8. Supersymmetric corrections to M_W and $\sin^2\theta^{lept}_{eff}$ in mSUGRA [1]

8.1 Introduction

Specific patterns of supersymmetry (SUSY) breaking provide relationships between various sparticle masses. In mSUGRA for instance, the GUT-scale scalar masses are set to m_0, the gaugino masses $M_{1/2}$ and the universal scalar SUSY breaking trilinear coupling A_0. These degeneracies are broken by renormalisation group effects between the GUT scale and M_Z. It is by now well known that various regions of mSUGRA parameter space are ruled out by direct sparticle search constraints, which place lower bounds upon the sparticle masses.

Sparticles may appear in loop corrections to electroweak observables, therefore affecting the values of the latter as predicted within the Standard Model once a set of independent physical input parameter is chosen, such as the electromagnetic couplings, G_F from decay, M_Z and other SM particle masses. Two such precision observables are the W boson mass, M_W, as measured at LEPII and the Tevatron and the effective leptonic mixing angle, $\sin^2\theta^{lept}_{eff}$, derived from the lepton asymmetries measured at LEPI and SLD. The former is related to the electric charge $e = \sqrt{4\pi\alpha}$, the weak mixing angle $s_w^2 = 1 - M_W^2/M_Z^2$, G_F, and M_Z via

$$\frac{G_F}{\sqrt{2}} = \frac{e^2}{8 s_w^2 M_W^2}(1 + \Delta r); \tag{1}$$

where the parameter Δr is a model dependent quantity which accounts for all higher order corrections to the muon decay (this includes self energies, vertex and box corrections in a given model, see ref. [93] for a recent discussion in the context of the MSSM). The M_W value which solves the above relation constitutes the model specific prediction of M_W for a given fixed set of Standard Model and new physics parameters. Similarly, one can express the effective leptonic mixing angle as

$$\sin^2\theta^{lept}_{eff} = s_w^2(1 + \Delta\kappa); \tag{2}$$

where the model dependent higher order corrections to the leptonic Z boson decay, $Z \to l\bar{l}$, enter via $\Delta\kappa$ (details concerning $\sin^2\theta^{lept}_{eff}$ in the general MSSM can be found in ref. [94]). The prefactor $s_w^2 = 1 - M_W^2/M_Z^2$, and thus also $\sin^2\theta^{lept}_{eff}$, is furthermore sensitive to radiative corrections via M_W. It is convenient to split the MSSM higher order corrections into Standard Model and SUSY type contributions [93, 94]

$$\Delta r = \Delta r^{SM}|_{M_H^{SM} = M_h} + \Delta r^{SUSY}; \qquad \Delta\kappa = \Delta\kappa^{SM}|_{M_H^{SM} = M_h} + \Delta\kappa^{SUSY}; \tag{3}$$

with the Standard Model Higgs boson mass M_H^{SM} set to the lightest MSSM Higgs mass M_h. Direct search constraints put lower bounds upon sparticle masses, limiting the size of the SUSY contributions, which are propagator suppressed by large sparticle masses.

Empirical constraints on M_W and $\sin^2\theta^{lept}_{eff}$ are very tight: they are taken here to be [95, 96]

$$M_W = 80.398 \pm 0.027\,\text{GeV}; \qquad \sin^2\theta^{lept}_{eff} = 0.23153 \pm 0.000175. \tag{4}$$

One may ask how large the SUSY contributions to the electroweak observables are, given the current strong constraints upon sparticle masses from LEP2 and the Tevatron. If the SUSY contributions are much smaller than experimental errors upon the relevant observables, then there is no need to include them in any fit. Here, we use results from a previous fit of mSUGRA to dark matter and other indirect data (including the direct search constraints) in order to see how big the SUSY contribution to M_W and $\sin^2\theta^{lept}_{eff}$ may be.

8.2 The fits

In refs. [95], multi-dimensional fits to mSUGRA were presented using the `SOFTSUSY2.0.10` [97] spectrum calculator and the `micrOMEGAs1.3.6` [98] dark matter code. m_0, A_0, $\tan\beta$, $M_{1/2}$, m_t, m_b, $\alpha_s(M_Z)$ and were all scanned simultaneously using the Metropolis algorithm in a Markov Chain Monte Carlo technique. It was assumed that the WMAP-constrained relic density of dark matter $\Omega_{DM}h^2$ consisted entirely of the lightest neutralino, which is stable by the assumption of R-parity. The following data were included in the fit: the anomalous magnetic moment of the muon, $(g-2)_\mu$, $BR(b \to s\gamma)$, Tevatron $BR(B_s \to \mu^+\mu^-)$ constraints, $\Omega_{DM}h^2$, M_W, $\sin^2\theta^{lept}_{eff}$, LEP2 Higgs constraints as well as other constraints upon sparticle masses from direct searches. Data on m_t, m_b, $\alpha_s(M_Z)$ and were also included in the likelihood. We refer the reader to ref. [95] for the details. We

[1] B.C. Allanach, F. Boudjema and A.M. Weber

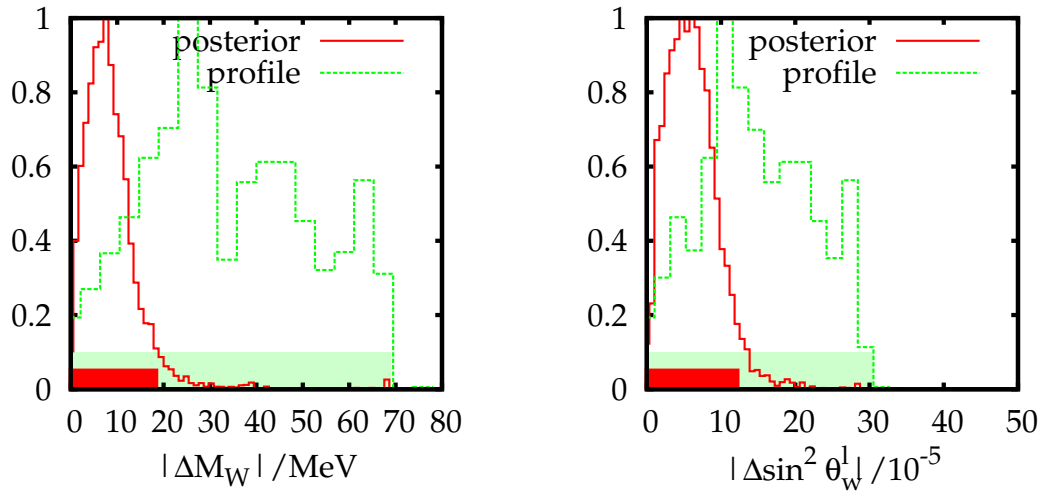

Fig. 1: Distributions to the SUSY contribution to the electroweak observables M_W and $\sin^2\theta_w^l$ from mSUGRA fits. The posterior probability distribution function (pdf) is shown in red (dark) whereas the profile likelihood is shown in green (light). Each histogram has an arbitrary normalisation. Horizontal bands display the one-sided 95% Bayesian credibility (condidence level) regions for the posterior pdf (profile likelihood).

note here that M_W and $\sin^2\theta_w^l$ were determined using am embryonic version of the SUSYPOPE [99] code, which is a state-of-the-art MSSM calculation [93, 94] of the electroweak observables[2]. SUSYPOPE is also capable of calculating the Standard Model value prediction for M_W given other Standard Model input parameters and the Higgs mass. A list of 500 000 weighted mSUGRA parameter space points, with weighted frequency proportional to their combined likelihoods, was the result of the fit. This set of points is referred to as KISMET (**K**iller **I**nference in **S**usy **M**eteorology). The points are presented for public use on URL

`http://users.hepforge.org/~allanach/benchmarks/kismet.html`

In ref. [95], the fits were presented in several ways: the ways relevant to our discussion here will be the frequentist fashion (utilising the *profile likelihood*) and a Bayesian fit with flat priors in the inputs listed above. While the profile likelihood takes into account only the best fit parameters, the Bayesian fit includes volume effects. Volume effects take into account the volume of the probability distribution: for instance, a region which has a very large volume in marginalised (or averaged) parameter directions but a less good fit can still have an appreciable effect on the marginalised posterior probability distribution. However, as is well known, the Bayesian interpretation is dependent upon the subjective prior choice unless the data are plentiful and precise. As was pointed out in ref. [95], the indirect data used in the fits are currently not plentiful and precise enough. We therefore display both methods and use the difference between the two as an indication of the size of inherent uncertainty in our interpretation of the fits.

8.3 The W mass and the weak mixing angle

We take the KISMET points and re-weight them, taking off the likelihood contributions from M_W and $\sin^2\theta_w^l$. By marginalising against these two variables, we may then examine what size of SUSY contribution to each is expected from fits to the other indirect data. In order to calculate the one-sided 95% limits upon the *magnitude* of the SUSY corrections to each observable, we re-bin in terms of $|M_W|$ and $|\sin^2\theta_w^l|$. M_W is the difference between the mSUGRA prediction and the Standard Model one with α_s, m_t, m_b and M_h identical to those associated with

[2]The SOFTSUSY determination of M_W and $\sin^2\theta_w^l$ is not to a sufficient accuracy, given the tiny empirical errors upon their measured values.

the mSUGRA point in question. The posterior pdf with flat priors gives us a 95% Bayesian credibility interval of

$$|M_W| < 19\,\text{MeV}; \qquad |\sin^2\theta_w| < 12 \times 10^{-5}. \tag{5}$$

The 95% upper confidence limit in the frequentist interpretation is obtained in each case from the profile likelihood:

$$|M_W| < 70\,\text{MeV}; \qquad |\sin^2\theta_w| < 30 \times 10^{-5}. \tag{6}$$

Thus, the frequentist constraints are somewhat (two and a half times) more relaxed than the Bayesian constraints with flat priors. These numbers are to be compared with the empirical uncertainties quoted in Eq. 4 of 17.5 MeV and 27×10^{-5}, respectively. Even the tighter 95% Bayesian constraints are around the same values and so we conclude that the SUSY contribution to the likelihood cannot be neglected.

Acknowledgements

This work has been partially supported by the STFC.

9. LHC and the muon's anomalous magnetic moment [1]

9.1 Introduction

The strongest hint for a TeV-scale modification of the Standard Model originates from the anomalous magnetic moment of the muon. This parameter has been evaluated both in experiment and in theory to unprecedented precision. We use the experimental value [100]

$$a^{(Exp)} \quad (g \quad 2)=2 = 116592080(63) \quad 10^{\ 11} \ : \tag{1}$$

In contrast, the Standard Model prediction is smaller [101, 102]

$$a^{(SM\ )} = 116591785(61) \quad 10^{\ 11} \ ; \tag{2}$$

where we use the number using $e^+ e$ data, as the discrepancy with tau data is still large [103]. This difference corresponds to a $3{:}4$ deviation between theory and experiment, suggesting a new–physics effect. Supersymmetry provides a particularly attractive explanation of this discrepancy. Contributions from the supersymmetric partners of the muon, the muon-neutrino and the gauge and Higgs bosons modify the Standard–Model prediction. The masses of the new particles responsible for this signal should be of the order of several hundred GeV, a mass range well accessible to the LHC [104, 105]. Therefore, LHC will be able to test the hypothesis that this discrepancy is caused by TeV-scale supersymmetry.

However, the benefit of such a test will go in both ways: after the LHC will have measured observables like the masses of supersymmetric particles or kinematic edges involving such particles [106, 61], the question will arise what the fundamental parameters of the Lagrangian are [31, 32]. Since $(g \quad 2)$ at leading order is proportional to $\tan$ it includes useful information [107], which can significantly improve the extraction of $\tan$.

As an example we use the experimentally well-studied parameter point SPS1a [21]. Its theory prediction for a is $a^{(SPS1a)} = a^{(SM\ )} + 282 \quad 10^{11}$. This leads to a deviation from the experimentally observed value of $a = 13 \quad 10^{11}$, which is well below the experimental error bounds. Therefore, we can safely use the experimental value without further modifications.

Our analysis uses the parameter extraction tool SFitter [31] where we have added the necessary modules to calculate the anomalous magnetic moment. To obtain a good balance between precision and required time to perform the scans we use the one-loop expression for $(g \quad 2)$ with additional leading two-loop QED-logarithms. Note that in this study we are not mainly interested in the best–fitting MSSM parameter point, but in the errors of the MSSM parameters, so this simplification is appropriate.

9.2 Weak–scale MSSM analysis

The determination of the weak–scale MSSM Lagrangian at the LHC is clearly preferable to tests of SUSY–breaking assumptions, as long as we have enough information available at the LHC. The extracted model parameter can then be run to a higher scale, to test for example unification patterns [31]. However, some model parameters can be fixed, because neither LHC nor $(g \quad 2)$ will include any information on them. Properly including the top-quark mass as a free parameter we assume a 19-dimensional weak–scale MSSM parameter space listed in Table 1. As we have shown in Ref. [31], even this reduced parameter space cannot be determined completely at the LHC. In the parameter point SPS1a, we for example find an eightfold degeneracy in the gaugino–higgsino sub-sector. Because only three of the neutralinos and none of the charginos can be observed at the LHC, the connection between their masses and the model parameters M_1, M_2 and is not unique. In addition the sign of is not determined by LHC data alone [108].

This is where the anomalous magnetic moment of the muon adds important information. First, the deviation from the Standard Model prediction is proportional to the sign of , the parameter which couples the two Higgs superfields in the superpotential. Including $(g \quad 2)$ data will clearly favor one sign of , namely the > 0, thereby reducing the degeneracy by a factor of two.

When reconstructing the fundamental parameters of the Lagrangian the central values have to be accompanied with the correct error bars. There are three different types of experimental errors on the observables: a statistical error and the two (correlated) systematic errors for the jet and lepton energy scales. All experimental errors are Gaussian shaped. In addition, we include flat theory errors of 1% for all colored particle masses and $0{:}5\%$ for all others. For $(g \quad 2)$ we use the values given in Eqs.(1, 2). The convolution of these errors is described

[1] M. Alexander, S. Kreiss, R. Lafaye, T. Plehn, M. Rauch, and D. Zerwas

	only experimental errors				including flat theory errors				SPS1a
	LHC		LHC ($g-2$)		LHC		LHC ($g-2$)		
$\tan\beta$	**9.8**	**2.3**	**9.7**	**2.0**	**10.0**	**4.5**	**10.3**	**2.0**	**10.0**
M_1	101.5	4.6	101.1	3.6	102.1	7.8	102.7	5.9	103.1
M_2	191.7	4.8	191.4	3.5	193.3	7.8	193.2	5.8	192.9
M_3	575.7	7.7	575.4	7.3	577.2	14.5	578.2	12.1	577.9
$M_{\tilde{\ell}_L}$	196.2	$\mathcal{O}(10^2)$	263.4	$\mathcal{O}(10^2)$	227.8	$\mathcal{O}(10^3)$	253.7	$\mathcal{O}(10^2)$	193.6
$M_{\tilde{\ell}_R}$	136.2	$\mathcal{O}(10^2)$	156.8	$\mathcal{O}(10^2)$	164.1	$\mathcal{O}(10^3)$	134.1	$\mathcal{O}(10^2)$	133.4
$M_{\tilde{\nu}_{e_L}}$	192.6	5.3	192.3	4.5	193.2	8.8	194.0	6.8	194.4
$M_{\tilde{\nu}_{e_R}}$	134.0	4.8	133.6	3.9	135.0	8.3	135.6	6.3	135.8
$M_{\tilde{e}_L}$	192.7	5.3	192.2	4.5	193.3	8.8	194.0	6.7	194.4
$M_{\tilde{e}_R}$	134.0	4.8	133.6	3.9	135.0	8.3	135.6	6.3	135.8
$M_{\tilde{\tau}_{3_L}}$	478.2	9.4	476.1	7.5	481.4	22.0	485.6	22.4	480.8
$M_{\tilde{t}_R}$	429.5	$\mathcal{O}(10^2)$	704.0	$\mathcal{O}(10^2)$	415.8	$\mathcal{O}(10^2)$	439.0	$\mathcal{O}(10^2)$	408.3
$M_{\tilde{b}_R}$	501.2	10.0	502.4	7.8	501.7	17.9	499.2	19.3	502.9
$M_{\tilde{q}_L}$	523.6	8.4	523.0	7.5	524.6	14.5	525.5	10.6	526.6
$M_{\tilde{q}_R}$	506.2	11.7	505.8	11.4	507.3	17.5	507.6	15.8	508.1
A_ℓ	fixed 0		fixed 0		fixed 0		fixed 0		-249.4
A_t	-500.6	58.4	-519.8	64.3	-509.1	86.7	-530.6	116.6	-490.9
A_b	fixed 0		fixed 0		fixed 0		fixed 0		-763.4
m_A	446.1	$\mathcal{O}(10^3)$	473.9	$\mathcal{O}(10^2)$	406.3	$\mathcal{O}(10^3)$	411.1	$\mathcal{O}(10^2)$	394.9
	350.9	7.3	350.2	6.5	350.5	14.5	352.5	10.8	353.7
m_t	171.4	1.0	171.4	1.0	171.4	1.0	171.4	0.90	171.4

Table 1: Result for the general MSSM parameter determination at the LHC in SPS1a. The left part neglects all theory errors, the right one assumes flat theory errors. In all cases a set of 20 kinematic endpoints and the top-quark and lightest Higgs–mass measurements have been used. In the third and fifth column we include the current measurement of $(g-2)$. All masses are given in GeV.

in Ref. [31]. To determine the errors on the model parameter we randomly smear the nominal values for SPS1a. The corresponding random numbers obey a distribution according to the associated errors. Then we minimize ^{2} for each pseudo–measurement and repeat this procedure 10000 times. The emerging distribution of the parameters is simply the result of the correct error propagation. Using a Gaussian fit we then extract the central value and the 1 standard deviation of each parameter.

Table 1 shows the result of our SPS1a analysis. For comparison and to make the effect of the additional $(g-2)$ data easily visible, we include the result without $(g-2)$ data from Tables VIII and IX of Ref. [31]. We give results with experimental errors only (columns 2 and 3) and including theory errors (columns 4 and 5). The effect of the additional information on the accuracy of the parameter determination is clearly visible. It is particularly significant for $\tan\beta$, which is not well determined by the measurements of kinematic endpoints at the LHC. The best source of information on $\tan\beta$ is the light MSSM Higgs mass [109], but this observable strongly relies on the assumed minimal structure of the Higgs sector, on the knowledge of many other MSSM parameters, and on the estimate of the theory errors due to higher orders. Because of a lack of complementary measurements (for example A_t) a change in $\tan\beta$ can always be compensated by an appropriate change in other MSSM parameters, leaving the value of all LHC observables unchanged. Additional sources of a $\tan\beta$ measurement are the production rate for heavy Higgs bosons [110] and rare decays like $B_s \to \mu^+\mu^-$, which we study elsewhere in this volume, but both of them only work for large enough values of $\tan\beta$.

The $(g-2)$ prediction has a leading linear dependence on $\tan\beta$. Therefore, the improvement of the $\tan\beta$ errors by more than a factor of two can be easily understood. This improved accuracy of $\tan\beta$ influences those parameters which must be re-rotated when $\tan\beta$ is changed to reproduce the same physical observables. Correlations and loop corrections propagate the improvement over almost the complete parameter space.

9.3 SLHAio

The link between the main SFitter modules and the (g 2) module is provided by SLHAio. SLHAio is a library which allows for a smooth communication between different programs according to the SUSY Les Houches Accord (SLHA) [72] and its extension SLHA2 [111]. With such an interface, for example a (g 2) code can easily be used in a large–scale program like SFitter.

The separation of actual calculations and SLHA interface creates a simple structure. SLHAio itself has an easy instruction set with a concept similar to the XML Path Language (XPath) [112]. Each data field in SLHA is associated with a leaf in a tree. The leafs are accessed and manipulated with a path. The path itself is similar to the path used for navigation in file systems.

The tree has no predefined structure. Its size is determined by the amount of information stored. It can of course grow beyond the fields defined in SLHA and SLHA2. This feature we use for the smuon mass matrix, where SLHA restricts itself to third–generation particles. There are two data types for each field: string and double. Conversions are done automatically. Setting a leaf with a string and afterwards reading a double is possible, as long as the string can be converted. The library assures the highest precision possible. Strings which are never changed through doubles remain strings, because this representation has the highest precision. Conversions to strings are done in the format defined in SLHA. One part of SLHAio is a templated container class for matrices. This class is fully integrated into SLHAio, so matrices can be read, stored and printed with a single command.

As discussed above, the (g 2) code can be used stand–alone and within SFitter. When used with SFitter, data is shared directly via SLHAio. This is a huge increase in performance, because no files need to be written and doubles do not need to be converted to strings and back again. It also means that once the tree is set up, parameter changes are as fast as the access to a double pointer. At this stage, no SLHAio functions are involved. While SLHAio is used in the SFitter extraction tool, it will in the future become publicly available.

9.4 Conclusions

Supersymmetry provides a particularly convincing explanation for the currently observed $3{:}4$ discrepancy between the experimental value for the anomalous magnetic moment of the muon and its Standard–Model prediction. If this signal proves to be correct, there exist new particles in a mass range accessible to the LHC. When we attempt to reconstruct weak–scale MSSM parameters from LHC observables, the numerical value of (g 2) provides an attractive additional handle on the MSSM parameters. Using the parameter point SPS1a as an example, we have shown that (g 2) essentially determines the sign of in the weak–scale MSSM, cutting the number of discrete solutions obtained in the general MSSM in half. In addition, many of the parameter errors are reduced, most notably the error on the extraction of the notoriously difficult parameter $\tan$.

Acknowledgements

We would like to thank the organizers of the great Les Houches 2007 workshop *Physics at TeV-Scale Colliders.*

10. Towards combining cascade decays and flavor physics [1]

10.1 Determining supersymmetric parameters

For many years it has been known that the kinematics of cascade decays is particularly well suited to extract the masses of the particles involved [106, 61]. More recently, we have seen how these masses can be used to determine the (running) TeV–scale Lagrangian parameters, with the ultimate goal of evolving these parameters to higher energy scales and extracting information on the mechanism of supersymmetry breaking. SFitter [31] and Fittino [32] are two computer tools specifically designed to determine TeV–scale supersymmetric parameters with the proper experimental and theory errors.

Most studies of cascade decays are based on the decays of (five) light–flavor squarks and gluinos. Hence, for example in SPS1a we would have convincing control over these squark masses and over the neutral gaugino masses. A crucial and yet notoriously hard parameter to extract is $\tan$, both in the neutralino/chargino sector and in the Higgs sector. In most analyses, we rely on the light MSSM Higgs mass for information on $\tan$ [109]. This extraction depends on a large number of supersymmetric parameters, on the strict MSSM assumption, and on a reliable estimate of the theory errors. Elsewhere in this volume we show how a measurement of $(g \quad 2)$ can be used to determine $\tan$ from the lepton sector. In a former Les Houches project it was shown that $\tan$ can be extracted from the production rate of heavy MSSM Higgs bosons, which for large values of $\tan$ is typically proportional to $m_b^2 \tan^2$. Combining all errors entering the cross–section measurements this study predicts a total error of 12% to 16% on the $bbA=bbH$ Yukawa coupling, which is proportional to $\tan$ [110].

Another strategy for an indirect $\tan$ measurement are flavor–physics observables. For example the rare decay rate for $B_s \; ! \; ''$ is proportional to $\tan^6 =m_A^4$. This steep behavior makes it a prime suspect to extract $\tan$ [113]. A major problem of such an extraction is the correct estimate of the theory error on the observable. The second problem is the dependence of the effective $bsfh;H;Ag$ couplings on the stop and chargino masses appearing in the loop. In this article we briefly report on a pre-study done for SFitter, to give a first estimate if these two problems will leave channels like $B_s \; ! \; ''$ promising candidates to be included in the SFitter set of observables.

Unfortunately, the usual parameter point SPS1a with $\tan = 10$ is not well suited to study the determination of $\tan$. Even if there should be a sensitivity from a measurement of $B_s \; ! \; ''$, it is unclear if we will observe any of the heavy Higgs bosons at the LHC. We therefore modify this parameter point in the direction of SPS1b, simply choosing a range of larger $\tan$ values. For simplicity we assume that the set of cascade observables is not altered by this change, including the sbottom mass determination. While this assumption might be quantitatively naive, it will serve our purpose of estimating the odds of combining different sources of information on $\tan$.

10.2 Combining flavor and cascades

FCNC processes involving down-type quarks in the Standard Model are both highly suppressed and sensitive to the mass and couplings of the top. This is because, beyond their loop suppression, the unitarity and hierarchical structure of the CKM matrix and the hierarchy $m_{t;W} \quad m_{u;c}$, entail strong GIM cancellations between the light–flavor loop contributions. Turning around this argument, they are sensitive probes of new–physics effects. In particular when the supersymmetric flavor structure is (close to) minimally flavor–violating [114, 115, 116], they provide a handle on stop and chargino masses. Of special interest are FCNC mediated by neutral Higgs exchange, which exhibit a double enhancement: first, they involve the large bottom Yukawa coupling $y_b \; / \; y_b^{SM} \tan$. Secondly, the loop–induced contribution of $v_u \quad hH_u i \quad v_d$ to the down-type fermion mass matrix destroys the alignment of the mass matrix with the Yukawa couplings and renders the latter flavor-nondiagonal [117, 118, 119, 120, 121, 122, 123], leading to an additional factor $\tan$. For minimal flavor violation, the corresponding FCNC Higgs couplings have the form [123, 124, 125]

$$L_e \quad b_R s_L \; _i x_i V_{tb} V_{ts} \frac{y_t^2 y_b}{\cos} \frac{Y}{(1 + (\ _0 + y_t^2 \ _Y)\tan \ )(1 + \ _0 \tan \ )}; \tag{1}$$

where $x_H = \sin(\quad)$ and $x_A = i$. The FCNC couplings of h are suppressed by a factor $x_h = \cos(\quad)$, offsetting the $\tan$ enhancement. The parameters $_0$ and $_Y$ parameterize loop-induced "wrong-Higgs" contributions to the down-quark mass matrix. The sensitivity to MSSM parameters becomes most transparent in the limit $v \quad M_{SUSY}$, when

$$_Y = \frac{1}{16^{\ 2}} \frac{A_t}{y_t} \left[\frac{x \ln x}{(1 \quad x)(x \quad y)} + \frac{y \ln y}{(1 \quad y)(y \quad x)} \right]; \tag{2}$$

[1] S. Jäger, T. Plehn and M. Spannowsky

with $x = m^2_{\tilde{t}_L} / {}^2$ and $y = m^2_{\tilde{t}_R} / {}^2$. The observables most sensitive to these couplings are $B_{s,d} \to {}^+ {}^-$, where the tree-level H ;A exchange contributes at the amplitude level as [123, 124, 125, 126, 127]

$$A(B_q \to {}^+ {}^-)^{H\,A} \;/\; \frac{y_b y_{} \tan}{\cos\, m^2_A} \;/\; \frac{1\, m_b m_{} \tan^3}{m^2_A} : \tag{3}$$

Among the modes accessible at LHCb, ATLAS, and CMS, $B_s \to {}^+$ has the largest branching fraction [113], which can be dominated by the neutral-Higgs contribution.

The usual cascade measurements we assume with this simple study include $g \to \tilde{t}_1 t \to t\tilde{t} {}^0_1$, $g \to \tilde{t}_1 t \to tb\,{}^+_1$, $\tilde{q}_L \to {}^0_3 q \to {}^0_2 Z q \to \tilde{}_R\, Z q \to {}^1_0\, q Z$, $\tilde{q} \to {}^+_2 q \to {}^+_1 Z q \to q W\, {}^0_1 Z q \to q q' q'' {}^0_1 Z$, where the ${}^+_2$ cascade is strictly speaking not necessary for our analysis. In our simple parameter points $M_0 = 150$, $M_{1=2} = 250$, $A_0 = \;\; 100$, $\;\; > 0$, and $\tan \;\; = (30;40)$ [128], these cascades should be visible. In our Minuit fit we include 10 observables listed in Table 1, including $BR(B \to \;\;)$ and the edge measurement m_{tb} [129]. In addition, we need to include some very basic information on the chargino–stop sector. The measurement of the three neutralino masses gives us information on the chargino mass parameters M_2 and $\;\;$. The left–handed stop mass is linked to the left–handed sbottom mass via SU(2). However, the right–handed stop mass as well as the off–diagonal entry into the mass matrix are not determined by cascade decays. The latter is dominated by the trilinear coupling A_t, which enters for example the calculation of the light Higgs mass [130]. Extracting A_t, however, requires a measurement of the dominant heavy Higgs mass parameter, which again limits us to reasonably large values of $\tan \;\;$. We assume m_A to be known either directly or via the charged Higgs mass, similarly to Ref. [110].

The modified SPS1a parameter point for two example values of $\tan \;\;$ is specified in Table 2, together with the best-fit values and the errors from our Minuit fit. For $B_s \to \;\;$, LHCb alone expects about 100 events at the Standard–Model rate after 5 years of running [113]. For our study we assume an integrated luminosity of $10\ \text{fb}^{-1}$ for the B_s sample. The Higgs–mediated contributions always increases the corresponding events number. As a consequence, the theory error, which at present ranges around 30%, will soon dominate the total uncertainty, unless it can be reduced. It is mainly due to the decay constant f_{B_s}, which can be calculated using numerical lattice-QCD methods (see Ref. [131] for a recent review). For our study we simply assume a reduction of the error on f_{B_s} to 7%, about half its present value. Such a reduction is commonly believed to be realistic over the next five years.

For our study, we perform two sets of fits, one ignoring the theory error and one combining it in quadrature with the statistical error. A more refined treatment of the theory error is in progress and will use the proper Rfit ansatz [43], as implemented in Sfitter [31]. We indeed see that without taking into account the theory error, $\tan \;\;$ will be determined to 10% from the combined toy data sample. Including a realistic theory error increases this number to $15 \qquad 20\%$. The errors on the remaining parameters, shown in Table 2, remains largely unchanged. Slight shifts in either direction are at his stage well within the uncertainly on the determination of the error bars, and the central fit value for the top–mass parameter seems to be consistently lower than the input value (by roughly half a standard deviation). Comparing our error estimates on the mass parameters for example with the SFitter analysis [31], we expect the situation to improve for all model parameters once we include a more extensive set of measurements and properly correlated errors.

$\tan \;\;$	30		40	
	value	error	value	error
m_h	112.6	4.0	112.6	4.0
m_t	174.5	2.0	174.5	2.0
m_H	354.2	10.0	307.2	10.0
$m_{\;\;^0_1}$	98.4	4.8	98.7	4.8
$m_{\;\;^0_2}$	183.1	4.7	183.5	4.7
$m_{\;\;^0_3}$	353.0	5.1	350.7	5.1
$m_{\;\;^1}$	182.8	50.0	183.1	50.0
$m_{\tilde{g}}$	607.7	8.0	607.6	8.0
$BR(B_s \to \;\;)$	$7.3 \quad 10^9$	$\sqrt{N} \quad 15\%$	$3.2 \quad 10^8$	$\sqrt{N} \quad 15\%$
m_{tb}	404.2	5.0	404.2	5.0

Table 1: Set of toy measurements. The simple combined (absolute) errors are SPS1a–inspired.

	no theory error			BR=BR = 15%		no theory error			BR=BR = 15%	
	true	best	error	best	error	true	best	error	best	error
tan	30	29.5	3.4	29.5	6.5	40	39.2	4.4	39.2	5.8
M_A	344.3	344.4	33.8	344.3	31.2	295.5	304.4	35.4	295.6	33.9
M_1	101.7	100.9	16.3	100.9	16.4	101.9	101.0	16.3	101.0	16.3
M_2	192.0	200.3	18.9	200.3	18.8	192.3	200.3	20.0	200.7	18.9
	345.8	325.6	20.6	325.6	20.6	343.5	322.9	20.7	323.3	20.6
M_3	586.4	575.8	28.8	575.8	28.7	586.9	576.0	28.7	575.8	29.0
$M_{\tilde{Q}_L}$	494.4	494.4	78.1	494.3	78.0	487.1	487.6	79.4	487.5	78.9
M_{t_R}	430.0	400.4	79.5	399.8	79.5	431.5	399.2	86.7	399.1	82.6

Table 2: The modified SPS1a point and the errors from the parameter fit for the two values of tan = 30;40. Dimensionful quantities are in units of GeV. For the measurement of BR(B_s ! ‘‘) we assume either no theory error or an expected improvement to 15% , as compared to the current status.

10.3 Caveats

Note that the detailed results of this study should not be used at face value. First of all, it is not clear if the stop–mass measurement can be achieved in the SPS1a parameters point or with an increased value of tan . Secondly, for the charged Higgs mass we only use a toy measurement. And last but not least, we do not (yet) take into account error correlations at this stage. None of these omissions we expect to move the result of a complete analysis into a definite direction, but there is certainly room for the final error bars to move.

This study shows, however, that the parameter tan can indeed be extracted from a combined cascade and flavor data sample. Already at this stage we can conclude that the combination of cascade–decay and flavor observables will crucially depend on the quality of the theory predictions in the flavor sector. In particular, an improved understanding of non-perturbative QCD effects in B_s ! ‘‘ decays is needed to meaningfully exploit this highly promising link. From the high–p_T point of view we also generally see that to measure tan we need to improve the analysis of the stop–chargino sector in the classic decay–kinematics analyses.

The problem with the measurement of tan from the light MSSM Higgs mass or from (g 2) or from rare B decays is that each of these indirect measurement rely on assumptions about the flavor and Higgs sectors. Moreover, these different measurements point to different parameters, not only from a renormalization point of view, but also because of large QCD effects distinguishing between them. The more direct extraction from cross sections times branching ratios of heavy Higgs bosons is at the same time plagued by large theory uncertainties, due to QCD corrections and uncertainties in the bottom–parton picture [132, 133]. If we should indeed find evidence for the MSSM in the LHC era we obviously expect a serious jigsaw approach to the tan determination.

Acknowledgments

We are grateful to Mihoko Nojiri and Giacomo Polessello for their ongoing encouragement. And of course we thank the organizers of the great Les Houches 2007 workshop *Physics at TeV-Scale Colliders*!

11. BBN lithium problem consequences at LHC [1]

11.1 Lithium problem

Recent measurements of the fluctuations of the microwave background radiation allowed for determination of the contribution of baryons to critical density $_{b}h^{2}$ $0{:}0224$ [36] which is the only free parameter of the standard BBN. SBBN previsions are in agreement with experimental estimates of abundances for deuterium and and helium 4 but have problem in explaining lithium 7 proliferation, which is about 3 times to high.

There is no agreement whether stated above discrepancy is a real problem because apparent primordial ^{7}Li abundance is derived only from the observation of so called Spite plateau [134] in low metallicity POP II stars. It is believed, that gas present in atmospheres of these very old starts have not changed composition since the BBN era. ^{7}Li is, however, fragile so in principle its depletion could be explained by some stellar evolution model but no fully satisfactory model have been proposed [135, 136]. Recently preliminary observation of similar plateau was done also for ^{6}Li [135] which was produced during SBBN but below detectable level. If confirmed, the plateau could suggest pre-galactic ^{6}Li origin corresponding to the primordial abundance at least an order of magnitude higher than SBBN predictions. Moreover, since ^{6}Li is by far more fragile than ^{7}Li, any model of its destruction will aggravate ^{6}Li problem.

Although above sketched lithium problems could have standard explanation it is very interesting to note beyond standard model solutions that alters BBN. All of them postulate long lived massive particles with lifetimes around 1ks or more. Their decays allow for late ^{6}Li production or late ^{7}Li destruction or both without altering abundances of other isotopes. If these particles could be negatively charged than also bound states must be taken into account. In the present letter there is no place for review all proposed solutions. We would concentrate on two, which are in agreement with cosmological constraints, and could have very interesting consequences for the LHC phenomenology. In both, an existence of long-lived stau is postulated. In the first [137] stau lifetime is of the order of 1ks. The solution for both lithium problems is found within CMSSM for stau mass of the order of 1 TeV which is, unfortunately, out of reach at LHC. However, solution of only ^{6}Li problem is possible for stau mass around few hundreds GeV. The second solution of both lithium problems is possible for very long stau lifetime of 1 Ms and stau mass of about 300 GeV [136].

11.2 Possible discovery at LHC

Both ATLAS and CMS experiments have developed strategies to look for charged massive particles (CHAMP) if they decay lengths exceed detector sizes.

Methods tested on full detector simulation are based on TOF measurements in the muon systems (CMS drift tubes, ATLAS drift tubes and RPCs) or specific ionization measurement in the tracker (CMS). Since in both experiments at least two independent measurements are performed it is possible to evaluate misidentification probabilities directly from data. If simulated performances will be confirmed almost background free selections with efficiency of the order of 10% could be designed. After collecting 10/fb of data this allows for the discovery if the cross section exceeds 10 pb which corresponds to stau mass around 300 GeV [138].

This provoke natural question about lifetime measurement of such CHAMP. Any estimate of it could be of crucial importance. The problem is, however, that interesting range of lifetimes is above 100 s. It is obvious that decays in flight are not only by far inefficient but also insensitive.

However, the first proposition in this direction was made already a decade ago [139]. The point was about using CMS muon system as a late electromagnetic calorimeter (so called CAL) in the following way. If significant fraction of energy release is electromagnetic and if the decay happens inside iron yoke at a distance to the next muon station equivalent to few radiation lengths, then developing electromagnetic cascade causes large accumulation of hits in the station. By design the cascade ends in the next yoke section. So the signal is large accumulation of hits in one muon station. Despite the fact, that this proposal was made in the context of detection of decaying in flight neutralinos, it could be used also for decaying staus, but to measure long lifetimes these staus must stop inside the yoke. Unfortunately only small fraction of staus will do that. Larger fraction will be stopped in the concrete and rocks of the cavern.

There were proposals to drill out the cavern walls to recuperate the part with stopped CHAMP or to install water tanks for CHAMPs capture, but if CHAMPs are staus than there is also much simpler solution. 17% of stau decays produce muons. These muons could be detected not only for staus stopped inside detector but also for staus stooped in the cavern walls if muon is released backward. The first possibility is rather hopeless for the

[1] P. Zalewski

ATLAS detector because of air muon system but the second could be more efficient for ATLAS than for CMS because ATLAS is bigger and is closer to the cavern wall and so, it will have larger angular size when seen from the CHAMP decay point.

Although it is straight forward to estimate for a given model a probability for a muon from the stopped stau decay to cross again the detector full simulation is needed to know detector answer to such muon. In principle these muons are very similar to cosmic muons. The only difference is a homogeneous distribution of incoming directions in contrast to top bottom directions expected for cosmics.

Without full detector simulation (which already started, but no official results of it have been released) it is difficult to know if the sensitivity could be sufficient for measuring long lifetimes of stau. However, no such measurement is possible without cosmic trigger. Another problem is tracking of low momentum staus, which will go outside 25 ns window. Although triggering on such particles is not possible its offline recovery is not hopeless because drift tubes, thanks to their operation mode, remember data form many bunch crossings.

It is important to note, that cosmic trigger, even if possibly harmful for normal LHC operation, should be studied in detail, to be switched on if long lived CHAMPs will discovered at LHC.

11.3 Conclusions

It was underlined that lithium BBN problem could be solved by long lived CHAMPs, next, that such particles, if not to heavy, could be discovered at the LHC and that the most efficient way of measuring their very long lifetime is to design cosmic trigger for LHC detectors.

12. Precision measurements of the stop mass at the ILC [1]

12.1 Introduction

Supersymmetric particles are likely to be produced and observed in high-energy proton-proton collisions at the LHC. However, it will be difficult to confirm their identity as superpartners of the known Standard Model particles and to measure their properties precisely. For this, one needs experiments at a linear e^+e collider such as the proposed ILC at $\sqrt{s} = 500$ GeV. The importance of scalar top studies has been emphazised in the '2005 Les Houches' proceedings [140]. This work extends these studies.

An experiment at the ILC will be able to make many precise measurements from which particle properties, and ultimately, the outlines of a particle physics model may be inferred. Due to the high statistical precision expected at the ILC, the optimization of the systematic errors is of particular importance. We have studied one specific example, the extraction of the mass of a scalar top quark from cross-section measurements near threshold. We have devised a method which reduces most systematic uncertainties and leads to a potentially very accurate measurement of the stop quark mass. This method is general and could be applied to other particles that are pair-produced in an e^+e collider.

The method relies on the comparison of production rates at two different center-of-mass energies, and knowledge of how the cross-section varies as a function of $\sqrt{s}$ and the mass of the particle.

We have chosen the case of a light scalar top with a mass not much higher than the mass of the lightest neutralino since production of this particle was already extensively studied in an ILC context. It was concluded that a conventional approach to the measurement of the stop quark mass culminated in an uncertainty of about 1 GeV [141]. The new method improves substantially on this result. The presented results are preliminary and being finalized [142].

For this analysis, we have performed realistic simulations of the signal and backgrounds, and used two techniques to separate the signal from the background. The first technique is based on conventional sequential cuts, while the second employs an Iterative Discriminant Analysis (IDA). Furthermore, the hadronization followed by fragmentation of the stop has been included and we have carefully studied the systematic uncertainties arising from this and other sources.

There are theoretical motivations for studying a light stop quark with a small mass difference. Specifically, we evoke a scenario within the Minimal Supersymmetric extension of the Standard Model (MSSM) which is able to explain the dark matter density of the universe as well as the baryon asymmetry through the mechanism of electroweak baryogenesis [141].

A small mass difference between the stop and the lightest neutralino can help to bring the dark matter relic density into the observed region [36, 143] due to co-annihilation between the stop and the neutralino. For this mechanism to be effective, the typical mass difference is rather small, $m = m_{\tilde{t}_1} - m_{\tilde{\chi}^0_1} < 30$ GeV [144]. The dominant decay mode of the stop is $\tilde{t}_1 \to c\tilde{\chi}^0_1$, resulting in a final state with two soft charm jets and missing energy.

Previous methods to determine the scalar top quark mass were discussed for the SPS-5 benchmark ($m_{\tilde{t}_1} = 220.7$ GeV) [145] and results are summarized in Table 1. For the cosmology motivated benchmark with $m_{\tilde{t}_1} = 122.5$ GeV and $m_{\tilde{\chi}^0_1} = 107.2$ GeV, an experimental precision of $m_{\tilde{t}_1} = 1.0$ GeV was obtained [141], and about 1.2 GeV including theoretical uncertainties. The following study investigates the same signal scenario and it is based on the same background reactions and event preselection.

Method	$m_{\tilde{t}_1}$ (GeV)	luminosity
Polarization	0.57	$2 \times 500\,\text{fb}^{-1}$
Threshold scan	1.2	$300\,\text{fb}^{-1}$
End point	1.7	$500\,\text{fb}^{-1}$
Minimum mass	1.5	$500\,\text{fb}^{-1}$

Table 1: Comparison of precision for scalar top mass determination for the SPS-5 benchmark ($m_{\tilde{t}_1} = 220.7$ GeV).

12.2 Mass determination method

This method proposes to derive the stop mass from measurements at two center-of-mass energies, one measuring the stop production cross-section near the threshold (th), and the other measuring it at a center-of-mass energy where the cross-section has approximately a peak (pk). Using both measurements leads to a cancellation of sys-

[1] A. Sopczak, A. Freitas, C. Milstène and M. Schmitt

tematic uncertainties in the mass determination. A parameter Y is defined as

$$Y = \frac{N_{th}}{N_{pk}} - \frac{B_{th}}{B_{pk}} = \frac{_{th}}{_{pk}} \quad \frac{_{th}}{_{pk}} \quad \frac{L_{th}}{L_{pk}}; \tag{1}$$

where N is the total number of expected events after event selection and B the number of corresponding background events, is the stop production cross-section, the selection efficiency, and L the luminosity. The center-of-mass energies 260 and 500 GeV have been chosen. Near the threshold, the production cross-section is very sensitive to the stop mass.

In this study we assume that the ILC will operate primarily at $\sqrt{s} = 500$ GeV with a total luminosity of $L = 500$ fb^{-1}, and a small luminosity of $L = 50$ fb^{-1} will be collected at $\sqrt{s} = 260$ GeV. Table 2 summarizes the expected production cross-sections. The detector response was modeled with the SIMDET package [146] including the LCFI [147] vertex detector concept.

The relation of the observable Y and the stop mass is used to determine the stop mass with precision. For example a variation of Y by 3% in a realistic scenario would lead to an uncertainty of the stop mass $m_{\tilde{t}_1} = 0.2$ GeV as illustrated in Fig. 1.

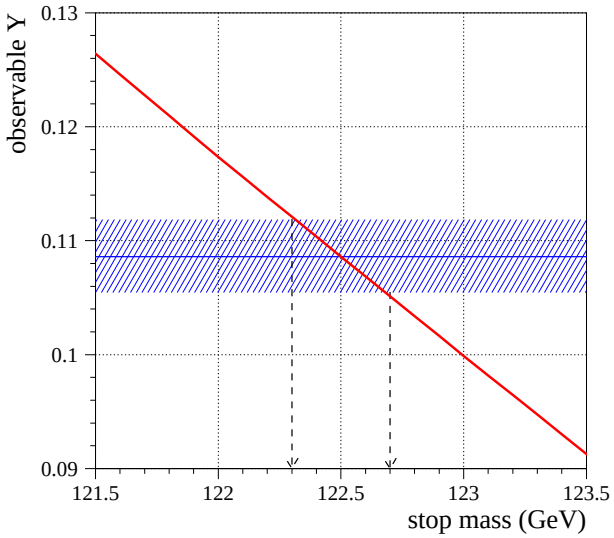

Fig. 1: Example of mass uncertainty derivation from the uncertainty of the observable Y.

12.3 Sequential-cut analysis

In order to cancel the systematic uncertainties to a large extent with the described method, the same sequential cuts are applied for the $\sqrt{s} = 260$ and 500 GeV analyses. Details of the event selection are given in Table 3 and the results are given in Table 4.

Table 2: Cross-sections for the stop signal [148] and Standard Model background processes for $\sqrt{s} = 260$ GeV and $\sqrt{s} = 500$ GeV and different polarization combinations. The signal is given for a right-chiral stop of $m_{\tilde{t}} = 122.5$ GeV. Negative polarization values refer to left-handed polarization and positive values to right-handed polarization.

Process	(pb) at $\sqrt{s} = 260$ GeV			(pb) at $\sqrt{s} = 500$ GeV		
$P(e^-)P(e^+)$	0/0	-.8/+.6	+.8/-.6	0/0	-.8/+.6	+.8/-.6
$\tilde{t}_1\tilde{t}_1$	0.032	0.017	0.077	0.118	0.072	0.276
W^+W^-	16.9	48.6	1.77	8.6	24.5	0.77
ZZ	1.12	2.28	0.99	0.49	1.02	0.44
$We\nu$	1.73	3.04	0.50	6.14	10.6	1.82
$ee(Z/\gamma)$	5.1	6.0	4.3	7.5	8.5	6.2
$qq(\gamma/Z)$, $q \neq t$	49.5	92.7	53.1	13.1	25.4	14.9
$t\bar{t}$	0.0	0.0	0.0	0.55	1.13	0.50
2-photon $p_T > 5$ GeV	786			936		

Table 3: Selection cuts for $\sqrt{s} = 260$ and 500 GeV. Also listed are the selection efficiencies optimized for right-chiral stop quarks.

Variable	$\sqrt{s} = 260$ GeV	$\sqrt{s} = 500$ GeV
number of charged tracks	$5 \le N_{tracks} \le 25$	$5 \le N_{tracks} \le 20$
visible energy E_{vis}	$0.1 < E_{vis}/\sqrt{s} < 0.3$	$0.1 < E_{vis}/\sqrt{s} < 0.3$
event long. momentum	$\lvert p_L/p_{tot}\rvert < 0.85$	$\lvert p_L/p_{tot}\rvert < 0.85$
event transv. momentum p_T	$15 < p_T < 45$ GeV	$22 < p_T < 50$ GeV
thrust T	$0.77 < T < 0.97$	$0.55 < T < 0.90$
Number of jets N_{jets}	$N_{jets} \ge 2$	$N_{jets} \ge 2$
extra-jet veto	$E_{jet} < 25$ GeV	$E_{jet} < 25$ GeV
charm tagging likelihood P_c	$P_c > 0.6$	$P_c > 0.6$
di-jet invariant mass m_{jj}	$m^2_{jj} < 5500$ GeV^2 or $m^2_{jj} > 8000$ GeV^2	$m^2_{jj} < 5500$ GeV^2 or $m^2_{jj} > 10000$ GeV^2
signal efficiency	0.340	0.212

Table 4: Numbers of generated events, and expected events for the sequential-cut analysis at $\sqrt{s} = 260$ and 500 GeV for total luminosities of 50 fb^{-1} and 200 fb^{-1} with unpolarized and polarized beams.

	$\sqrt{s} = 260$ GeV			$\sqrt{s} = 500$ GeV		
	generated	$L = 50$ fb^{-1}		generated	$L = 200$ fb^{-1}	
$P(e^-)=P(e^+)$		0/0	.8/-.6		0/0	.8/-.6
$\tilde{t}_1\tilde{t}_1$	50,000	544	1309	50,000	5170	12093
W^+W^-	180,000	38	4	210;000	16	2
ZZ	30,000	8	7	30;000	36	32
$We\nu$	210,000	208	60	210;000	7416	2198
$ee\nu\nu$	210,000	2	2	210;000	< 7	< 6
$q\bar{q}, q\bar{q}g$	350,000	42	45	350;000	15	17
$t\bar{t}$	—	0	0	180;000	7	7
2-photon	1:6 10^6	53	53	8:5 10^6	12	12
total background	—	351	171	—	7509	2274

12.4 Iterative discriminant analysis

The Iterative Discriminant Analysis (IDA) [149] is applied to increase the discriminant power between signal and background compared to the sequential-cut-based analysis, and thus reduce the statistical uncertainty in the stop mass measurement. Figure 2 gives the results of expected number of background events as a function of the signal efficiency. The chosen working points have efficiencies of 38.7% and 41.6% for the $\sqrt{s} = 260$ and 500 GeV analyses, respectively. Table 5 lists the corresponding expected background events.

	$\sqrt{s} = 260$ GeV			$\sqrt{s} = 500$ GeV		
	generated	$L = 50$ fb^{-1}		generated	$L = 200$ fb^{-1}	
$P(e^-)=P(e^+)$		0/0	.8/-.6		0/0	.8/-.6
$\tilde{t}_1\tilde{t}_1$	50,000	619	1489	50,000	9815	22958
W^+W^-	180,000	11	1	210;000	< 8	< 1
ZZ	30,000	< 2	< 2	30;000	20	18
$We\nu$	210,000	68	20	210;000	1719	510
$ee\nu\nu$	210,000	3	2	210;000	< 7	< 6
$q\bar{q}, q\bar{q}g$	350,000	16	17	350;000	18	21
$t\bar{t}$	—	0	0	180;000	1	1
2-photon	1:6 10^6	27	27	8:5 10^6	294	294
total background	—	125	67	—	2067	851

Table 5: Numbers of generated events, and expected events for the IDA at $\sqrt{s} = 260$ and 500 GeV for total luminosities of 50 fb^{-1} and 200 fb^{-1} with unpolarized and polarized beams.

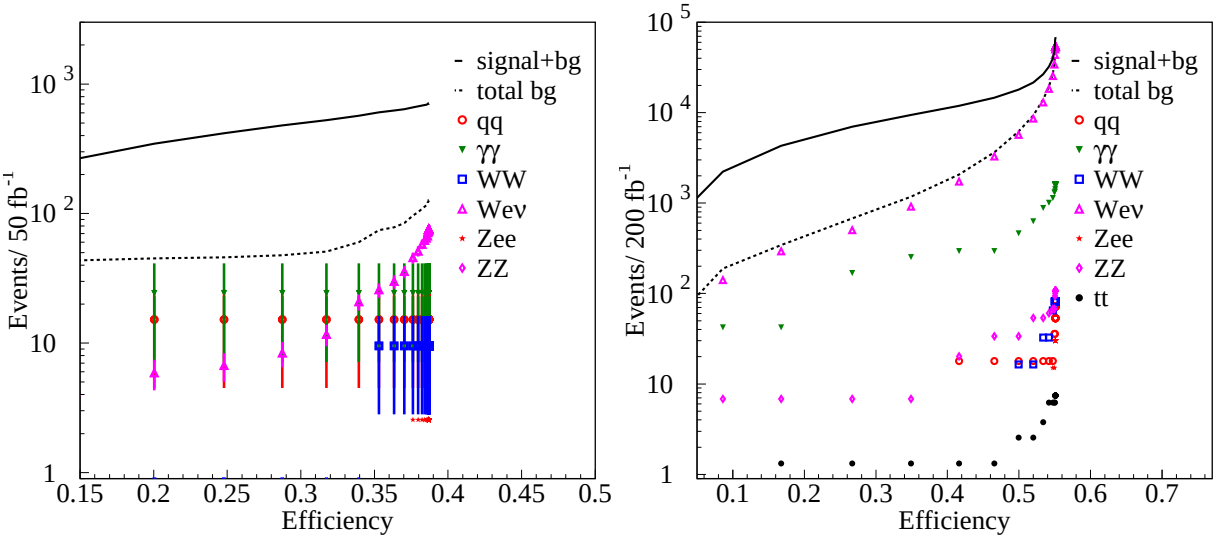

Fig. 2: IDA: Expected background events as a function of the signal efficiency. Left: $L = 50$ fb^{-1} at $\sqrt{s} = 260$ GeV. Right: $L = 200$ fb^{-1} at $\sqrt{s} = 500$ GeV.

12.5 Systematic uncertainties

Both the sequential-cut-based analysis and the IDA method lead to a small statistical uncertainty resulting in $m_{\tilde{t}_1} < 0.2$ GeV and thus systematic uncertainties are particularly important to evaluate. Three classes of systematic uncertainties are distinguished:

instrumental uncertainties related to the detector and accelerator: detector calibration (energy scale), track reconstruction efficiency, charm-quark tagging efficiency, and integrated luminosity.

Monte Carlo modeling uncertainty of the signal: charm and stop fragmentation effects. The Peterson fragmentation function [150] was used with $_c = 0.031 \quad 0.011$ (OPAL) [151]. For $_b = 0.0041 \quad 0.0004$ (OPAL) [152] and $_b = 0.0031 \quad 0.0006$ (ALEPH) [153] an average uncertainty of 15% was taken, and a factor 2 improvement at the ILC has been assumed, leading to $_{\tilde{t}_1} = 0.6 \quad 10^{-6}$ where $_{\tilde{t}_1} = {}_b(m_b/m_{m_{\tilde{t}_1}})^2$ [150, 154]. Fragmentation effects and gluon radiation increase the number of jets significantly and the importance of c-quark tagging is stressed in order to resolve the combinatorics.

neutralino mass $108.2 \quad 0.3$ GeV [155].

theoretical uncertainties on the signal and background. Some improvement compared to the current loop calculation techniques is assumed, and an even larger reduction of this uncertainty is anticipated before the start of the ILC operation.

Tables 6 and 7 list the systematic uncertainties for the sequential-cut analysis and the IDA. The systematic uncertainty using the IDA method from detector calibration (energy scale) is larger. This is because the sequential-cut analysis pays particular attention to cancellation of this uncertainty between the two analyses at the different center-of-mass energies.

Table 6: Sequential-cut analysis experimental systematic uncertainties on the signal efficiency. The first column indicates the variable that is cut on. The second column contains the expected systematic uncertainty for this variable based on experience from LEP. The third column shows by how much the signal efficiency for $\sqrt{s} = 260$ GeV varies as a result of varying the cut value by this uncertainty. The fourth column shows the same for $\sqrt{s} = 500$ GeV, and the fifth column lists the resulting error on the observable Y.

variable	error on variable	rel. shift on signal eff. 260 GeV	500 GeV	error on Y
energy scale	1%	3.7%	3.1%	0.6%
N_{tracks}	0.5%		negligible	
charm tagging	0.5%		taken to be 0.5%	
luminosity	–	0.4%	0.2%	0.4%
charm fragmentation	0.011	0.3%	0.8%	0.6%
stop fragmentation	$0.6 \quad 10^{-6}$	0.6%	0.2%	0.7%
neutralino mass	0.3 GeV	3.8%	3.0%	0.8%
background estimate	–	0.8%	0.1%	0.8%

Table 7: IDA experimental systematic uncertainties.

variable	error on variable	rel. shift on signal eff. 260 GeV	500 GeV	error on Y
energy scale	1%	3.4%	1.3%	2.3%
N_{tracks}	0.5%		negligible	
charm tagging	0.5%		taken to be 0.5%	
luminosity	–	0.4%	0.2%	0.4%
charm fragmentation	0.011	0.1%	0.6%	0.5%
stop fragmentation	$0.6 \quad 10^{-6}$	0.1%	0.8%	0.7%
neutralino mass	0.3 GeV	3.7%	1.6%	2.2%
background estimate	–	0.3%	0.2%	0.1%

12.6 Mass determination

The assessment of the achievable stop mass precision is based on the statistical and systematic uncertainties on the observable Y (eq. (1)) as summarized in Table 8. The IDA method has a smaller statistical uncertainty, and also a smaller background uncertainty due to a smaller number of expected background events. The expected stop mass uncertainty is inferred from the uncertainty on Y as given in Table 9.

Table 8: Summary of statistical and systematic uncertainties on the observable Y.

error source for Y	sequential cuts	IDA method
statistical	3.1%	2.7%
detector effects	0.9%	2.4%
charm fragmentation	0.6%	0.5%
stop fragmentation	0.7%	0.7%
neutralino mass	0.8%	2.2%
background estimate	0.8%	0.1%
sum of experimental systematics	1.7%	3.4%
sum of experimental errors	3.5%	4.3%
theory for signal cross-section	5.5%	5.5%
total error Y	6.5%	7.0%

Table 9: Estimated measurement errors (in GeV) on the stop quark mass.

	measurement error $m_{\tilde{t}_1}$ (GeV)	
error category	sequential cuts	IDA method
statistical	0.19	0.17
sum of experimental systematics	0.10	0.21
beam spectrum and calibration	0.1	0.1
sum of experimental errors	0.24	0.28
sum of all exp. and th. errors	0.42	0.44

12.7 Cold dark matter interpretation

The chosen benchmark parameters are compatible with the mechanism of electroweak baryogenesis [141]. They correspond to a value for the dark matter relic abundance within the WMAP bounds, $_{CDM}h^2 = 0.109$ [36]. The relic dark matter density has been computed as in Ref. [141][2]. In the investigated scenario, the stop and lightest neutralino masses are $m_{\tilde{t}_1} = 122.5$ GeV and $m_{\tilde{\chi}_1^0} = 107.2$ GeV, and the stop mixing angle is $\cos_{\tilde{t}} = 0.0105$, i.e. the light stop is almost completely right-chiral. The improvement compared to Ref. [141] regarding the CDM precision determination is shown in Fig. 3 and summarized in Table 10.

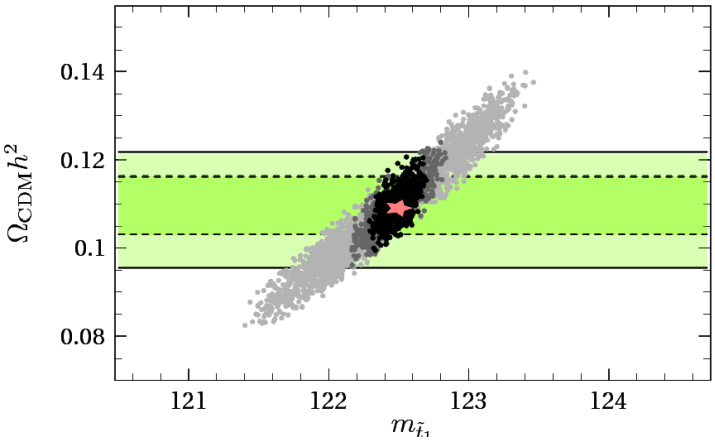

Fig. 3: Computation of dark matter relic abundance $_{CDM}h^2$ taking into account estimated experimental errors for stop, chargino, neutralino sector measurements at the future ILC. The black dots correspond to a scan over the 1 (^{2} 1) region including the total expected experimental uncertainties (detector and simulation), the grey-dotted region includes also the theory uncertainty, and the light grey-dotted area are the previous results [141]. The red star indicates the best-fit point. The horizontal shaded bands show the 1 and 2 constraints on the relic density measured by WMAP.

[2] The assumed benchmark parameters changed slighty (larger slepton masses assumed) and $_{CDM}h^2$ changed from 0.1122 [141] to 0.109.

Table 10: Estimated precision for the determination of stop mass and dark matter relic density for different assumptions about the systematic errors.

	$m_{\tilde{t}_1}$ (GeV)	$_{CDM}h^2$
exp. and th. errors	0.42	$0{:}109^{+\,0{:}015}_{\,0{:}013}$
stat. and exp. errors only		
sequential-cut analysis	0.24	$0{:}109^{+\,0{:}012}_{\,0{:}010}$
IDA	0.28	$0{:}109^{+\,0{:}012}_{\,0{:}010}$

Conclusions

Scalar top quarks could be studied with precision at a future International Linear Collider (ILC). The simulations for small stop-neutralino mass difference are motivated by cosmology. The precision mass determination at the future ILC is possible with a method using two center-of-mass energies, e.g. $\sqrt{s} = 260$ and 500 GeV. This method can also be applied to other analyses to improve the mass resolution in searches for new particles. The precision of two independent analysis methods, one with a sequential-cuts and the other with an Interative Discriminant Analysis (IDA) lead to very similar results. The new proposed method increases the mass precision by about a factor of three due to the error cancellation using two center-of-mass energies with one near the production threshold. Including experimental and theoretical uncertainties, the mass of a 122.5 GeV scalar top could be determined with a precision of 0.42 GeV. The interpretation of this benchmark scenario leads to a uncertainty on $_{CDM}h^2$ of $0{:}013$ and $+\,0{:}015$ which is about a factor two better compared to previous results, and comparable to current cosmological (WMAP) measurement uncertainties. With the new stop mass determination, the stop mass uncertainty is no longer the dominant uncertainty in the $_{CDM}h^2$ calculation.

Acknowledgements

We would like to thank the organizers of the 2005 and 2007 editions of the Les Houches workshops “Physics at TeV Colliders’, where part of this work was carried out.

13. Comparison of SUSY spectrum codes: the NUHM case [1]

13.1 Introduction

Recent analyses of uncertainties in SUSY spectrum calculations [156, 157] have triggered important improvements in the various spectrum codes. This concerns in particular the treatment of the top and bottom Yukawa couplings, and the finite corrections in translating $\overline{DR}$ parameters to on-shell masses and mixing angles, see e.g. [158]. Moreover, all public codes now apply full two-loop renormalization group (RG) evolution of the SUSY-breaking parameters, plus one-loop self-energy corrections for sparticle masses.

So far, comparisons of spectrum computations have concentrated on the constrained MSSM or mSUGRA models. In this contribution, we extend these studies to models with non-universal Higgs masses (NUHM). We use the most recent versions of the four public spectrum codes, ISAJET 7.75 [159, 158], SOFTSUSY 2.0.14 [97], SPHENO 2.2.3 [18] and SUSPECT 2.3 [37]. We first compare the results from the four public codes for the NUHM benchmark points of [160], hence also comparing with the private code SSARD. It turns out that there is good agreement once the different sign convention in SSARD as compared to the other codes is taken into account. Then we discuss the case of gaugino mediation, for which 10% differences in left-chiral slepton masses can occur for very large $m_{H_d}^2 \quad m_{H_u}^2$.

13.2 NUHM benchmarks

NUHM models have recently become very popular because they lead to very interesting phenomenological effects beyond the well-studied CMSSM case, see e.g. [161, 162, 163]. In general, the non-universality of the Higgs doublets can be specified either through GUT-scale masses $m_{H_u}^2$ and $m_{H_d}^2$, or though and m_A at the weak scale.[2] In particular, the group around Baer uses $m_{H_{u,d}}^2$, while the group around Ellis and Olive follows the second approach. From the four public spectrum codes, only two currently have the $(; m_A)$ approach implemented. We therefore start our discussion by reproducing the NUHM benchmark points proposed in [160] with a scan in the $m_{H_u}^2 - m_{H_d}^2$ plane.

Figure 1 shows contours of constant and m_A from the four public spectrum codes in the plane of m_{H_u} versus m_{H_d}, $m_{H_{u,d}} \quad \mathrm{sign}(m_{H_{u,d}}^2) \sqrt{|m_{H_{u,d}}^2|}$ for the NUHM benchmark scenarios , , of [160]. Each benchmark point is approximately reproduced where the respective contours of and m_A intersect. As can be seen, the solutions for the various codes lie close to each other. One can therefore also expect good agreement on the resulting physical spectrum.

That this is indeed the case is examplified in Table 1 for benchmark point . We find agreement of about 1–2% on the sparticle and Higgs masses, and about 10% on the relic density, which we compute using MICROMEGAS [98, 20] for the ISAJET, SOFTSUSY, SPHENO and SUSPECT spectra. Note also that the agreement within the public codes themselves is better than the overall agreement including SSARD, cf. Table 1. For point , there is also 1–2% agreement on the masses. For the relic density, however, the spectra of the public codes interfaced to MICROMEGAS give $h^2 \quad 0{:}07$ with 15% variation, while SSARD gives $h^2 = 0{:}1$. The source of the difference is the A-funnel annihilation cross section.

In SOFTSUSY, there is also the option to input and m_A instead of $m_{H_{u,d}}^2$ at M_{GUT}. To this aim, the progam makes an initial guess of the GUT-scale $m_{H_{u,d}}^2$ for the first iteration. For later iterations, only the EWSB-scale boundary conditions are used for $m_{H_{u,d}}^2$. The procedure works extremely well, giving exactly the same results irrespective of whether one uses GUT-scale $m_{H_{u,d}}^2$ or EWSB-scale , m_A as inputs —at least for the cases we have tried.

There is an analogous option in ISAJET, through the NUSUG keywords. However, the procedure applied is more complicated, using boundary conditions for $m_{H_{u,d}}^2$ at both the GUT and the EWSB scales. The results slightly depend on what kind of input is used. For example, for point , input of $= 375\,\mathrm{GeV}$ and $m_A = 265\,\mathrm{GeV}$ gives $m_{H_u}^2 = (250)^2\ \mathrm{GeV}^2$ and $m_{H_d}^2 = (320{:}2)^2\ \mathrm{GeV}^2$ at M_{GUT}. On the other hand, GUT-scale input of $m_{H_u}^2 = (250)^2\ \mathrm{GeV}^2$ and $m_{H_d}^2 = (320{:}2)^2\ \mathrm{GeV}^2$ gives $= 378\,\mathrm{GeV}$ and $m_A = 274{:}6\,\mathrm{GeV}$ at the weak scale.

SPHENO and SUSPECT do not yet have and m_A input for SUGRA scenarios.

---

[1] S. Kraml and S. Sekmen

[2] We take (M_{EWSB}), where M_{EWSB} is the scale of electroweak symmetry breaking, and $m_A \quad m_A(\mathrm{pole})$.

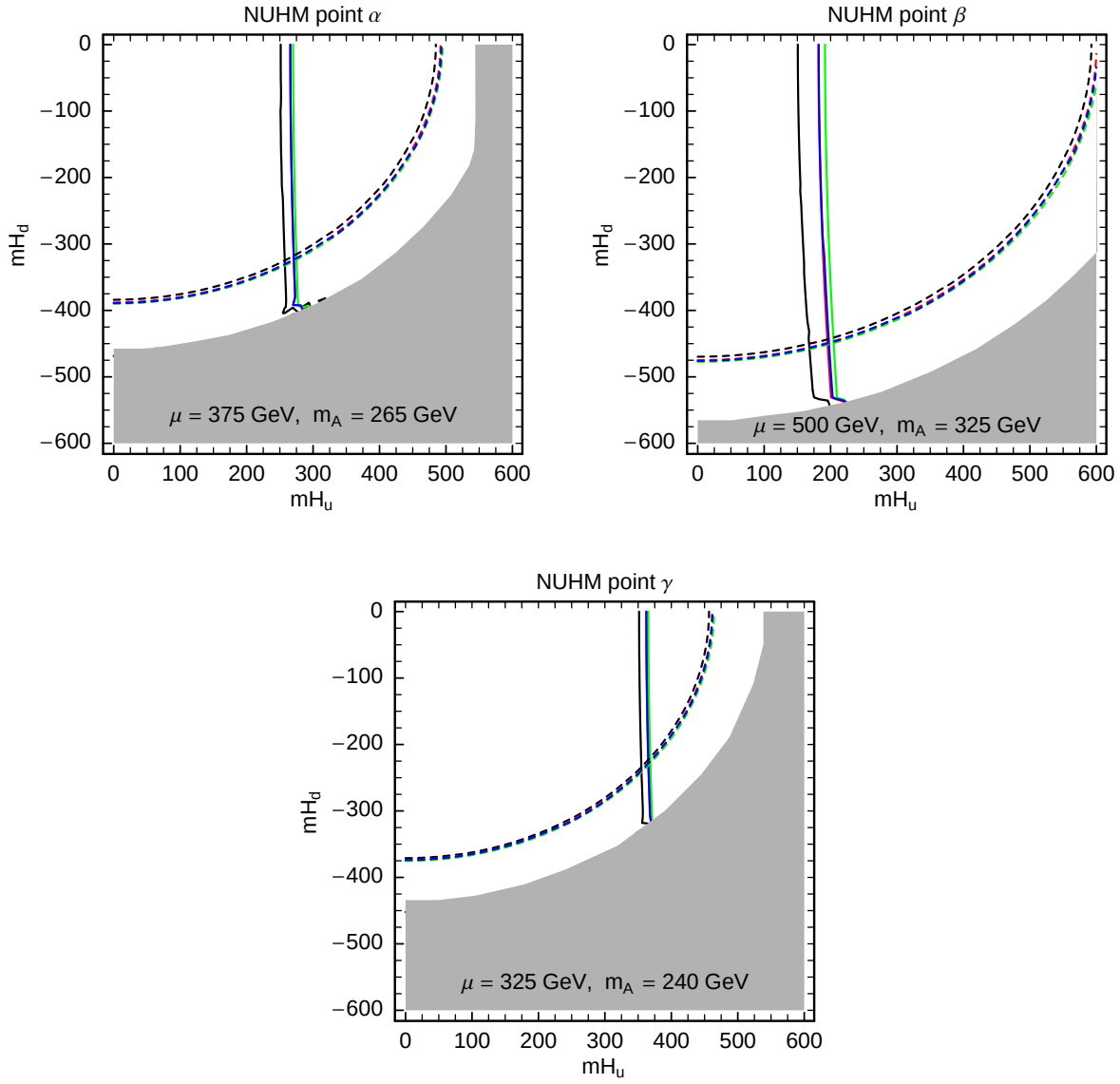

Fig. 1: Contours of constant (solid lines) and m_A (dashed lines) from the four public spectrum codes in the m_{H_u} versus m_{H_d} plane for the NUHM benchmark scenarios , , of [160]. The black, red, green and blue lines are for ISAJET, SOFTSUSY, SPHENO and SUSPECT, respectively. Each benchmark point is approximately reproduced where the respective contours of and m_A intersect. In the grey areas no solution is obtained.

	SSARD [160]	ISAJET	SOFTSUSY	SPHENO	SUSPECT	[%]
$m^2_{H_u}(M_{GUT})$	$(333)^2$	$+(257.4)^2$	$+(271.0)^2$	$+(275.0)^2$	$+(271.1)^2$	
$m^2_{H_d}(M_{GUT})$	$+(294)^2$	$(325.0)^2$	$(323.6)^2$	$(323.7)^2$	$(323.7)^2$	
h^0	115	112.0	112.5	112.7	112.5	2.66
H^0	266	265.0	265.0	265.7	265.7	0.38
A^0	265	265.0	265.0	265.0	265.0	—
H^+	277	280.0	277.0	277.1	277.1	1.08
$\tilde{u}_R$	637	647.2	644.9	646.3	643.9	1.58
$\tilde{u}_L$	648	659.7	653.1	659.3	656.1	1.79
$\tilde{d}_R$	630	639.3	633.2	638.1	635.8	1.46
$\tilde{d}_L$	653	664.8	659.3	663.9	660.8	1.79
$\tilde{t}_1$	471	475.1	475.5	477.1	476.9	1.28
$\tilde{t}_2$	652	655.3	652.7	654.9	655.1	0.50
$\tilde{b}_1$	590	599.7	591.9	594.4	597.8	1.63
$\tilde{b}_2$	629	637.4	630.5	637.0	635.4	1.33
$\tilde{e}_R$	216	218.8	219.3	218.9	218.1	1.51
$\tilde{e}_L$	296	296.9	296.7	296.7	295.1	0.61
$\tilde{\nu}_e$	285	285.1	285.2	285.7	284.6	0.39
$\tilde{\tau}_1$	212	216.3	215.9	215.4	214.8	2.00
$\tilde{\tau}_2$	298	297.9	298.3	298.3	296.8	0.50
$\tilde{\nu}_\tau$	285	284.0	284.9	285.4	284.3	0.49
$\tilde{\chi}^0_1$	115	112.4	111.7	111.9	112.2	1.16
$\tilde{\chi}^0_2$	212	208.2	207.8	208.1	208.2	2.01
$\tilde{\chi}^0_3$	388	380.3	383.8	381.7	380.6	2.01
$\tilde{\chi}^0_4$	406	401.3	401.5	400.7	400.9	1.32
$\tilde{\chi}^+_1$	212	208.3	209.0	207.7	207.6	2.11
$\tilde{\chi}^+_2$	408	400.4	398.1	401.5	400.9	2.45
$\tilde{g}$	674	691.2	687.7	685.6	688.7	2.51
h^2	0.12	0.109	0.114	0.111	0.108	10.68

Table 1: Comparison of results for NUHM benchmark point given by $m_0 = 210$ GeV, $m_{1=2} = 285$ GeV, $A_0 = 0$, $\tan = 10$, $m_t = 178$ GeV, $= 375$ GeV and $m_A = 265$ GeV.

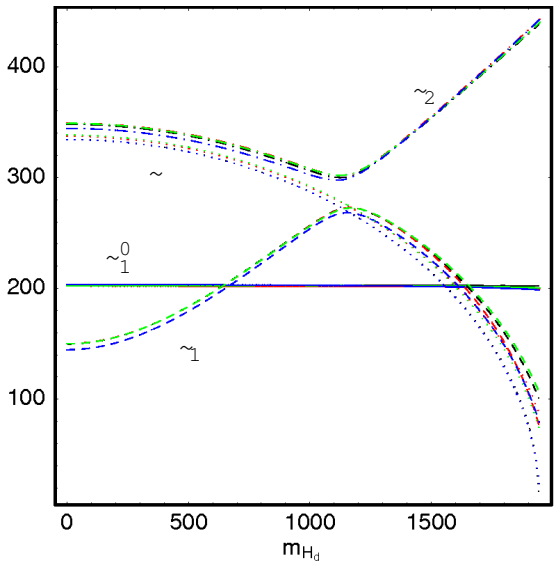

Fig. 2: Neutralino, stau and tau-sneutrino masses (in GeV) from the four public spectrum codes as a function of m_{H_d}, for $m_{1/2} = 500$ GeV, $\tan\beta = 10$, $m_0 = A_0 = m_{H_u} = 500$. The black, red, green and blue lines are for ISAJET, SOFTSUSY, SPHENO and SUSPECT, respectively.

13.3 Slepton masses in gaugino mediation

In general, in SUSY-breaking models with universal scalar and gaugino masses, the right-chiral charged sleptons, $\tilde{\ell}_R$, are lighter than the left-chiral ones and the sneutrinos, $\tilde{\ell}_L$ and $\tilde{\nu}_\ell$ ($\ell = e, \mu, \tau$). However, owing to D-term contributions in the RG evolution, for large enough $m^2_{H_d} - m^2_{H_u} > 0$, $\tilde{\ell}_L$ and/or $\tilde{\nu}_\ell$ can become lighter than $\tilde{\ell}_R$, and even lighter than the $\tilde{\chi}_1^0$ [161, 162, 163]. In such a setup, if R parity is conserved, the lightest SUSY particle (LSP) should be a gravitino or axino, and the next-to-lightest one (NLSP) a $\tilde{\tau}_1$ or $\tilde{\nu}_\tau$. This has recently attracted quite some interest in the context of gaugino mediation [164, 165, 166, 167].

In gaugino mediation [168, 169], gauge couplings and gaugino masses each unify at the compactification scale M_C, while there are no-scale boundary conditions for sfermion masses and trilinear couplings, i.e. $m_0 = A_0 = 0$) [169]. The free parameters of the model are hence $m_{1/2}$, $m^2_{H_u}$, $m^2_{H_d}$, $\tan\beta$, and the sign of μ; $|\mu|$being determined by radiative electroweak symmetry breaking. Following [164, 165, 166, 167], we take $M_C = M_{GUT}$ and $m_t = 172.5$ GeV.

Figure 2 shows the $\tilde{\chi}_1^0$, $\tilde{\tau}_{1,2}$ and $\tilde{\nu}_\tau$ masses as a function of m_{H_d}, for $m_{1/2} = 500$ GeV, $\tan\beta = 10$, $m_{H_u} = 500$.[3] As can be seen, for $m_{H_d} \lesssim 1.2$ TeV, the left-ciral sleptons become lighter than the right-chiral ones; for $m_{H_d} \lesssim 1.6$ TeV, they are lighter than the lightest neutralino. Moreover, there is an overall good agreement between the codes. Only for very large $m^2_{H_d} - m^2_{H_u}$, when there are large D-term corrections, the differences in the left-chiral slepton masses reach $\sim 10\%$. This is also the region where the stau or sneutrino is the (pseudo) LSP. Explicit numbers are given in Tables 2 and 3 for $m_{H_d} = 900$ GeV and 1.8 TeV, respectively. Note also that there is ~ 3–4% difference in μ. The masses of coloured sparticles and Higgs bosons are not shown due to lack of space; they agree to $\sim 1\%$ or better.

13.4 Conclusions

We have compared results of the latest versions of the public SUSY spectrum codes ISAJET, SOFTSUSY, SPHENO and SUSPECT for models with non-universal Higgs masses. We find very good agreement for the mass spectra and the resulting h^2. Only for edges of parameter space, the differences in the most sensitive masses become large. For instance, we have found differences in slepton masses of the order of 10% for large $m^2_{H_d} - m^2_{H_u}$.

[3] In SUSPECT we use $m_0 = 10^3$, since this code does not give a spectrum for $m_0 \lesssim 0$.

	ISAJET	SOFTSUSY	SPHENO	SUSPECT	m [%]
$\tilde{e}_R$	253.6	256.7	256.7	254.1	1.25
$\tilde{e}_L$	318.8	317.4	316.7	311.4	2.34
$\tilde{\nu}_e$	304.8	305.2	306.4	301.5	1.61
$\tilde{\tau}_1$	241.3	241.1	240.9	238.2	1.29
$\tilde{\tau}_2$	313.7	315.7	315.2	310.0	1.82
$\tilde{\nu}_\tau$	296.6	300.4	301.6	296.7	1.67
$\tilde{\chi}_1^0$	203.0	201.8	202.6	202.8	0.59
$\tilde{\chi}_2^0$	364.4	365.6	367.8	367.2	0.93
$\tilde{\chi}_3^0$	463.5	477.3	481.2	477.7	3.73
$\tilde{\chi}_4^0$	500.2	508.4	513.4	511.1	2.6
$\tilde{\chi}_1^\pm$	365.0	367.3	367.3	366.3	0.63
$\tilde{\chi}_2^\pm$	499.1	504.9	513.1	510.2	2.76

Table 2: Comparison of neutralino, chargino, and slepton masses for a gaugino-mediation scenario with $m_0 = A_0 = 0$, $m_{1=2} = 500$ GeV, $\tan\beta = 10$, $m_{H_u} = 500$ and $m_{H_d} = 900$ GeV.

	ISAJET	SOFTSUSY	SPHENO	SUSPECT	m [%]
$\tilde{e}_R$	432.1	436.2	433.8	436.0	0.94
$\tilde{e}_L$	199.4	182.7	192.3	180.1	10.23
$\tilde{\nu}_e$	170.3	179.9	175.0	162.5	10.12
$\tilde{\tau}_1$	159.9	151.1	163.4	148.6	9.5
$\tilde{\tau}_2$	410.5	413.3	411.1	413.0	0.68
$\tilde{\nu}_\tau$	130.6	149.5	144.5	148.6	13.19
$\tilde{\chi}_1^0$	202.5	200.9	201.3	200.1	1.19
$\tilde{\chi}_2^0$	351.7	353.6	357.2	356.4	1.55
$\tilde{\chi}_3^0$	425.3	439.4	444.5	440.9	4.39
$\tilde{\chi}_4^0$	474.9	481.1	486.7	484.6	2.45
$\tilde{\chi}_1^\pm$	351.8	355.6	356.2	355.0	1.24
$\tilde{\chi}_2^\pm$	473.0	478.9	486.3	483.6	2.77

Table 3: Same as Table 2 but for $m_{H_d} = 1.8$ TeV.

Acknowledgements

SS acknowledges the support by TÜBİTAK grant 106T457 (TBAG-HD 190).

14. The SLHA2 Conventions [1]

14.1 Introduction

The states and couplings appearing in the general minimal supersymmetric standard model (MSSM) can be defined in a number of ways. In principle, this is not a problem, as translations between different conventions can usually be carried out without ambiguity. From the point of view of practical application, however, such translations are, at best, tedious, and at worst they introduce an unnecessary possibility for error. To deal with this problem, and to create a more transparent situation for non-experts, the original SUSY Les Houches Accord (SLHA1) was proposed [72]. However, SLHA1 was designed exclusively with the MSSM with real parameters and R-parity conservation in mind. We here summarize conventions [170] relevant for R-parity violation (RPV), flavour violation, and CP-violation (CPV) in the minimal supersymmetric standard model. We also consider next-to-minimal models which we shall collectively label NMSSM. For simplicity, we still limit the scope of the SLHA2 in two regards: for the MSSM, we restrict our attention to *either* CPV or RPV, but not both. For the NMSSM, we define one catch-all model and extend the SLHA1 mixing only to include the new states, with CP, R-parity, and flavour still assumed conserved. For brevity, this document only describes our convention choices and not the full ASCII data structures that go with them (these are the focus of a complementary summary [171]). The complete SLHA2 is described in detail in [170].

14.2 Extensions of SLHA1

Firstly, we allow for using either the A^0 or H^+ pole masses, respectively, as input instead of the parameter $m_A^2(M_{input})$ defined in [72]. Secondly, we also optionally allow for different parameters to be defined at different scales (e.g., defined at M_{EWSB}, the remaining parameters defined at M_{input}).

To define the general properties of the model, we introduce new global switches for field content (either MSSM or NMSSM), RPV (either off or on), CPV (either no CPV, just the CKM phase, or general CPV), and flavour violation (either no flavour violation or quark and/or lepton flavour violation).

Also note the recent proposal [172] for a joint SLHA+LHEF (Les Houches Event File [173]) format for BSM event generation.

14.3 Flavour violation

In the Super-CKM basis of the squarks [174], the quark mass matrix is diagonal, and the squarks are rotated in parallel to their superpartners. This implies that only physically measurable parameters are present. Actually, once the electroweak symmetry is broken, a rotation in flavour space

$$D^\circ = V_d D\,; \qquad U^\circ = V_u U\,; \qquad D^\circ = U_d D\,; \qquad U^\circ = U_u U\,; \tag{1}$$

of all matter superfields in the (s)quark superpotential

$$W_Q = \epsilon_{ab}\left[(Y_D)_{ij} H_1^a Q_i^{b\circ} D_j^\circ + (Y_U)_{ij} H_2^b Q_i^{a\circ} U_j^\circ\right] \tag{2}$$

brings fermions from the interaction eigenstate basis $\{d_L^\circ, u_L^\circ, d_R^\circ, u_R^\circ\}$ to their mass eigenstate basis $\{d_L, u_L, d_R, u_R\}$: $d_L^\circ = V_d d_L$, $u_L^\circ = V_u u_L$, $d_R^\circ = U_d d_R$, $u_R^\circ = U_u u_R$, and the scalar superpartners to the basis $\{\tilde{d}_L, \tilde{u}_L, \tilde{d}_R, \tilde{u}_R\}$. Through this rotation, the Yukawa matrices Y_D and Y_U are reduced to their diagonal form $\hat{Y}_D$ and $\hat{Y}_U$:

$$(\hat{Y}_D)_{ii} = (U_d^y Y_D^T V_d)_{ii} = \frac{\sqrt{2} m_{di}}{v_1}\,; \qquad (\hat{Y}_U)_{ii} = (U_u^y Y_U^T V_u)_{ii} = \frac{\sqrt{2} m_{ui}}{v_2}\,: \tag{3}$$

Tree-level mixing terms among quarks of different generations are due to the misalignment of V_d and V_u, expressed via the CKM matrix [175, 176], $V_{CKM} = V_u^y V_d$, which is proportional to the tree-level $u_{Li} d_{Lj} W^+$, $u_{Li} d_{Rj} H^+$, and $u_{Ri} d_{Lj} H^+$ couplings ($i,j = 1,2,3$).

In the super-CKM basis the 6×6 mass matrices for the up- and down-type squarks are defined as

$$L_{\tilde{q}}^{mass} = \ldots\, {}^y_u M^2_{\tilde{u}}\, u \ldots\, {}^y_d M^2_{\tilde{d}}\, d\,; \tag{4}$$

[1] participating/corresponding authors: B.C. Allanach, P. Skands and P. Slavich

where $\psi_u = (\tilde{u}_L, \tilde{c}_L, \tilde{t}_L, \tilde{u}_R, \tilde{c}_R, \tilde{t}_R)^T$ and $\psi_d = (\tilde{d}_L, \tilde{s}_L, \tilde{b}_L, \tilde{d}_R, \tilde{s}_R, \tilde{b}_R)^T$. We diagonalise the squark mass matrices via 6×6 unitary matrices $R_{u,d}$, such that $R_{u,d} M^2_{\tilde{u},\tilde{d}} R^\dagger_{u,d}$ are diagonal matrices with increasing mass squared values. The flavour-mixed mass matrices read:

$$M^2_{\tilde{u}} = \begin{pmatrix} V_{CKM}\, \hat{m}^2_{\tilde{Q}}\, V^\dagger_{CKM} + m_u^2 + D_{uLL} & \frac{v_2}{\sqrt{2}} \hat{T}^\dagger_U - m_u \cot\beta \\ \frac{v_2}{\sqrt{2}} \hat{T}_U - m_u \cot\beta & \hat{m}^2_{\tilde{u}} + m_u^2 + D_{uRR} \end{pmatrix}; \tag{5}$$

$$M^2_{\tilde{d}} = \begin{pmatrix} \hat{m}^2_{\tilde{Q}} + m_d^2 + D_{dLL} & \frac{v_1}{\sqrt{2}} \hat{T}^\dagger_D - m_d \tan\beta \\ \frac{v_1}{\sqrt{2}} \hat{T}_D - m_d \tan\beta & \hat{m}^2_{\tilde{d}} + m_d^2 + D_{dRR} \end{pmatrix}. \tag{6}$$

In the equations above we introduced the 3×3 matrices

$$\hat{m}^2_{\tilde{Q}} \equiv V_d^\dagger m^2_{\tilde{Q}} V_d\,; \quad \hat{m}^2_{\tilde{u},\tilde{d}} \equiv U^\dagger_{u,d} m^{2\,T}_{\tilde{u},\tilde{d}} U_{u,d}\,; \quad \hat{T}_U \equiv U_u^\dagger T_U^T V_u\,; \quad \hat{T}_D \equiv U_d^\dagger T_D^T V_d\,; \tag{7}$$

where the un-hatted mass matrices $m^2_{Q,u,d}$ and trilinear interaction matrices $T_{U,D}$ are given in the electroweak basis of [72], in which the soft SUSY-breaking potentials V_3 and V_2 have the following forms:

$$V_3 = \sum_{ab} \sum_{ij} \Big[(T_E)_{ij} H_1^a \tilde{L}^b_{i_L} \tilde{e}_{j_R} + (T_D)_{ij} H_1^a \tilde{Q}^b_{i_L} \tilde{d}_{j_R} + (T_U)_{ij} H_2^b \tilde{Q}^a_{i_L} \tilde{u}_{j_R} \Big] + h.c.; \tag{8}$$

$$V_2 = m^2_{H_1} H_{1a} H_1^a + m^2_{H_2} H_{2a} H_2^a + \tilde{Q}^*_{i_L a} (m^2_{\tilde{Q}})_{ij} \tilde{Q}^a_{j_L} + \tilde{L}^*_{i_L a} (m^2_{\tilde{L}})_{ij} \tilde{L}^a_{j_L} + \tilde{u}^*_{i_R} (m^2_{\tilde{u}})_{ij} \tilde{u}_{j_R} + \tilde{d}^*_{i_R} (m^2_{\tilde{d}})_{ij} \tilde{d}_{j_R} + \tilde{e}^*_{i_R} (m^2_{\tilde{e}})_{ij} \tilde{e}_{j_R} - (m^2_3)_{ab} H_1^a H_2^b + h.c.). \tag{9}$$

The matrices $m_{u,d}$ are the diagonal up-type and down-type quark masses and $D_{fLL,RR}$ are the D-terms given by:

$$D_{fLL,RR} = \cos 2\beta \left(m_Z^2 \left(T_f^3 - Q_f \sin^2\theta_W \right) \right) \mathbb{1}_3\,; \tag{10}$$

which are also flavour diagonal, and Q_f is the electric charge of the left-handed chiral supermultiplet to which the squark belongs, i.e., it is $2/3$ for U and $-2/3$ for U^c. Note that the up-type and down-type squark mass matrices in eqs. (5) and (6) cannot be simultaneously flavour-diagonal unless $\hat{m}^2_{\tilde{Q}}$ is flavour-universal.

For the lepton sector, we adopt a super-PMNS basis and cover all cases that lead to a low energy effective field theory with Majorana neutrino masses and one sneutrino per family. In terms of this low energy effective theory, the lepton mixing phenomenon is analogous to the quark mixing case. After electroweak symmetry breaking, the neutrino sector of the MSSM contains the Lagrangian pieces

$$L = -\frac{1}{2} \nu^{oT} (m_\nu) \nu^o + h.c.; \tag{11}$$

where m_ν is a 3×3 symmetric matrix. The interaction eigenstate basis neutrino fields ν^o are related to the mass eigenstate ones ν by $\nu^o = V_\nu \nu$, reducing the mass matrix m_ν to its diagonal form $\hat{m}_\nu$

$$(\hat{m}_\nu)_{ii} = (V_\nu^T m_\nu V_\nu)_{ii} = m_{\nu_i}. \tag{12}$$

The charged lepton fields have a 3×3 Yukawa coupling matrix defined in the superpotential piece [72]

$$W_E = \sum_{ab} (Y_E)_{ij} H_1^a L_i^b E^o_j; \tag{13}$$

where the charged lepton interaction eigenstates $\{e^o_L, e^o_R\}$ are related to the mass eigenstates by $e^o_L = V_e e_L$ and $e^o_R = U_e e_R$. The equivalent diagonalised charged lepton Yukawa matrix is

$$(\hat{Y}_E)_{ii} = (U_e^\dagger Y_E^T V_e)_{ii} = \frac{\sqrt{2} m_{ei}}{v_1}. \tag{14}$$

Lepton mixing in the charged current interaction can then be characterised by the PMNS matrix [177, 178], $U_{PMNS} = V_e^\dagger V_\nu$, which is proportional to the tree-level $e_{Li}\nu_j W^-$ and $e_{Ri}\nu_j H^-$ couplings.

Rotating the interaction eigenstates of the sleptons identically to their leptonic counterparts, we obtain the super-PMNS basis for the charged sleptons and the sneutrinos, described by the Lagrangian (neglecting the possible term $\tilde{\nu}^T M^{\hat{}\,2}_{\tilde{\nu}} \tilde{\nu}$)

$$L_I^{mass} = -\tilde{e}^\dagger M^2_{\tilde{e}} \tilde{e} - \tilde{\nu}^\dagger M^2_{\tilde{\nu}} \tilde{\nu}; \tag{15}$$

where $\quad = (\tilde{e}_{;}\tilde{\ } ;\tilde{\ })^{T}$ and $\ _{e} = (e_{L} ;\tilde{}_{L} ;\tilde{}_{L} ;e_{R} ;\tilde{}_{R})^{T}$. $M\ ^{2}_{e}$ is the $6\quad 6$ matrix

$$M\ ^{2}_{e} = \begin{pmatrix} \hat{m}\ ^{2}_{L} + m\ ^{2}_{e} + D_{eLL} & \frac{v_1}{\sqrt{2}}\hat{T}^{y}_{E} \\ \frac{v_1}{\sqrt{2}}\hat{T}_{E} & m_e \tan \end{pmatrix} \quad m_e \tan \quad \hat{m}\ ^{2}_{e} + m\ ^{2}_{e} + D_{eRR} \quad ; \tag{16}$$

and $M\ ^{2}_{\tilde{}}$ is the $3\quad 3$ matrix

$$M\ ^{2}_{\tilde{}} = U^{y}_{PMNS}\, \hat{m}\ ^{2}_{L}\, U_{PMNS} + D\ _{LL} ; \tag{17}$$

where D_{eLL} and $D\ _{LL}$ are given in eq. (10). In the equations above we introduced the $3\quad 3$ matrices

$$\hat{m}\ ^{2}_{L} \quad V^{y}_{e}\, m\ ^{2}_{L}\, V_e ; \quad \hat{m}\ ^{2}_{e} \quad U^{y}_{e}\, m\ ^{2^{T}}_{e}\, U_e ; \quad \hat{T}_{E} \quad U^{y}_{e}\, T^{T}_{E}\, V_e ; \tag{18}$$

where the un-hatted matrices $m\ ^{2}_{L,e}$ and T_E are given in the interaction basis of ref. [72]. We diagonalise the charged slepton and sneutrino mass matrices via the unitary $6\quad 6$ and $3\quad 3$ matrices $R_{\tilde{e}}$, respectively. Thus, R_{e}; $M\ ^{2}_{e;\tilde{}} R^{y}_{e;}$ are diagonal with increasing entries toward the bottom right of each matrix.

14.4 R-parity violation

We write the R-parity violating superpotential in the interaction basis as

$$W_{RPV} \quad {}_{ab}\ \frac{1}{2}\ _{ijk} L^{a}_{i} L^{b}_{j} E_{k} + \ ^{0}_{ijk} L^{a}_{i} Q^{bx}_{j} D_{kx} \quad {}_{i} L^{a}_{i} H^{b}_{2} + \frac{1}{2}\ ^{00}_{ijk}\ _{xyz} U^{x}_{i} D^{y}_{j} D^{z}_{k} ; \tag{19}$$

where $x;y;z = 1;:::;3$ are fundamental SU(3)$_C$ indices and ^{xyz} is the antisymmetric tensor in 3 dimensions with $^{123} = +1$. In eq. (19), $_{ijk}$; $^{0}_{ijk}$ and $_{i}$ break lepton number, whereas $^{00}_{ijk}$ violate baryon number. To ensure proton stability, either lepton number conservation or baryon number conservation is usually still assumed, resulting in either $_{ijk} = \ ^{0}_{ijk} = \ _{i} = 0$ or $\ ^{00}_{ijk} = 0$ for all $i;j;k = 1;2;3$.

The trilinear R-parity violating terms in the soft SUSY-breaking potential are

$$V_{3;RPV} \quad {}_{ab}\ \frac{1}{2}(T\ )_{ijk} \tilde{L}^{a}_{iL} \tilde{L}^{b}_{jL} e_{kR} + (T^{\ 0})_{ijk} \tilde{L}^{a}_{iL} \tilde{Q}^{b}_{jL} d_{kR} \quad + \frac{1}{2}(T^{\ 00})_{ijk}\ _{xyz} \tilde{d}^{x}_{iR} \tilde{d}^{y}_{jR} \tilde{d}^{z}_{kR} + h.c. : \tag{20}$$

Note that we do not factor out the couplings (e.g. as in $T_{ijk} = \ _{ijk} \quad A\ _{;ijk}$) in order to avoid potential problems with $_{ijk} = 0$ but $T_{ijk} \neq 0$. This usage is consistent with the convention for the R-conserving sector elsewhere in this report.

The bilinear R-parity violating soft terms (all lepton number violating) are

$$V_{2;RPV} \quad {}_{ab} D_{i} \tilde{L}^{a}_{iL} H^{b}_{2} + \tilde{L}^{y}_{iaL}\, m\ ^{2}_{\tilde{L}_i H_1}\, H^{a}_{1} + h.c. : \tag{21}$$

When lepton number is not conserved the sneutrinos may acquire vacuum expectation values (VEVs) $h\tilde{}_{e;\ ;}\ i \quad v_{e;\ ;} = \sqrt{2}$. We generalise the SLHA1 parameter v to:

$$v = \sqrt{v_1^2 + v_2^2 + v_e^2 + v^2 + v^2} = 246\ GeV : \tag{22}$$

The addition of sneutrino VEVs allows for various different definitions of $\tan$, but we here choose to keep the SLHA1 definition $\tan = v_2/v_1$.

We use the super-CKM/PMNS basis throughout, as defined in subsection 14.3, with the following considerations specific to the R-parity violating case. Firstly, the d-quark mass matrices are given by

$$(m_d)_{ij} = (Y_D\ )_{ij} v_1 + \ ^{0}_{kij} v_k : \tag{23}$$

where v_k are the sneutrino VEVs. Secondly, in the lepton number violating case, we restrict our attention to scenarios in which there are no right-handed neutrinos and, thus, neutrino masses are generated solely by the RPV couplings. In this case, the PMNS matrix is not an independent input but an output.

We define the super-CKM basis as the one where the Yukawa couplings Y_D and Y_U are diagonal. The PMNS basis is defined as the basis where Y_E is diagonal and the loop-induced neutrino mass matrix is diagonalised.

In this way one obtains a uniquely defined set of parameters:

$$\hat{}_{ijk} \quad {}_{rst}V^{*}{}_{;ri}V_{e;sj}U^{y}_{e;tk} \; ; \tag{24}$$

$$\hat{}^{0}_{ijk} \quad {}^{0}_{rst}V^{*}{}_{;ri}V_{d;sj}U^{y}_{d;tk} \; ; \tag{25}$$

$$\hat{}_{i} \quad {}_{r}V_{e;ri} \; ; \tag{26}$$

$$\hat{}^{00}_{ijk} \quad {}^{00}_{rst}U^{y}_{u;ri}U^{y}_{d;sj}U^{y}_{d;tk} \; ; \tag{27}$$

where the fermion mixing matrices are defined in subsection 14.3. The Lagrangian for the quark-slepton interactions then takes the following form:

$$L = \hat{}^{0}_{ijk}\tilde{}_{i}d_{R\,k}d_{L\,j} + \hat{}^{0}_{rsk}U^{y}_{P\,M\,N\,S;ri}V^{y}_{C\,K\,M\;;sj}\tilde{L}_{i}d_{R\,k}u_{L\,j} + h\!:\!c\!:\!: \tag{28}$$

Similarly one obtains the soft SUSY breaking couplings in this basis by replacing the superpotential quantities in eqs. (24)–(27) by the corresponding soft SUSY breaking couplings. In addition we define:

$$m^{2}_{\tilde{L}_{i}H_{1}} \quad V^{y}_{e;ir}m^{2}_{\tilde{L}_{r}H_{1}} \; : \tag{29}$$

As for the R-conserving MSSM, the bilinear terms (both SUSY-breaking and SUSY-respecting ones, including) and the VEVs are not independent parameters. Specifically, out of the 12 parameters $_{i}$, D_{i}, sneutrino vevs, and $m^{2}_{\tilde{L}_{i}H_{1}}$, only 9 are independent.

Particle mixing

In general, the neutrinos mix with the neutralinos. This requires a change in the definition of the $4 \quad 4$ neutralino mixing matrix N to a $7 \quad 7$ matrix. The Lagrangian contains the (symmetric) neutrino/neutralino mass matrix as

$$L^{mass}_{\tilde{}^{0}} = \frac{1}{2}\tilde{}^{0T}M_{\tilde{}^{0}}\tilde{}^{0} + h\!:\!c\!:; \tag{30}$$

in the basis of 2–component spinors $\tilde{}^{0} = (\ _{e}; \ ; \ ; \ \tilde{b}; \ i\tilde{w}^{3};\tilde{h}_{1};\tilde{h}_{2})^{T}$. We define the unitary $7 \quad 7$ neutrino/neutralino mixing matrix N, such that:

$$\frac{1}{2}\tilde{}^{0T}M_{\tilde{}^{0}}\tilde{}^{0} = \frac{1}{2}\underbrace{\tilde{}^{0T}N^{T}}_{\tilde{}^{0T}}\underbrace{N^{*}M_{\tilde{}^{0}}N^{y}}_{diag(m_{\tilde{}^{0}})}\underbrace{N\tilde{}^{0}}_{\tilde{}^{0}} \; ; \tag{31}$$

where the 7 (2–component) generalised neutrinos $\tilde{}^{0} = (\ _{1};:::;\ _{7})^{T}$ are defined strictly mass-ordered.

In the limit of CP conservation, the default convention is that N be a real matrix and one or more of the mass eigenstates may have an apparent negative mass. The minus sign may be removed by phase transformations on $\tilde{}^{0}_{i} \quad _{i}$ as explained in SLHA1 [72].

Charginos and charged leptons may also mix in the case of L-violation. In a similar spirit to the neutralino mixing, we define

$$L^{mass}_{\tilde{}^{+}} = \frac{1}{2}\tilde{} \ {}^{T}M_{\tilde{}^{+}}\tilde{}^{+} + h\!:\!c\!:; \tag{32}$$

in the basis of 2–component spinors $\tilde{}^{+} = (e^{+}; \ ^{+}; \ ^{+}; \ i\tilde{w}^{+};\tilde{h}^{+}_{2})^{T}$, $\tilde{} \ = (e \ ; \ \ ; \ \ ; \ i\tilde{w} \ ;\tilde{h}_{1} \ )^{T}$ where $\tilde{w} \ = (\tilde{w}^{1} \quad \tilde{w}^{2})=\sqrt{2}$. Note that, in the limit of no RPV the lepton fields are mass eigenstates.

We define the unitary $5 \quad 5$ charged fermion mixing matrices $U;V$ such that:

$$\frac{1}{2}\tilde{} \ {}^{T}M_{\tilde{}^{+}}\tilde{}^{+} = \frac{1}{2}\underbrace{\tilde{} \ {}^{T}U^{T}}_{\tilde{} \ {}^{T}}\underbrace{U^{*}M_{\tilde{}^{+}}V^{y}}_{diag(m_{\tilde{}^{+}})}\underbrace{V\tilde{}^{+}}_{\tilde{}^{+}} \; ; \tag{33}$$

where the generalised charged leptons $\tilde{}^{+} \quad (\tilde{e}^{+}_{1};e^{+}_{2};e^{+}_{3};e^{+}_{4};e^{+}_{5})$ are defined as strictly mass ordered. In the limit of CP conservation, U and V are chosen to be real by default.

R-parity violation via lepton number violation implies that the sneutrinos can mix with the Higgs bosons. In the limit of CP conservation the CP-even (-odd) Higgs bosons mix with real (imaginary) parts of the sneutrinos. We write the neutral scalars as $\sqrt{2}^{0} \quad \sqrt{2}<(H^{0}_{1};H^{0}_{2};\tilde{}_{e};\tilde{} \ ;\tilde{} \ )^{T}$, with the mass term

$$L = \frac{1}{2}\ {}^{0T}M^{2}{}_{0}\ {}^{0} \; ; \tag{34}$$

where M^2_0 is a 5×5 symmetric mass matrix. We define the orthogonal 5×5 mixing matrix $@$ by

$$ {}^{0T}M^2_0\,{}^0 = \underbrace{{}^{0T}@^T}_{{}^{0T}} \underbrace{@M^2_0@^T}_{\mathrm{diag}(m^2_0)} \underbrace{@\,{}^0}_{{}^0} ; \tag{35} $$

where ${}^0 \equiv (h^0_1; h^0_2; h^0_3; h^0_4; h^0_5)$ are the neutral scalar mass eigenstates in strictly increasing mass order.

We write the neutral pseudo-scalars as ${}^0 \equiv \sqrt{2}\,(H^0_1; H^0_2; \tilde{\nu}_e; \tilde{\nu}_\mu; \tilde{\nu}_\tau)^T$, with the mass term

$$ L = \frac{1}{2}\,{}^{0T}M^2_0\,{}^0 ; \tag{36} $$

where M^2_0 is a 5×5 symmetric mass matrix. We define the 4×5 mixing matrix $@$ by

$$ {}^{0T}M^2_0\,{}^0 = \underbrace{{}^{0T}@^T}_{{}^{0T}} \underbrace{@M^2_0@^T}_{\mathrm{diag}(m^2_0)} \underbrace{@\,{}^0}_{{}^0} ; \tag{37} $$

where ${}^0 \equiv (A^0_1; A^0_2; A^0_3; A^0_4)$ are the pseudoscalar mass eigenstates, again in increasing mass order.

The charged sleptons and charged Higgs bosons also mix in the 8×8 mass squared matrix M^2 which we diagonalize by a 7×8 matrix C:

$$ L = \underbrace{(H^-_1; H^-_2; \tilde{e}_{L_i}; \tilde{e}_{R_j})}_{{}^+} C^y \underbrace{CM^2C^y}_{\mathrm{diag}(M^2)} C \begin{pmatrix} H^+_1 \\ H^+_2 \\ \tilde{e}_{L_k} \\ \tilde{e}_{R_l} \end{pmatrix} ; \tag{38} $$

where $i; j; k; l \in \{1; 2; 3\}$ and ${}^+ \equiv {}^{y} \equiv (h^+_1; h^+_2; h^+_3; h^+_4; h^+_5; h^+_6; h^+_7)$.

R-parity violation may also generate contributions to down-squark mixing via additional left-right mixing terms,

$$ \frac{1}{\sqrt{2}} v_l \hat{T}^y_{D,ij} \qquad m_{d,i} \tan \beta_{ij} + \frac{v_k}{\sqrt{2}} \hat{T}^y_{0,kij} \tag{39} $$

where v_k are the sneutrino vevs. However, this only mixes the six down-type squarks amongst themselves and so is identical to the effects of flavour mixing. This is covered in subsection 14.3.

14.5 CP violation

In general, we write complex parameters in terms of their real and imaginary parts, rather than in terms of phase and modulus. (The SLHA1 data structures are then understood to refer to the real parts, and the imaginary parts are provided in data blocks of the same name but prefaced by `IM`.) The defaults for all imaginary parameters will be zero.

One special case is the μ parameter. When $|\mu|$ is determined by the conditions for electroweak symmetry breaking, only the phase ϕ_μ is taken as an input parameter, see [170].

When CP symmetry is broken, quantum corrections cause mixing between the CP-even and CP-odd Higgs states. Writing the neutral scalar interaction eigenstates as ${}^0 \equiv \sqrt{2}\,(<H^0_1; <H^0_2; =H^0_1; =H^0_2)^T$ we define the 3×4 mixing matrix S by

$$ {}^{0T}M^2_0\,{}^0 = \underbrace{{}^{0T}S^T}_{{}^{0T}} \underbrace{SM^2_0S^y}_{\mathrm{diag}(m^2_0)} \underbrace{S\,{}^0}_{{}^0} ; \tag{40} $$

where ${}^0 \equiv (h^0_1; h^0_2; h^0_3)^T$ are the mass eigenstates.

For the neutralino and chargino mixing matrices, the default convention in SLHA1 is that they be real. One or more mass eigenvalues may then have an apparent negative sign, which can be removed by a phase transformation on $\tilde{\chi}_i$ as explained in SLHA1 [72]. When going to CPV, the reason for introducing the negative-mass convention in the first place, namely maintaining the mixing matrices strictly real, disappears. In the CP violating case, we therefore take all masses real and positive, with N, U, and V complex.

14.6 The next-to-minimal supersymmetric standard model

We write the most general CP conserving NMSSM superpotential as:

$$W_{NMSSM} = W_{MSSM} \quad _{ab} SH_1^a H_2^b + \frac{1}{3} S^3 + {}^0 S^2 + {}_F S \; ; \tag{41}$$

where W_{MSSM} is the MSSM superpotential, in the conventions of ref. [72, eq. (3)]. A non-zero in combination with a VEV hSi of the singlet generates a contribution to the effective term $_e = hSi +$, where the MSSM term is normally assumed to be zero in NMSSM constructions, yielding $_e = hSi$. The remaining terms represent a general cubic potential for the singlet; is dimensionless, ^{0} has dimension of mass, and $_F$ has dimension of mass squared. The soft SUSY-breaking terms relevant to the NMSSM are

$$V_{soft} = V_{2;MSSM} + V_{3;MSSM} + m_S^2 \, S^2 + (\quad _{ab} A \; SH_1^a H_2^b + \frac{1}{3} A \; S^3 + m_S^{\,02} S^2 + {}_S S + hx:) ; \tag{42}$$

where $V_{i;MSSM}$ are the MSSM soft terms defined in eqs. (8) and (9), and we have introduced the notation $m_S^{\,02}$ $B^{\,0\,0}$.

At tree level, there are thus 15 parameters (in addition to m_Z which fixes the sum of the squared Higgs VEVs) that are relevant for the Higgs sector of the R-parity and CP-conserving NMSSM:

$$\tan \; ; \; ; m_{H_1}^2 ; m_{H_2}^2 ; m_3^2 ; \; ; \; ; A \; ; A \; ; \; {}^0 ; m_S^{\,02} ; \; _F ; \; _S ; \; hSi ; m_S^2 : \tag{43}$$

The minimisation of the effective potential imposes 3 conditions on these parameters, such that only 12 of them can be considered independent.

Note that we write the soft parameter m_3^2 in the form $m_3^2 = (\cos \quad \sin \quad)$, see [72]. The notation m_A^2 that was used for that parameter in the SLHA1 is no longer relevant in the NMSSM context, but by keeping the definition in terms of m_3^2 and $\cos \quad \sin$ unchanged, we maintain an economical and straightforward correspondence between the two cases.

Particle mixing

In the CP-conserving NMSSM, the CP-even interaction eigenstates are ${}^0 \quad \sqrt{2} < (H_1^{\,0} ; H_2^{\,0} ; S)^T$. We define the orthogonal $3 \quad 3$ mixing matrix S by

$$^{0T} M \; ^2{}_0 \; ^0 = \quad \underbrace{^{0T} S^T}_{^{0T}} \; \underbrace{SM \; ^2{}_0 S^T}_{diag(m \; ^2{}_0)} \; \underbrace{S \; ^0}_{^0} \; ; \tag{44}$$

where ${}^0 \quad (h_1^0 ; h_2^0 ; h_3^0)$ are the mass eigenstates ordered in mass.

In the CP-odd sector the interaction eigenstates are ${}^0 \quad \sqrt{2} = (H_1^{\,0} ; H_2^{\,0} ; S)^T$. We define the $2 \quad 3$ mixing matrix P by

$$^{0T} M \; ^2{}_0 \; ^0 = \quad \underbrace{^{0T} P^T}_{^{0T}} \; \underbrace{PM \; ^2{}_0 P^T}_{diag(m \; ^2{}_0)} \; \underbrace{P \; ^0}_{^0} \; ; \tag{45}$$

where ${}^0 \quad (A_1^0 ; A_2^0)$ are the mass eigenstates ordered in mass.

The neutralino sector of the NMSSM requires a change in the definition of the $4 \quad 4$ neutralino mixing matrix N to a $5 \quad 5$ matrix. The Lagrangian contains the (symmetric) neutralino mass matrix as

$$L_{\sim^0}^{mass} = \quad \frac{1}{2} \sim^{0T} M \; _{\sim_0} \sim^0 + hx:; \tag{46}$$

in the basis of 2–component spinors $\sim^0 = (\quad b ; \quad iw^3 ; \tilde{h}_1 ; \tilde{h}_2 ; s)^T$. We define the unitary $5 \quad 5$ neutralino mixing matrix N such that:

$$\frac{1}{2} \sim^{0T} M \; _{\sim_0} \sim^0 = \quad \frac{1}{2} \underbrace{\sim^{0T} N^T}_{\sim^{0T}} \; \underbrace{N \; M \; _{\sim_0} N^y}_{diag(m \; _{\sim_0})} \; \underbrace{N \sim^0}_{\sim^0} \; ; \tag{47}$$

where the 5 (2–component) neutralinos $\sim_i$ are defined such that the absolute value of their masses increase with i. As in SLHA1, our convention is that N be a real matrix. One or more mass eigenvalues may then have an apparent negative sign, which can be removed by a phase transformation on $\sim_i$.

14.7 Summary

The Supersymmetry Les Houches Accord (SLHA) [72] provides a universal set of conventions for supersymmetry analysis problems in high energy physics. Here, we summarise extensions of the conventions of the first SLHA to include various generalisations [170]: the minimal supersymmetric standard model with flavour violation, RPV, and CPV, as well as the simplest next-to-minimal model. For updates and examples, see
`http://home.fnal.gov/ skands/slha/`

References

[1] P. J. Fox, A. E. Nelson, and N. Weiner, *JHEP* **08** (2002) 035, [hep-ph/0206096].

[2] Z. Chacko, P. J. Fox, and H. Murayama, *Nucl. Phys.* **B706** (2005) 53–70, [hep-ph/0406142].

[3] L. M. Carpenter, P. J. Fox, and D. E. Kaplan, hep-ph/0503093.

[4] J. Hisano, M. Nagai, T. Naganawa, and M. Senami, *Phys. Lett.* **B644** (2007) 256–264, [hep-ph/0610383].

[5] M. M. Nojiri and M. Takeuchi, *Phys. Rev.* **D76** (2007) 015009, [hep-ph/0701190].

[6] K. Hsieh, arXiv:0708.3970 [hep-ph].

[7] I. Antoniadis, A. Delgado, K. Benakli, M. Quiros, and M. Tuckmantel, *Phys. Lett.* **B634** (2006) 302–306, [hep-ph/0507192].

[8] I. Antoniadis, K. Benakli, A. Delgado, M. Quiros, and M. Tuckmantel, *Nucl. Phys.* **B744** (2006) 156–179, [hep-th/0601003].

[9] I. Antoniadis, K. Benakli, A. Delgado, and M. Quiros, hep-ph/0610265.

[10] I. J. R. Aitchison, hep-ph/0505105.

[11] P. Fayet, *Nucl. Phys.* **B90** (1975) 104–124.

[12] H. P. Nilles, M. Srednicki, and D. Wyler, *Phys. Lett.* **B120** (1983) 346.

[13] J. M. Frere, D. R. T. Jones, and S. Raby, *Nucl. Phys.* **B222** (1983) 11.

[14] J. P. Derendinger and C. A. Savoy, *Nucl. Phys.* **B237** (1984) 307.

[15] S. Kraml *et. al.*, eds., *Workshop on CP studies and non-standard Higgs physics*, CERN, 2006. hep-ph/0608079.

[16] U. Ellwanger, J. F. Gunion, and C. Hugonie, *JHEP* **02** (2005) 066, [hep-ph/0406215].

[17] U. Ellwanger and C. Hugonie, *Comput. Phys. Commun.* **175** (2006) 290–303, [hep-ph/0508022].

[18] W. Porod, *Comput. Phys. Commun.* **153** (2003) 275–315, [hep-ph/0301101].

[19] G. Belanger, F. Boudjema, C. Hugonie, A. Pukhov, and A. Semenov, *JCAP* **0509** (2005) 001, [hep-ph/0505142].

[20] G. Belanger, F. Boudjema, A. Pukhov, and A. Semenov, *Comput. Phys. Commun.* **176** (2007) 367–382, [hep-ph/0607059].

[21] B. C. Allanach *et. al.*, hep-ph/0202233.

[22] J. Hamann, S. Hannestad, M. S. Sloth, and Y. Y. Y. Wong, *Phys. Rev.* **D75** (2007) 023522, [astro-ph/0611582].

[23] T. Sjostrand, S. Mrenna, and P. Skands, *JHEP* **05** (2006) 026, [hep-ph/0603175].

[24] E. Richter-Was, hep-ph/0207355.

[25] **ATLAS** Collaboration. CERN-LHCC-99-14.

[26] N. Arkani-Hamed and S. Dimopoulos, *JHEP* **06** (2005) 073, [hep-th/0405159].

[27] G. F. Giudice and A. Romanino, *Nucl. Phys.* **B699** (2004) 65–89, [hep-ph/0406088].

[28] J. D. Wells, *Phys. Rev.* **D71** (2005) 015013, [hep-ph/0411041].

[29] W. Kilian, T. Plehn, P. Richardson, and E. Schmidt, *Eur. Phys. J.* **C39** (2005) 229–243, [hep-ph/0408088].

[30] N. Bernal, A. Djouadi, and P. Slavich, *JHEP* **07** (2007) 016, [arXiv:0705.1496 [hep-ph]].

[31] R. Lafaye, T. Plehn, M. Rauch, and D. Zerwas, arXiv:0709.3985 [hep-ph].

[32] P. Bechtle, K. Desch, W. Porod, and P. Wienemann, *Eur. Phys. J.* **C46** (2006) 533–544, [hep-ph/0511006].

[33] M. Drees, hep-ph/0501106.

[34] A. C. Kraan, *Eur. Phys. J.* **C37** (2004) 91–104, [hep-ex/0404001].

[35] G. R. Farrar and P. Fayet, *Phys. Lett.* **B76** (1978) 575–579.

[36] D. N. Spergel *et. al.*,, **WMAP** Collaboration *Astrophys. J. Suppl.* **170** (2007) 377, [astro-ph/0603449].

[37] A. Djouadi, J.-L. Kneur, and G. Moultaka, *Comput. Phys. Commun.* **176** (2007) 426–455, [hep-ph/0211331].

[38] W. Beenakker, R. Hopker, M. Spira, and P. M. Zerwas, *Nucl. Phys.* **B492** (1997) 51–103, [hep-ph/9610490].

[39] W. Beenakker *et. al.*, *Phys. Rev. Lett.* **83** (1999) 3780–3783, [hep-ph/9906298].

[40] M. Bettinelli *et. al.*,. ATL-PHYS-PUB-2007-013.

[41] C. G. Lester, M. A. Parker, and M. J. White, *JHEP* **01** (2006) 080, [hep-ph/0508143].

[42] M. Muhlleitner, A. Djouadi, and Y. Mambrini, *Comput. Phys. Commun.* **168** (2005) 46–70, [hep-ph/0311167].

[43] A. Hocker, H. Lacker, S. Laplace, and F. Le Diberder, *Eur. Phys. J.* **C21** (2001) 225–259, [hep-ph/0104062].

[44] I. Hinchliffe, F. E. Paige, M. D. Shapiro, J. Soderqvist, and W. Yao, *Phys. Rev.* **D55** (1997) 5520–5540, [hep-ph/9610544].

[45] **ATLAS** Collaboration, *Inclusive SUGRA measurements*. No. CERN-LHCC-99-015 ATLAS-TDR-15. May, 1999. Sections 20.2.1.

[46] D. R. Tovey, *Phys. Lett.* **B498** (2001) 1–10, [hep-ph/0006276].

[47] C. G. Lester and D. J. Summers, *Phys. Lett.* **B463** (1999) [hep-ph/9906349].

[48] A. Barr, C. Lester, and P. Stephens, *J. Phys.* **G29** (2003) 2343–2363, [hep-ph/0304226].

[49] W. S. Cho, K. Choi, Y. G. Kim, and C. B. Park, arXiv:0709.0288 [hep-ph].

[50] B. Gripaios, arXiv:0709.2740 [hep-ph].

[51] A. J. Barr, B. Gripaios, and C. G. Lester, arXiv:0711.4008 [hep-ph].

[52] W. S. Cho, K. Choi, Y. G. Kim, and C. B. Park, arXiv:0711.4526 [hep-ph].

[53] G. Corcella *et. al.*, hep-ph/0210213.

[54] S. Moretti, K. Odagiri, P. Richardson, M. H. Seymour, and B. R. Webber, *JHEP* **04** (2002) 028, [hep-ph/0204123].

[55] G. Marchesini *et. al.*, *Comput. Phys. Commun.* **67** (1992) 465–508.

[56] S. Catani, Y. L. Dokshitzer, M. H. Seymour, and B. R. Webber, *Nucl. Phys.* **B406** (1993) 187–224.

[57] S. D. Ellis and D. E. Soper, *Phys. Rev.* **D48** (1993) 3160–3166, [hep-ph/9305266].

[58] H. Baer, F. E. Paige, S. D. Protopopescu, and X. Tata, hep-ph/0001086.

[59] C. Lester and A. Barr, *JHEP* **12** (2007) 102, [arXiv:0708.1028 [hep-ph]].

[60] I. Hinchliffe, F. E. Paige, M. D. Shapiro, J. Soderqvist, and W. Yao, *Phys. Rev.* **D55** (1997) 5520–5540, [hep-ph/9610544].

[61] B. C. Allanach, C. G. Lester, M. A. Parker, and B. R. Webber, *JHEP* **09** (2000) 004, [hep-ph/0007009].

[62] D. J. Miller, P. Osland, and A. R. Raklev, *JHEP* **03** (2006) 034, [hep-ph/0510356].

[63] G. Weiglein *et. al.*,, **LHC/LC Study Group** Collaboration *Phys. Rept.* **426** (2006) 47–358, [hep-ph/0410364].

[64] G. Corcella *et. al.*, *JHEP* **01** (2001) 010, [hep-ph/0011363].

[65] E. Richter-Was, hep-ph/0207355.

[66] F. James and M. Roos, *Comput. Phys. Commun.* **10** (1975) 343–367.

[67] CERN-LHCC-99-15.

[68] G. L. Bayatian *et. al.*,, **CMS** Collaboration *J. Phys.* **G34** (2007) 995–1579.

[69] S. Muanza, The Blind SUSY Search Project. http://www-clued0.fnal.gov/%7Emuanza/Blind_SUSY_Analysis.html.

[70] R. Brun and F. Rademakers, *Nucl. Instrum. Meth.* **A389** (1997) 81–86.

[71] T. Sjostrand, L. Lonnblad, S. Mrenna, and P. Skands, hep-ph/0308153.

[72] P. Skands *et. al.*, *JHEP* **07** (2004) 036, [hep-ph/0311123]. (See also Les Houches 'Physics at TeV Colliders 2003' Beyond the Standard Model Working Group: Summary report, hep-ph/0402295).

[73] S. Kretzer, H. L. Lai, F. I. Olness, and W. K. Tung, *Phys. Rev.* **D69** (2004) 114005, [hep-ph/0307022].

[74] D. Bourilkov, R. C. Group, and M. R. Whalley, hep-ph/0605240.

[75] S. Jadach, J. H. Kuhn, and Z. Was, *Comput. Phys. Commun.* **64** (1990) 275–299.

[76] E. Richter-Was, D. Froidevaux, and L. Poggioli, ATL-PHYS-98-131.

[77] ATLAS, ATLAS TDR-016. ATLAS High-Level Trigger, Data Acquisition and Controls.

[78] R. Brun, O. Couet, C. E. Vandoni, and P. Zanarini,. Prepared for International Workshop on Software Engineering, Artificial Intelligence and Expert Systems for High-energy and Nuclear Physics, Lyon, France, 19-24 Mar 1990.

[79] http://cc.in2p3.fr/article955.html?lang=en.

[80] http://cc.in2p3.fr/docenligne/281.

[81] B. C. Allanach *et. al.*, hep-ph/0602198.

[82] M. Rauch, R. Lafaye, T. Plehn, and D. Zerwas, arXiv:0710.2822 [hep-ph].

[83] P. Bechtle, K. Desch, and P. Wienemann, *ECONF* **C0508141** (2005) ALCPG0324, [hep-ph/0511137].

[84] D. Berdine, N. Kauer, and D. Rainwater, *Phys. Rev. Lett.* **99** (2007) 111601, [hep-ph/0703058].

[85] N. Kauer, *Phys. Lett.* **B649** (2007) 413–416, [hep-ph/0703077].

[86] J. A. Aguilar-Saavedra *et. al.*, *Eur. Phys. J.* **C46** (2006) 43–60, [hep-ph/0511344].

[87] J. Reuter *et. al.*, *ECONF* **C0508141** (2005) ALCPG0323, [hep-ph/0512012].

[88] C. F. Uhlemann, Diplomarbeit, Fakultät für Physik und Astronomie, Universität Würzburg, November, 2007.

[89] W. Beenakker, R. Hopker, and P. M. Zerwas, *Phys. Lett.* **B378** (1996) 159–166, [hep-ph/9602378].

[90] S. Kraml, H. Eberl, A. Bartl, W. Majerotto, and W. Porod, *Phys. Lett.* **B386** (1996) 175–182, [hep-ph/9605412].

[91] A. Djouadi, W. Hollik, and C. Junger, *Phys. Rev.* **D55** (1997) 6975–6985, [hep-ph/9609419].

[92] N. Kauer, arXiv:0708.1161 [hep-ph].

[93] S. Heinemeyer, W. Hollik, D. Stockinger, A. M. Weber, and G. Weiglein, *JHEP* **08** (2006) 052, [hep-ph/0604147].

[94] S. Heinemeyer, W. Hollik, A. M. Weber, and G. Weiglein, arXiv:0710.2972 [hep-ph]. submitted to JHEP.

[95] B. C. Allanach, K. Cranmer, C. G. Lester, and A. M. Weber, *JHEP* **08** (2007) 023, [arXiv:0705.0487 [hep-ph]].

[96] J. Alcaraz *et. al.*,, **LEP** Collaboration arXiv:0712.0929 [hep-ex].

[97] B. C. Allanach, *Comput. Phys. Commun.* **143** (2002) 305–331, [hep-ph/0104145].

[98] G. Belanger, F. Boudjema, A. Pukhov, and A. Semenov, *Comput. Phys. Commun.* **174** (2006) 577–604, [hep-ph/0405253].

[99] A. M. Weber *et. al.*, to appear.

[100] G. W. Bennett *et. al.*,, **Muon G-2** Collaboration *Phys. Rev.* **D73** (2006) 072003, [hep-ex/0602035].

[101] J. P. Miller, E. de Rafael, and B. L. Roberts, *Rept. Prog. Phys.* **70** (2007) 795, [hep-ph/0703049].

[102] K. Hagiwara, A. D. Martin, D. Nomura, and T. Teubner, *Phys. Lett.* **B649** (2007) 173–179, [hep-ph/0611102].

[103] M. Davier, *Nucl. Phys. Proc. Suppl.* **169** (2007) 288–296, [hep-ph/0701163].

[104] A. Czarnecki and W. J. Marciano, *Phys. Rev.* **D64** (2001) 013014, [hep-ph/0102122].

[105] D. Stockinger, *J. Phys.* **G34** (2007) R45–R92, [hep-ph/0609168].

[106] H. Bachacou, I. Hinchliffe, and F. E. Paige, *Phys. Rev.* **D62** (2000) 015009, [hep-ph/9907518].

[107] D. W. Hertzog, J. P. Miller, E. de Rafael, B. Lee Roberts, and D. Stockinger, arXiv:0705.4617 [hep-ph].

[108] B. C. Allanach, C. G. Lester, and A. M. Weber, *JHEP* **12** (2006) 065, [hep-ph/0609295].

[109] M. Frank *et. al.*, *JHEP* **02** (2007) 047, [hep-ph/0611326].

[110] R. Kinnunen, S. Lehti, F. Moortgat, A. Nikitenko, and M. Spira, *Eur. Phys. J.* **C40N5** (2005) 23–32, [hep-ph/0503075].

[111] B. Allanach *et. al.*, arXiv:0801.0045 [hep-ph].

[112] J. Clark and S. DeRose,. http://www.w3.org/TR/xpath.

[113] G. Buchalla *et. al.*, arXiv:0801.1833 [Unknown].

[114] L. J. Hall and L. Randall, *Phys. Rev. Lett.* **65** (1990) 2939–2942.

[115] A. J. Buras, P. Gambino, M. Gorbahn, S. Jäger, and L. Silvestrini, *Nucl. Phys.* **B592** (2001) 55–91, [hep-ph/0007313].

[116] G. D'Ambrosio, G. F. Giudice, G. Isidori, and A. Strumia, *Nucl. Phys.* **B645** (2002) 155–187, [hep-ph/0207036].

[117] L. J. Hall, R. Rattazzi, and U. Sarid, *Phys. Rev.* **D50** (1994) 7048–7065, [hep-ph/9306309].

[118] R. Hempfling, *Phys. Rev.* **D49** (1994) 6168–6172.

[119] M. S. Carena, M. Olechowski, S. Pokorski, and C. E. M. Wagner, *Nucl. Phys.* **B426** (1994) 269–300, [hep-ph/9402253].

[120] T. Blazek, S. Raby, and S. Pokorski, *Phys. Rev.* **D52** (1995) 4151–4158, [hep-ph/9504364].

[121] C. Hamzaoui, M. Pospelov, and M. Toharia, *Phys. Rev.* **D59** (1999) 095005, [hep-ph/9807350].

[122] M. S. Carena, D. Garcia, U. Nierste, and C. E. M. Wagner, *Nucl. Phys.* **B577** (2000) 88–120, [hep-ph/9912516].

[123] K. S. Babu and C. F. Kolda, *Phys. Rev. Lett.* **84** (2000) 228–231, [hep-ph/9909476].

[124] G. Isidori and A. Retico, *JHEP* **11** (2001) 001, [hep-ph/0110121].

[125] A. J. Buras, P. H. Chankowski, J. Rosiek, and L. Slawianowska, *Nucl. Phys.* **B659** (2003) 3, [hep-ph/0210145].

[126] S. R. Choudhury and N. Gaur, *Phys. Lett.* **B451** (1999) 86–92, [hep-ph/9810307].

[127] C. Bobeth, T. Ewerth, F. Kruger, and J. Urban, *Phys. Rev.* **D64** (2001) 074014, [hep-ph/0104284].

[128] A. Djouadi, M. M. Muhlleitner, and M. Spira, *Acta Phys. Polon.* **B38** (2007) 635–644, [hep-ph/0609292].

[129] J. Hisano, K. Kawagoe, and M. M. Nojiri, *Phys. Rev.* **D68** (2003) 035007, [hep-ph/0304214].

[130] T. Hahn, S. Heinemeyer, W. Hollik, H. Rzehak, and G. Weiglein, arXiv:0710.4891 [hep-ph].

[131] M. Della Morte, *PoS* **LAT2007** (2007) 008, [arXiv:0711.3160 [hep-lat]].

[132] T. Plehn, *Phys. Rev.* **D67** (2003) 014018, [hep-ph/0206121].

[133] E. Boos and T. Plehn, *Phys. Rev.* **D69** (2004) 094005, [hep-ph/0304034].

[134] F. Spite and M. Spite, *Astronomy and Astrophysics* **115** (1982) 357.

[135] M. Asplund, D. L. Lambert, P. E. Nissen, F. Primas, and V. V. Smith, *Astrophys. J.* **644** (2006) 229–259, [astro-ph/0510636].

[136] K. Jedamzik, arXiv:0707.2070 [astro-ph].

[137] K. Jedamzik, K.-Y. Choi, L. Roszkowski, and R. Ruiz de Austri, *JCAP* **0607** (2006) 007, [hep-ph/0512044].

[138] P. Zalewski, arXiv:0710.2647 [hep-ph].

[139] M. Kazana, G. Wrochna, and P. Zalewski,, **CMS** Collaboration CMS CR-1999/019.

[140] C. Balazs, A. Sopczak, *et. al., in "Les Houches 'Physics at TeV Colliders 2005' Beyond the Standard Model working group: summary report", hep-ph/0602198 (part 8), and references therein* (2006).

[141] M. S. Carena *et. al.*, *Phys. Rev.* **D72** (2005) 115008, [hep-ph/0508152].

[142] A. Freitas, C. Milstene, M. Schmitt, and A. Sopczak, arXiv:0712.4010 [hep-ph].

[143] M. Tegmark *et. al.*,, **SDSS** Collaboration *Astrophys. J.* **606** (2004) 702–740, [astro-ph/0310725].

[144] C. Balazs, M. S. Carena, and C. E. M. Wagner, *Phys. Rev.* **D70** (2004) 015007, [hep-ph/0403224].

[145] A. Sopczak *et. al.*, hep-ph/0605225.

[146] M. Pohl and H. J. Schreiber, hep-ex/0206009.

[147] **LCFI** Collaboration , http://hepwww.rl.ac.uk/lcfi.

[148] H. Eberl, A. Bartl, and W. Majerotto, *Nucl. Phys.* **B472** (1996) 481–494, [hep-ph/9603206].

[149] T. G. M. Malmgren and K. E. Johansson, *Nucl. Instrum. Meth.* **A403** (1998) 481–489.

[150] C. Peterson, D. Schlatter, I. Schmitt, and P. M. Zerwas, *Phys. Rev.* **D27** (1983) 105.

[151] G. Alexander *et. al.*,, **OPAL** Collaboration *Z. Phys.* **C69** (1996) 543–560.

[152] G. Abbiendi *et. al.*,, **OPAL** Collaboration *Eur. Phys. J.* **C29** (2003) 463–478, [hep-ex/0210031].

[153] A. Heister *et. al.*,, **ALEPH** Collaboration *Phys. Lett.* **B512** (2001) 30–48, [hep-ex/0106051].

[154] K. Ackerstaff *et. al.*,, **OPAL** Collaboration *Eur. Phys. J.* **C6** (1999) 225–238, [hep-ex/9808026].

[155] M. S. Carena and A. Freitas, *Phys. Rev.* **D74** (2006) 095004, [hep-ph/0608255].

[156] B. C. Allanach, S. Kraml, and W. Porod, *JHEP* **03** (2003) 016, [hep-ph/0302102].

[157] G. Belanger, S. Kraml, and A. Pukhov, *Phys. Rev.* **D72** (2005) 015003, [hep-ph/0502079].

[158] H. Baer, J. Ferrandis, S. Kraml, and W. Porod, *Phys. Rev.* **D73** (2006) 015010, [hep-ph/0511123].

[159] F. E. Paige, S. D. Protopopescu, H. Baer, and X. Tata, hep-ph/0312045.

[160] A. De Roeck *et. al.*, *Eur. Phys. J.* **C49** (2007) 1041–1066, [hep-ph/0508198].

[161] P. Nath and R. Arnowitt, *Phys. Rev.* **D56** (1997) 2820–2832, [hep-ph/9701301].

[162] J. R. Ellis, T. Falk, K. A. Olive, and Y. Santoso, *Nucl. Phys.* **B652** (2003) 259–347, [hep-ph/0210205].

[163] H. Baer, A. Mustafayev, S. Profumo, A. Belyaev, and X. Tata, *JHEP* **07** (2005) 065, [hep-ph/0504001].

[164] W. Buchmuller, J. Kersten, and K. Schmidt-Hoberg, *JHEP* **02** (2006) 069, [hep-ph/0512152].

[165] W. Buchmuller, L. Covi, J. Kersten, and K. Schmidt-Hoberg, *JCAP* **0611** (2006) 007, [hep-ph/0609142].

[166] L. Covi and S. Kraml, *JHEP* **08** (2007) 015, [hep-ph/0703130].

[167] S. Kraml and D. T. Nhung, arXiv:0712.1986 [hep-ph].

[168] D. E. Kaplan, G. D. Kribs, and M. Schmaltz, *Phys. Rev.* **D62** (2000) 035010, [hep-ph/9911293].

[169] Z. Chacko, M. A. Luty, A. E. Nelson, and E. Ponton, *JHEP* **01** (2000) 003, [hep-ph/9911323].

[170] B. Allanach *et. al.*, arXiv:0801.0045 [hep-ph].

[171] P. Skands,. FERMILAB-CONF-07-586-T, in 'Collider aspects of flavour physics at high Q', arXiv:0801.1800.

[172] J. Alwall *et. al.*, arXiv:0712.3311 [hep-ph].

[173] J. Alwall *et. al.*, *Comput. Phys. Commun.* **176** (2007) 300–304, [hep-ph/0609017].

[174] L. J. Hall, V. A. Kostelecky, and S. Raby, *Nucl. Phys.* **B267** (1986) 415.

[175] N. Cabibbo, *Phys. Rev. Lett.* **10** (1963) 531–532.

[176] M. Kobayashi and T. Maskawa, *Prog. Theor. Phys.* **49** (1973) 652–657.

[177] Z. Maki, M. Nakagawa, and S. Sakata, *Prog. Theor. Phys.* **28** (1962) 870.

[178] B. Pontecorvo, *Sov. Phys. JETP* **26** (1968) 984–988.